Effluent Stream Monitoring at the Dynamic Stripping Demonstration Using Fourier-Transform Infrared Spectroscopy

Contents

EFFLUENT STREAM MONITORING AT THE DYNAMIC STRIPPING DEMONSTRATION USING FOURIER-TRANSFORM INFRARED SPECTROSCOPY

Kevin C. Langry and Thomas J. Kulp

Abstract: A standard fourier transform infrared (FT-IR) spectrometer equipped with a gas sample cell was used to monitor the vapor effluent stream at the Gasoline Spill Site during a portion of the Dynamic Stripping Demonstration. The vacuum-extracted effluent vapor was passed directly through a sample line to the FT-IR for on-line analysis of the spectral region between 400 and 4000 cm^{-1}. Spectra of the effluent were recorded at six to ten minute intervals during eight days of the demonstration. The data collected with this spectral range and frequency of sampling show that on-line FT-IR spectroscopy can be used to monitor water vapor concentrations, carbon dioxide levels, and bulk alkane concentrations in the process stream essentially in real-time. In this report, representative spectra of Spill Site effluent vapor are presented to illustrate the type of data collected during the monitoring period and to demonstrate the utility of on-line analysis with FT-IR spectroscopy.

INTRODUCTION

This report summarizes an effort to use an in-line Fourier transform infrared (FT-IR) spectrometer to monitor the vapor effluent stream of the LLNL Dynamic Stripping Demonstration Facility (DSDF). The test was carried out during the period between June 25 to July 2, 1993, (days 33 to 40 of the DSDF operation). Because the test was not planned as part of the overall demonstration, it was carried out in an impromptu fashion using off-the-shelf

equipment that was not specifically tailored for the task. Nonetheless, the results of the trial indicate that in-line FT-IR spectroscopy shows considerable promise for monitoring a process stream of this nature. Data collected demonstrate the ability of the FT-IR to characterize aspects of the chemical composition of the effluent stream at a rate that is essentially real-time for a process of this type (sampling period of a few minutes or less). Although the data collected were not sufficiently detailed to allow quantitative determination of the flow stream constituents, they do allow certain conclusions to be drawn about the nature of its composition. For example, the data demonstrate a concentration of CO_2 that is considerably higher than ambient. Also, the data indicate that the organic composition of the flow stream is primarily aliphatic at the sampling point. The temporal dependence of the integrated absorbance in the C-H-stretch region gives an indication of the overall hydrocarbon content of the flow stream. Finally, comparisons of the time data obtained with the FT-IR closely parallel the data obtained with the Oak Ridge National Laboratory (ORNL) Differential UV Absorption Sensor (DUVAS).

In the remainder of this report, the implementation of the FT-IR at the DSDF will be described and the results of its use will be presented. Spectra obtained during the demonstration will be compared with library spectra of a series of known constituents of the effluent stream. Temporal plots of band-integrated spectral data will also be presented and compared with data obtained from the ORNL DUVAS sensor. The report will conclude with a discussion of future applications using FT-IR for process stream monitoring during site remediation.

BACKGROUND

Infrared spectroscopy is a type of absorption spectroscopy that is used to interrogate the types of bonds that exist within molecules. The bonds between atoms of a molecule undergo two basic motions: a stretching motion where the distance between two covalently linked nuclei is altered along the bonding axis, and a bending motion where a change in the bond angle occurs between bonds with a common atom (see Figure 1). When these vibrations produce a change in the dipole moment of the bond, infrared radiation can be absorbed by the molecule. The frequency of the radiation absorbed is a function of the vibrational frequency of the bonds, and the intensity of the absorption depends on the magnitude of the change in the dipole moment. In a classical interpretation, the bond vibrational frequency, and consequently the infrared absorption frequency, is related to the masses of the bonded elements and to the force constant of the bond.

The infrared spectra of the effluent from the Gasoline Spill Site will depend on the kinds of molecules that comprise the vapor stream. The bulk of pre-clean air era gasoline generally consists of a variety of C_6 to C_8 alkanes in addition to an aromatic fraction of octane boosters comprised of alkylated benzene components. With this mixture the infrared spectra of the effluent will

be characterized primarily by the C-H stretching (2800-3000 cm^{-1}) and bending (1300-1500 cm^{-1}) modes of the alkane components and the aromatic C-H stretching (3000 to 3100 cm^{-1}) and out-of-plane bending (660-900 cm^{-1}) vibrations of the substituted benzene compounds. In addition, there may be other vapor components, such as water and ammonia, that may show hydrogen-heteroatom stretching and bending absorptions. Carbon dioxide will likely be present and exhibit its infrared-active C-O bond absorptions (stretching 2350 cm^{-1}; bending 667 cm^{-1}).

FT-IR APPARATUS DESCRIPTION

The location of the FT-IR in the DSDF process stream is indicated in Figure 2. The instrument was incorporated into a sampling line that branched off from the primary effluent stream at a point just before the vapor stream entered the gas combustion engine. About 10 m of 0.25 in o.d. stainless steel tubing was used to convey the effluent vapor from the branch point into an air conditioned mobile laboratory van that housed an on-line gas chromatograph (GC) in addition to the FT-IR gas sampling system. Because the primary vapor stream was about 7.6 cm Hg (10.13 kPa) less than atmospheric pressure, a metal bellows pump was used to draw the effluent from the main line and elevate the vapor to a pressure between 40 cm Hg (53.3 kPa) and 50 cm Hg (66.7 kPa) above atmospheric. A small portion of this gas stream was then directed into the GC through a tee in the line while the remaining portion of the flow was sent to the FT-IR. The temperature of the van was kept between 16 and 22 °C.

The sample cell used in the FT-IR consisted of a cylindrical quartz body that was terminated with anti-reflection coated zinc selenide windows. The optical pathlength of the cell was 12 cm, and its diameter was 2.5 cm. The sample cell was suspended in the FT-IR sample compartment by its quartz inlet and outlet tubes which routed the vapor through the cell. Upon exiting the cell, the vapor was piped outside the van and vented to the atmosphere. The cell inlet and outlet tubes protruded through the upper sealing plate of the spectrometer's sample chamber and were sealed in place with a silicone rubber cement. Thus, it was possible to maintain the entire FT-IR sample compartment under an atmosphere of dry nitrogen with the cell in place. The quartz body of the cell was wrapped with a resistive heater wire that was connected to a thermostatted current source that was used to regulate the cell temperature. During the run, the cell was maintained at a temperature of about 35 °C in order to prevent condensation within it. Cell temperature was monitored using a thermocouple and flow through the cell was monitored using an in-line rotometer. The flow of effluent vapor through the cell was fairly constant at 10 L/min. Additional prevention against liquid buildup within the cell was accomplished by flowing the vapor effluent through a glass-bead filled trap just prior to its introduction into the spectral cell. Occasionally buildup of fluid (water + organic layer) within this trap was discovered during the monitoring period. At times, it was

not emptied until several milliliters of fluid had accumulated, as there was only limited direct monitoring of the apparatus by personnel. Thus, it is conceivable that this buildup may, at times, influence the experimental results by producing a constant level of higher readings caused by evaporation of the neat liquid.

The FT-IR spectrometer used was a Polaris model produced by Mattson Instruments, Inc. of Madison, Wisconsin. It was controlled by a Wyse 286 PC and was operated at all times at a resolution of 4 cm^{-1}. Detection was accomplished with a liquid nitrogen-cooled mercury cadmium telluride (MCT) detector. For the first two days of the experiment, power was provided to the instrument by a portable gasoline-powered generator; thereafter standard line current was used. The instrument and sample compartment were continually purged with dry nitrogen. When sampling, the instrument was programmed to collect and transform 16 scans in 30 seconds to provide a full infrared spectrum (400-4000 cm^{-1}) at regular intervals for a given period of time. Initially, time intervals of 6 minutes were used; later this was changed to 10 minutes. The total collection time for a run was initially set at 2 hours but was later extended to 24 hours. A reference spectrum was obtained at the beginning of each run as the sample cell was flushed with dry nitrogen. During the extended runs, it was necessary to periodically fill the detector dewar and to fill the gas tank of the portable generator. Occasionally, a maintenance visit was missed and the detector warmed, causing data to be lost for a period of time. Ultimately, for long field experiments, it would be desirable to incorporate a closed-cycle refrigerator into the system to chill the detector.

REPRESENTATIVE SPECTRAL DATA

Figure 3 contains a representative spectrum obtained during the monitoring process. Also shown in that figure is a spectrum taken in the laboratory in which ambient room air occupied the cell. Note in both cases the presence of the CO_2 bands centered at 2370 cm^{-1} and 667 cm^{-1} and the water bands between 4000-3500 cm^{-1} and 2050-1300 cm^{-1}. Several points may be made. (1) Despite the essentially saturated humidity conditions of the gas stream during the run, clear windows exist between the water vapor absorption bands that allow the unhindered measurement of vibrational bands of organic species. It should, however, be noted that the water may become more of a problem (although probably not intractably so) if longer sample pathlengths are used. (2) As will be seen later in this report, the water bands do, nonetheless, obscure *some* weak organic vibrational bands. (3) From a comparison of the ratio of the CO_2 to water bands in both spectra, and consideration of the fact that the water vapor in the gas stream spectrum is probably near saturation, it is apparent that there is a considerably higher concentration of CO_2 in the gas stream than is present in the ambient atmosphere. The source of this CO_2 is not known to us at this time; however, subsurface oxidation or biodegradation has been suggested as a possible source.

Features attributable to organic species of the vapor effluent are expected to occur in the C-H stretching region (2700-3200 cm^{-1}, Fig. 3.3) and in the molecular fingerprint region between 500 and 1500 cm^{-1} (Fig. 3.5 and 3.6). The absorptions caused by effluent stream organic constituents in the spectra of Figure 3 are the C-H stretching feature at 2970 cm^{-1} and the C-H bending bands located at 1465 cm^{-1} (overlapped by the lower energy branch of the water vapor absorption band). Other features, primarily those of aromatic bond vibrations, expected in the region between 400 and 2000 cm^{-1} (Fig. 3.6) are not visible at this level of magnification. Further expansion of this region reveals some additional bands, as shown in the spectra of Figure 4. These absorptions are obviously quite weak and their detection could be improved by increasing the optical pathlength and, possibly, by averaging more scans. In the future, a variable dynamic range system could be implemented using a variable pathlength multipass cell as the measurement chamber.

IDENTIFICATION OF THE INFRARED SPECTRAL FEATURES

The gas stream of the DSDF contains a relatively complex mixture of organic species, all of which are IR absorbing. The spectral features observed in the FT-IR data can be compared with features in reference spectra of the chemical constituents that are known to be present in the effluent stream. A listing of species that were reported in the GC-MS data of M. Jovanovich is provided in Table 1. We used this list as the basis for selecting library spectra to compare with the gaspad spectral results (see Figure 5). The comparisons are made for three separate regions: 2700-3200 cm^{-1}, 500-2000 cm^{-1}, and 800-2000 cm^{-1}. In some of the spectra, the data in the latter region is magnified to show comparisons of the C-H bending regions and to accentuate the weak mid-region bands.

The most intense feature of the effluent stream spectrum is the C-H stretching band centered around 2950 cm^{-1} that contains overlapping contributions from many of the components of the organic vapor; however, those absorptions are nondistinct in shape and provide very little structural information. The 1465 cm^{-1} band, attributable to C-H bending vibrations, provides some additional structural information, as do the wavelengths of the weak fingerprint features of Figures 4 and 5. Despite the wealth of unique spectral information found in the library reference spectra, the effluent vapor possesses too few characteristic absorption bands with sufficient intensity to generate a comprehensive identification of species from the FT-IR spectra. This result could be anticipated by reviewing the physical properties of the effluent stream constituents. The vapor pressure and boiling point data in Table 1 indicate that the alkane portion of the effluent will be at least an order of magnitude higher in concentration than the most volatile of the aromatic compounds. This does not impugn the potential of in-line FT-IR spectroscopy

for vapor analysis, it merely suggests that a longer pathlength cell is required to gain signal intensity for those more dilute components of the vapor stream.

TIME-DEPENDENT CHANGES IN THE EFFLUENT VAPOR SPECTRA

The first analyses of the vapor effluent were initiated by collecting a background spectrum of the gas cell purged with nitrogen. This spectrum was then subtracted automatically from all subsequent scans in the collection interval to provide spectra solely of the effluent vapor. The first set of data collected is shown in Figure 6. These spectra are a series of 20 consecutive scans collected over a 2 hour interval. The simplicity in the spectra belies several significant features found in this series. Most significant of all is the remarkable stability of the baseline with less than 1% drift occurring in the baseline at 1000 cm^{-1} over the 2 hour monitoring period (based on 1.6 full-scale absorbance). Juxtaposed to the stable baseline is the dramatic change in the integrated band intensity of the C-H alkane stretching band centered at 2950 cm^{-1} (see Fig. 6.2). This band experiences a 50% change over its base value, indicating a 50% change in the concentration of alkane components in the vapor stream. A similar change is noticeable within the lower energy portion of the water envelope that contains the overlapping portion of the alkyl C-H bending modes around 1385 cm^{-1} and 1485 cm^{-1} (Fig. 6.5). A very interesting feature of the water band between 1500 cm^{-1} and 1600 cm^{-1} is that the band structure is virtually unchanged over the course of the collection period providing clear evidence that, while the vapor remains saturated with water the concentration of the organic components is changing. Even the concentration of carbon dioxide appears to vary slightly during the two hour interval (see Fig. 6.2 and 6.7).

The first collection interval was only two hours so that the instrument could be adjusted and collection parameters modified for more extended periods of data collection. Consequently, subsequent monitoring intervals were increased to 12 and then 24 hours. In these longer term runs the baseline no longer remains stable but begins to drift substantially. Figure 7 shows some of the scans collected over 17 hours and these spectra exhibit considerable drift in the baseline, particularly at higher frequencies. The origin of the drift is not known but may result from temperature fluctuations in the IR source. Nevertheless, it should be possible to overcome this drift problem by collecting background scans more frequently.

The drifting baseline does not necessarily diminish the quality of the data because the spectra can automatically be base-line corrected. However, to insure that the drift only affected the baseline and not the integrated band values, the instrument was evaluated in the laboratory for drift behavior. Figure 8 shows some representative scans from a set of 46 spectra of room air collected during a three hour sampling interval. This figure shows there is a substantial shift in the baseline intensity, almost uniformly, over the entire 4000 to 400 cm^{-1} region. However, even though the baseline shifts by more than 20%, the integrated band

intensities for the water bending manifold (2100 to 1200 cm^{-1}) and carbon dioxide (2500 to 2200 cm^{-1}) remain relatively constant with the water band changing by less than 1.5% and the CO_2 band intensity changing by less than 3%. Unfortunately, the drift of the baseline does appear to be related to the increasing values of the integrated intensities (see Figure 9). This relation may be coincidental but in view of the substantial changes in the integrated values found for the alkane vapor concentration it may not be significant if more frequent background spectra are collected and used.

ON-LINE TEMPORAL MONITORING OF THE DYNAMIC STRIPPING PROCESS

An indication of the progress of the Dynamic Stripping process can be mapped by plotting the band-integrated intensities of certain spectral features as a function of time. Given the limited degree of chemical identification that is possible with the data set collected during the demonstration, we chose to monitor the C-H stretch absorption feature at 2950 cm^{-1}, whose intensity gives an rough indication of total organic content of the effluent stream. These data are plotted in Figure 10, which shows the raw data of the integrated band intensity for the C-H stretch absorbance obtained from each scan during the entire monitoring period. Note that the plot shows a period in time in which the combustion engine shut down (causing a stop in effluent flow) and some periods in which the detector warmed because the deware was not recharged with liquid nitrogen (where the signal becomes very noisy). In the beginning of each individual run (i.e. the start of each segment in the plot) a low point is plotted that results from the sampling stream entering the purged cell following a reference scan. Despite the disruptions in the data collection, the intervals exhibit good continuity from one sequence to the next. The concern over shifting baselines during the monitoring period may be exaggerated because, as the data demonstrates in this figure, even after the gas cell has been purged the trend of decreasing alkane concentration in the vapor stream is continuous.

Figure 11 contains an edited version of the CH-stretch data from Figure 10, in which unusable points have been removed. Also plotted in that figure is a time-curve corresponding to the integrated band intensity for the CO_2 band at 667 cm^{-1}. Note that the same general trend is paralleled in each curve, although the organic curve is reduced in intensity by about 60 percent during the dip while the CO_2 curve is reduced by only about 20 percent of its original value. Note also that the low-intensity fluctuation occurs in each curve, and that the pattern of these fluctuations appears to be correlated between curves. These fluctuations are not due to baseline noise in the spectra, and are also not attributable to baseline drift. The up-swing in the data at about 920 h corresponds to steam injection into well 819 at 897 h into the second pass operation. Careful examination of Figure 11 indicates that the CO_2 band is first to exhibit an increase in vapor concentration, as might be expected to occur as the subsurface is heated and the more volatile components are boiled off or degassed from the soil matrix.

The temporal data obtained with the FT-IR can be compared with data provided by the ORNL DUVAS. The purpose of this is not to judge the instruments against one another, but only to correlate trends to improve confidence in the readings from either instrument. Figure 12 contains a plot of the CH-stretch data plotted against the total aromatic signal from the DUVAS; Figure 13 contains a plot of the benzene signal. Each DUVAS trace contains some down-times as does the FT-IR data. The DUVAS data was obtained at sparser time resolution (30 min between data points) and do not, therefore, show the detailed temporal fluctuations seen in figures of FT-IR data. Nonetheless, the degree of fluctuation in those data is comparable to that of the FT-IR. The longer term (24 hr period) variations in the DUVAS results that were attributed to some type of diurnal heating and cooling of the system were not observed in the FT-IR data. It should be noted, however, that the DUVAS and the FT-IR were located in two different locations in the stream, and that the discrepancies may be due to factors peculiar to those locations. Also, the DUVAS is responsive to heavier aromatics while the FT-IR data appears to reflect primarily alkane concentrations. Nonetheless, the general shape of the FT-IR temporal curves and those of the DUVAS appear qualitatively similar.

ESTIMATION OF COMPONENT CONCENTRATION IN THE EFFLUENT GAS

The absorption of radiation in the infrared region follows Beer's absorption law which relates the absorbance, A, to a linear function of the vapor concentration as expressed in the equation:

$$A = abc,$$

where a is the molar absorptivity and is characteristic for a specific sample at a particular wavelength, b is the cell pathlength, and c is the molar concentration of the sample in the cell. Although a calibration curve for water and carbon dioxide were not prepared, assuming that the effluent vapor absorbances for these two components is in a linear portion of their concentration profile, the amount of water and CO_2 in the off-gas stream can be estimated by comparing the integrated band intensities for the corresponding absorbances to those of the room air spectrum. The concentration of CO_2 in ambient room air is generally fixed at 0.034 mole-%. The water in the laboratory room air for the spectrum shown was measured with a psychrometer and found to be 9.4 g/m^3 at 22.5 °C. Given these values, and the integrated band intensity for the water band of the vapor effluent being a factor of 1.9 greater than the room air band intensity, an estimated value for the water concentration in the vapor stream is 17.9 g/m^3, which is essentially the value expected for water-saturated air. For the effluent spectrum shown in Figure 3, the CO_2 concentration is calculated by the same method to be 10 times that of ambient air, or 0.34 mole-% of the vapor stream. However, as shown in Figure 11, the concentration of CO_2 changes during the course of the Dynamic Stripping demonstration.

An evaluation of the organic component concentration presents a more difficult task. A detailed gas chromatographic analysis of the vapor stream in the primary gas line was not available to us at the time of this report; however, liquid that was collected from the gasoline -water separators shows that the condensed phase effluent was composed of more than 40 principle components consisting of both alkane and aromatic compounds (see Figure 14). The aromatic constituents, except for benzene, all possessed various alkyl ring substituents that ranged from a single methyl group (toluene) to more highly substituted ethyl and propyl alkylated xylenes. The alkane fraction was no less complex and comprised primarily of C6 to C9 alkanes. The gas chromatographic and mass spectral data was not sufficiently detailed to provide the identifies of these hydrocarbons, but the petroleum distillates found in gasoline normally are an array of branched chain positional isomers in addition to the linear hydrocarbons homologs. This complex nature of the gas stream makes it difficult to quantify any specific component of the mixture.

However, because the vapor fraction monitored by the FT-IR was largely composed of alkane components, it may be possible to estimate the gross alkane concentration, with some conditions, based on a comparisons of the effluent alkane infrared absorptions to those of a standard gas. This generalization is similar to the approach taken to quantitate the alkane fraction using GC. In gas chromatographic analysis, one or two compounds are chosen as standards to generate a detector response curve for given concentrations of the standard. All the other components are then assumed to have similar molar response factors. Applying this approach, a standard curve was generated in the laboratory using the same gas cell that was employed at the Gasoline Spill Site. Pentane was chosen as the standard alkane because it has a very high vapor pressure and this would insure that the prepared standards would all be gas phase samples. Figure 14 shows the calibration curve generated with pentane as the standard gas. Using the data of Figure 10, the estimated alkane concentration is determined to be about 15,000 ppm in the vapor phase at 840 h into the second pass of the steam injection sequence. Obviously, this number only represents an estimated value and better calibration curves could be generated with standards that more closely resemble the structures of the alkane vapor components.

CONCLUSION

This report summarizes an effort to use an in-line FT-IR spectrometer to monitor the vapor effluent stream of the LLNL Dynamic Stripping Demonstration Facility. The results of the trial indicate that in-line FT-IR spectroscopy shows considerable promise for monitoring vapor phase effluent streams of this nature. Data collected demonstrate the ability of the FT-IR to characterize aspects of the chemical composition of the effluent stream at a rate that is essentially real-time for a process where the interval between sampling can be as short as a minute. Although the data collected in this test were not sufficiently detailed to allow quantitative determination of most of the flow

stream constituents, they do allow certain conclusions to be drawn about the nature of its composition. The data also demonstrate that uniquely identifiable absorbances can be used to quantify some of the constituents of the vapor stream. The well resolved absorbances of water vapor and CO_2 are examples of this capability. As with other analytical methods, this test shows that there are trade-offs between rapid analysis and complete analysis. While FT-IR spectroscopy can provide essentially real-time data analysis for classes of compounds, it is not able identify specific compounds within a group of functionally similar constituents. However, as this test shows, FT-IR can be used quite productively in applications of process stream monitoring providing both qualitative and quantitative information for selected chemical components.

The conclusions more specifically related to the analysis of the Gasoline Spill vapor effluent show that FT-IR spectroscopy can be used to monitor the alkane component of the effluent vapor flow stream. The temporal dependence of the integrated absorbance in the C-H-stretch region gives an indication of the overall hydrocarbon content of the effluent stream. Finally, comparisons of the time data obtained with the FT-IR closely parallel the data obtained with the Oak Ridge National Laboratory (ORNL) Differential UV Absorption Sensor (DUVAS).

REFERENCES

Colthup, N. B.; Daly, L. H.; and Wiberley, S. E. (1990), *Introduction to Infrared and Raman Spectroscopy,* 3rd ed. (Academic Press, Inc., San Diego).

Silverstein, R. M.; Bassler, G. C.; and Morrill, T. C. (1974), *Spectrometric Identification of Organic Compounds*, 3rd ed. (John Wiley & Sons, Inc., New York).

CRC Handbook of Chemistry and Physics, 73rd ed.(1992), D. R. Lide, Ed. (CRC Press, Boca Raton).

Table 1. Physical Properties of Condensed Phase Effluent Constituents

Entry	Chemical Name [CAS No.]	Mass[a]	bp[b]	vp[c]	% at Saturation[d]
1	2-methylpentane [107-83-5]	86	62	176	23
2	methyl cyclopentane [96-37-7]	84	72	109	14
3	2-methylhexane [591-76-4]	100	90	52	6.8
4	3-methylhexane [589-34-4]	100	91	48	6.3
5	heptane [142-82-5]	100	98	36	4.7
6	toluene [108-88-3]	92	111	21	2.8
7	octane [111-65-9]	114	125	10	1.3
8	ethylbenzene [100-41-4]	106	136	7	0.9
9	m-xylene [108-38-3]	106	139	6[e]	0.8
10	p-xylene [106-42-3]	106	138	6[e]	0.8
11	o-xylene [95-47-6]	106	144	5[e]	0.7
12	propylbenzene [103-65-1]	120	159	3[e]	0.4
13	1-ethyl-2-methylbenzene [611-14-3]	120	165	3[e]	0.4
14	1-ethyl-3-methylbenzene [620-14-4]	120	161	3[e]	0.4
15	1,3,5-trimethylbenzene [108-67-8]	120	165	3[e]	0.4
16	1,2,3-trimethylbenzene [526-73-8]	120	176	2[e]	0.3
17	1,2,4-trimethylbenzene [95-63-6]	120	169	2[e]	0.3
18	water [7732-18-5]	18	100	17.5	2.3

[a] molecular weight in grams/mole.
[b] boiling point at 760 torr in °C.
[c] vapor pressure at 20 °C, 760 torr.
[d] mole % of atmosphere at 20 °C, 760 torr.
[e] Calculated from CRC Handbook of Chemistry and Physics reference data.

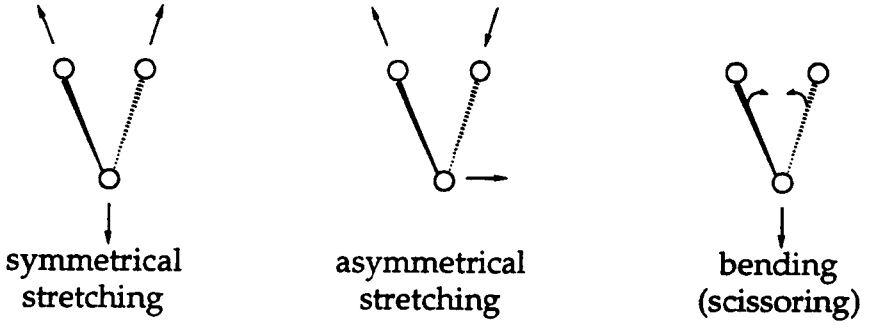

Figure 1. The three fundamental vibrations of a nonlinear molecule are depicted as symmetrical stretching, asymmetrical stretching, and bending.

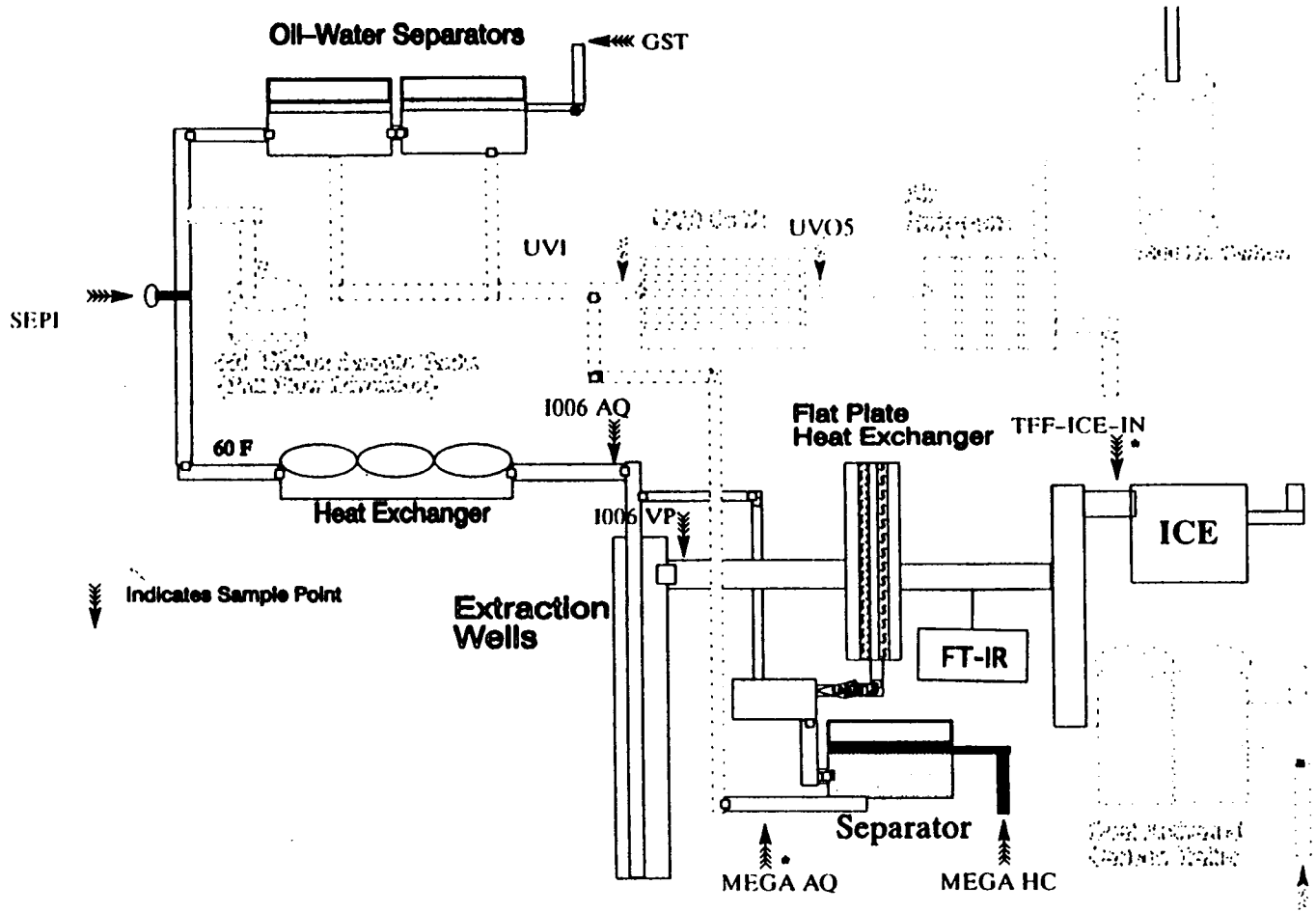

Figure 2. Relative location of the Fourier-transform infrared (FT-IR) spectrometer and gas sampling line at the Gasoline Spill Site of the Dynamic Stripping Demonstration Facility (DSDF).

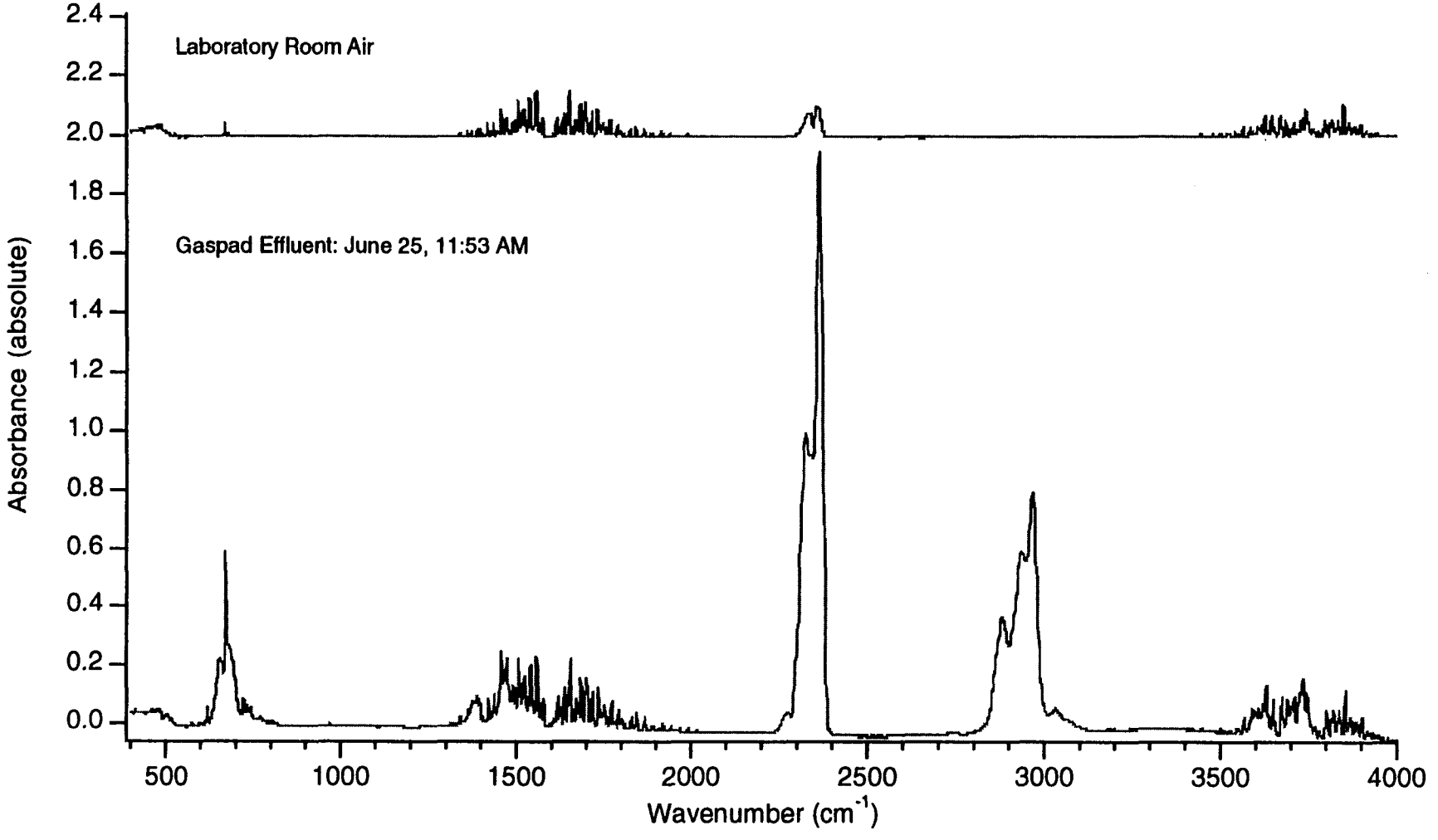

Figure 3.1. A spectrum of the gaspad vapor effluent collected on June 25, is compared to a spectrum of normal laboratory room air. Both spectra were obtained from gas samples in the 12 cm gas cell and are displayed in this spectral series at their absolute absorbances. The concentration of carbon dioxide in this sample of effluent, calculated by measuring the integrated peak intensity of the CO_2 band centered at 2350 cm^{-1}, is nearly 10 times that of room air. The water content of the room air was measured using a electric fan psychrometer and found to be 9.4 g/m^3. The concentration of carbon dioxide in air is generally 0.034 mole %.

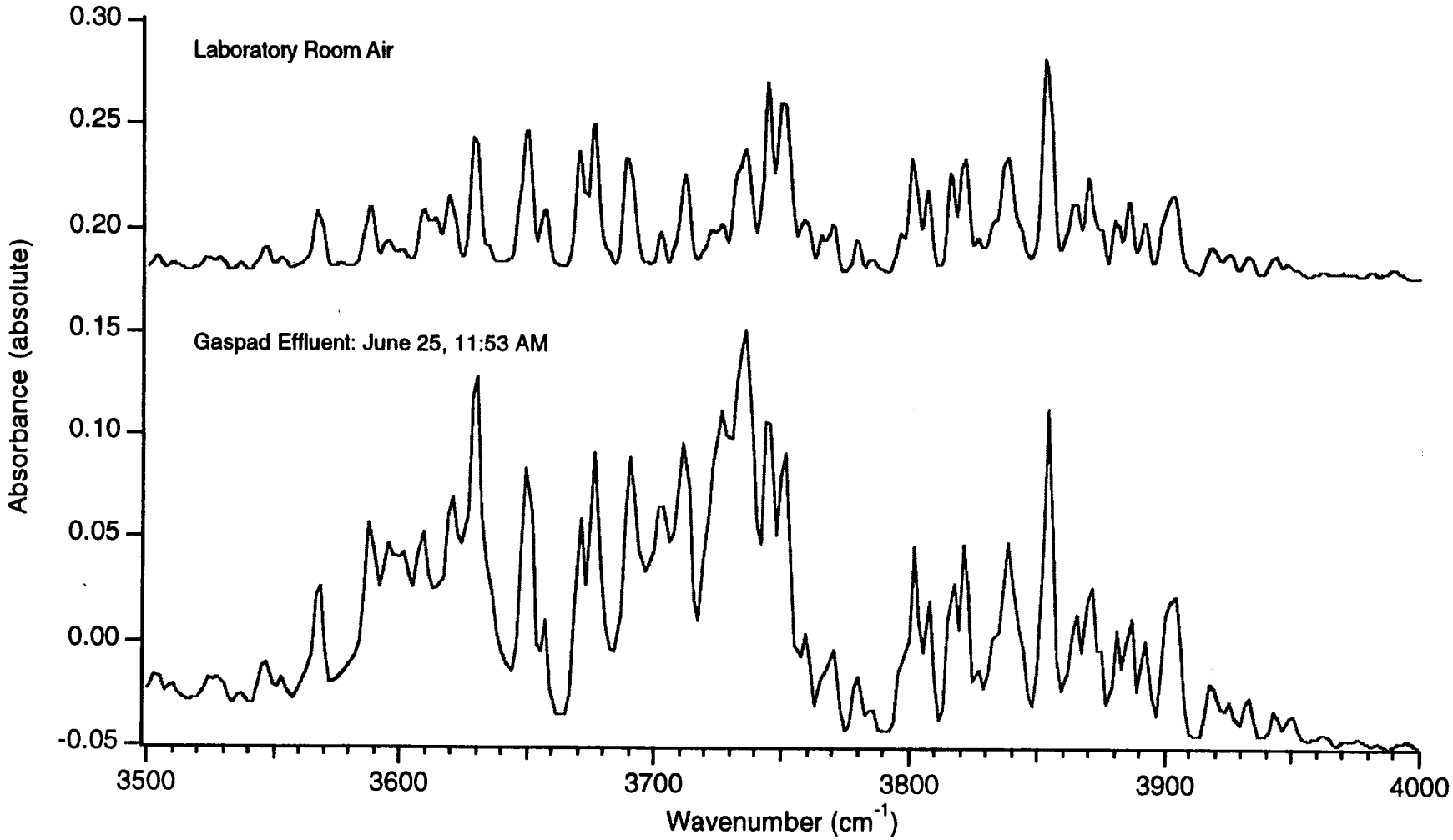

Figure 3.2. The infrared spectra of Figure 3.1 are expanded to show the high energy portion that contains the O-H stretching region. The spectrum of gaspad vapor effluent collected on June 25 is compared to a spectrum of normal laboratory room air. The absorbances in the 3500-4000 cm^{-1} region generally result from stretching vibrations in the bonds linking heteroatoms with hydrogen. In the spectra shown here this type of absorbance is limited to water, although alcohols and amines, compounds not found in the effluent vapor, do exhibit strong absorbances in the 3500 cm^{-1} region.

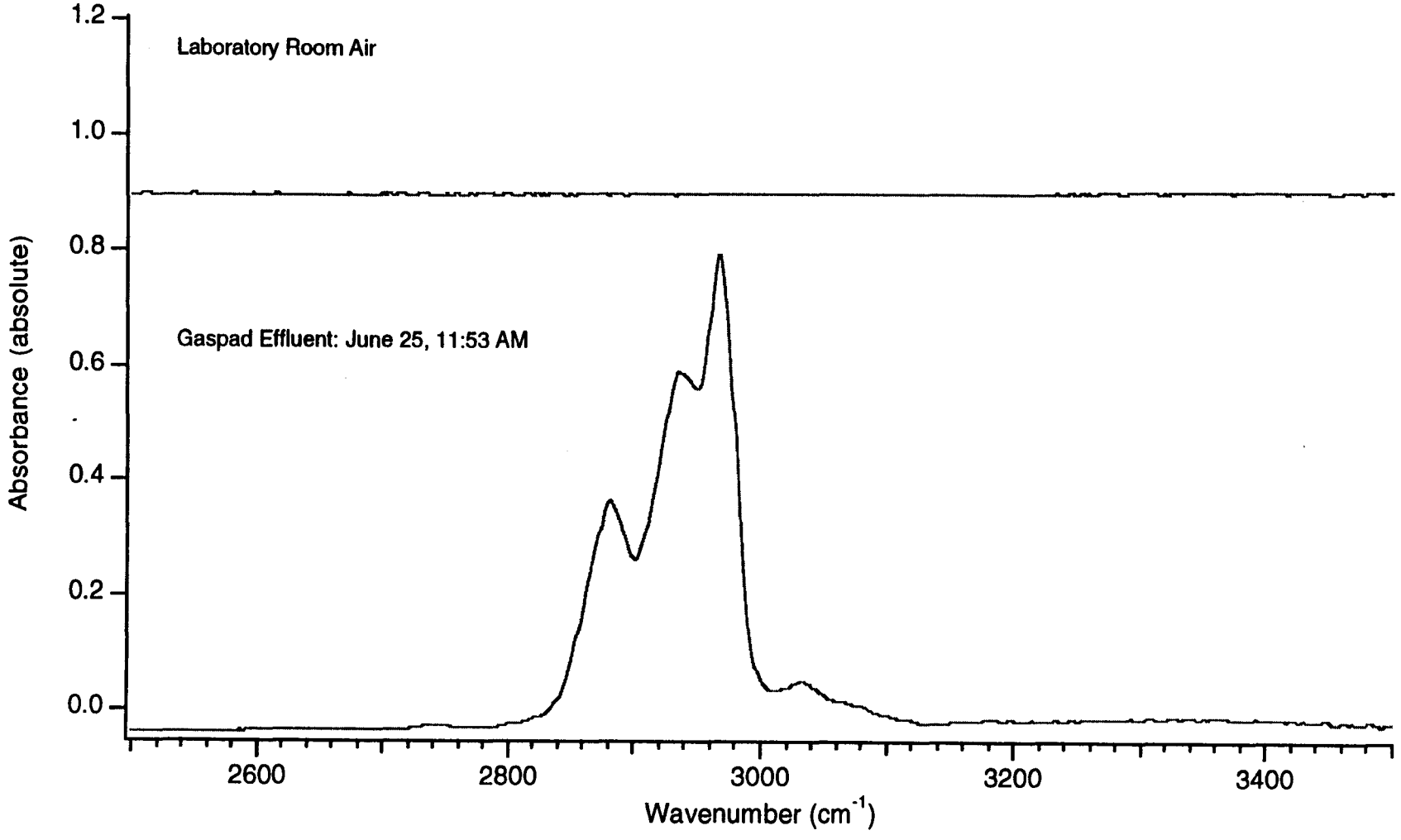

Figure 3.3. The infrared spectra of Figure 3.1 are expanded to show the C-H stretching region. Air does not usually contain compounds that possess C-H bonds so this leaves a clear window to observe the alkyl constituents of gasoline and other petroleum-based hydrocarbons. The three discernible peaks from the gaspad effluent result from overlap of the C-H stretching vibrations of alkyl CH_3 groups (2960 cm^{-1}, out of phase; and 2870 cm^{-1}, in-phase) and CH_2 groups (2925 cm^{-1}, out of phase; and 2850 cm^{-1}, in-phase).

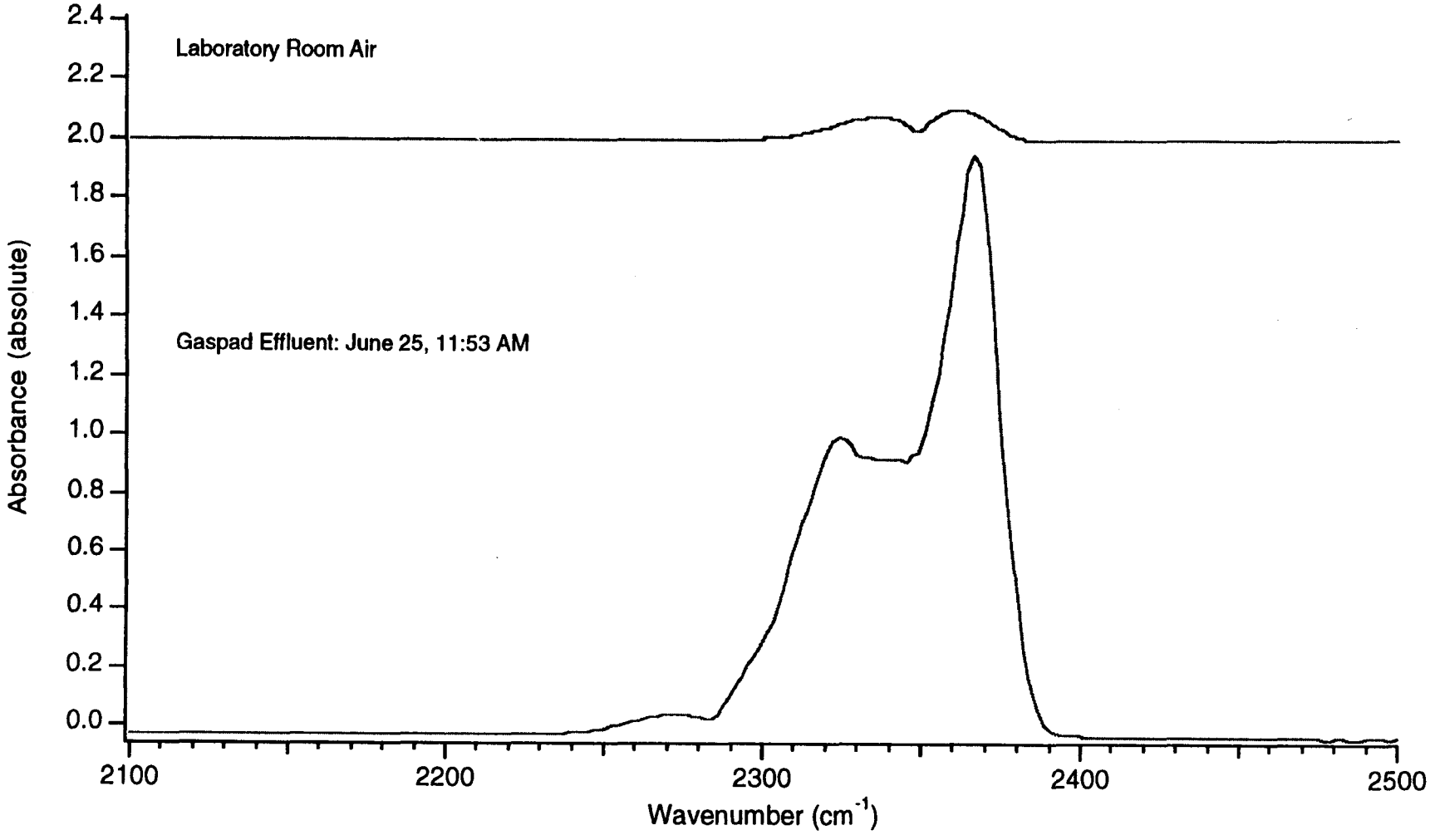

Figure 3.4. The infrared spectra of Figure 3.1 are expanded to show the C-O stretching bands of carbon dioxide. This region of the infrared spectrum is generally limited to vibrational stretching modes of triple bonds and cumulated double bonds (e.g., -N=N=N, -C≡N, and -C≡C-). The lack of symmetry shown in the CO_2 bands of the gaspad effluent may result from collisonally-induced line broadening that often occurs in concentrated gas samples.

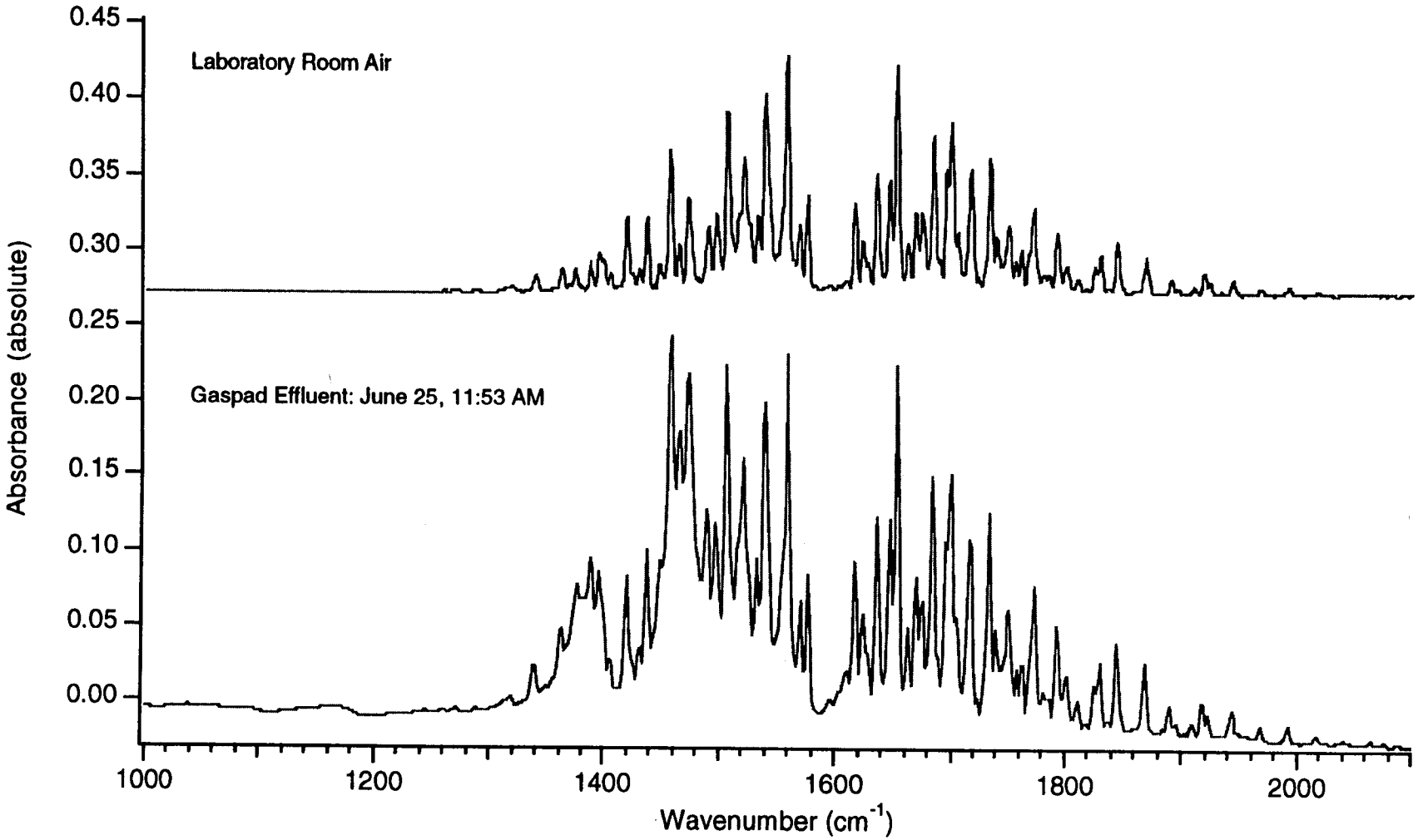

Figure 3.5. This portion of Figure 3.1 shows part of the fingerprint region of the infrared spectrum where a variety of bending and stretching modes appear. In both the air and effluent spectra shown, the multiple band structure of water is the dominant feature. However, in the gaspad spectrum there are two enhanced regions, 1380 and 1465 cm^{-1}, that are common absorbances for several C-H bending modes of both CH_3 and CH_2 groups of alkanes. The higher energy portion of the water manifold extending from 1600 to 2000 cm^{-1} is not normally occupied by gasoline-based compounds so integration of these bands represents a plausible way to measure the concentration of water in the effluent vapor.

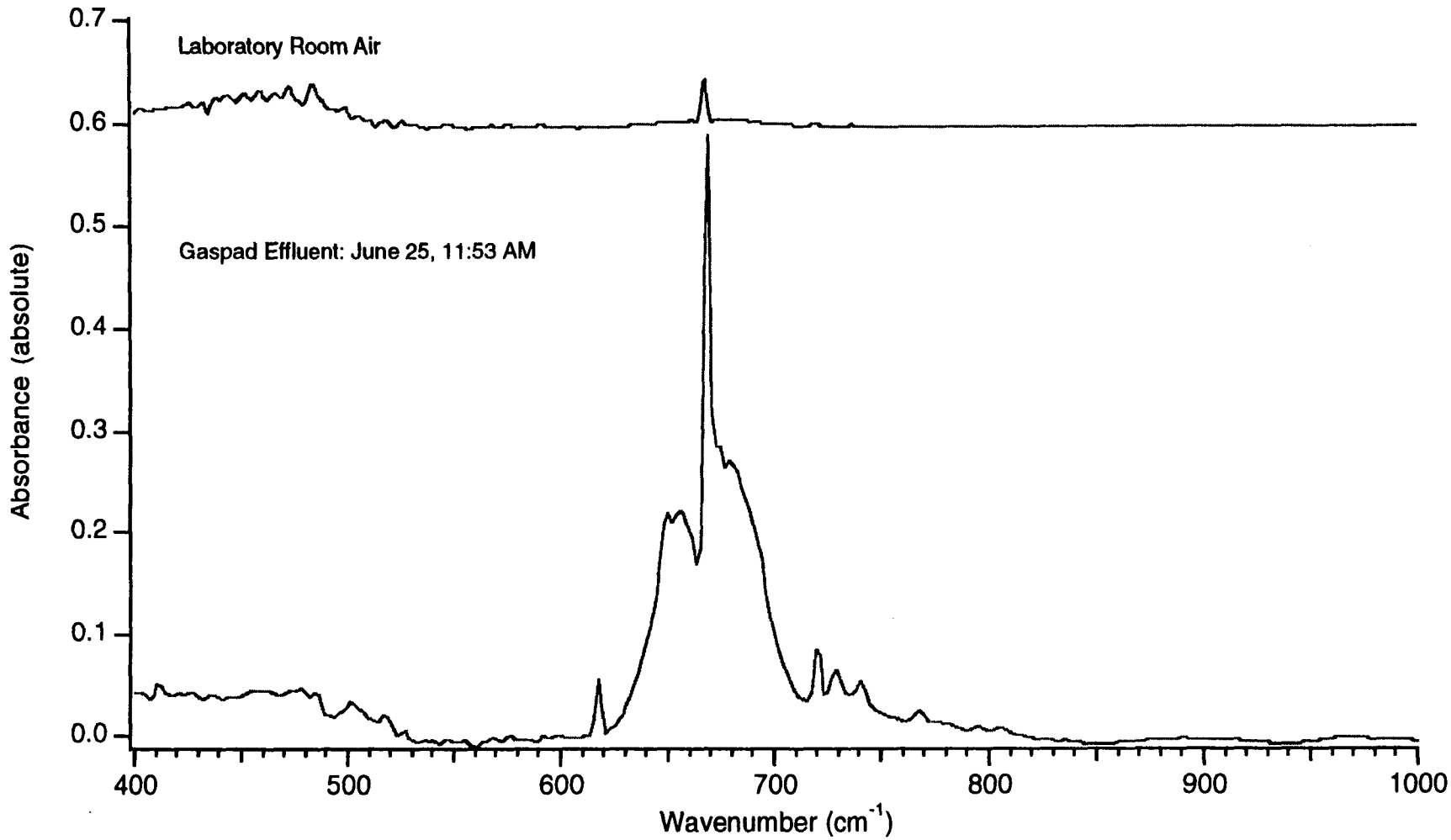

Figure 3.6. This portion of Figure 3.1 shows the lowest energy region of the infrared spectrum where a variety of bending modes appear. Aromatic compounds have weak absorbances in this region that are characteristic of their substitution pattern . In the spectra shown, the predominate feature of the effluent stream vapor is the absorbance that results from the fundamental CO_2 bending vibration at 667 cm^{-1}.

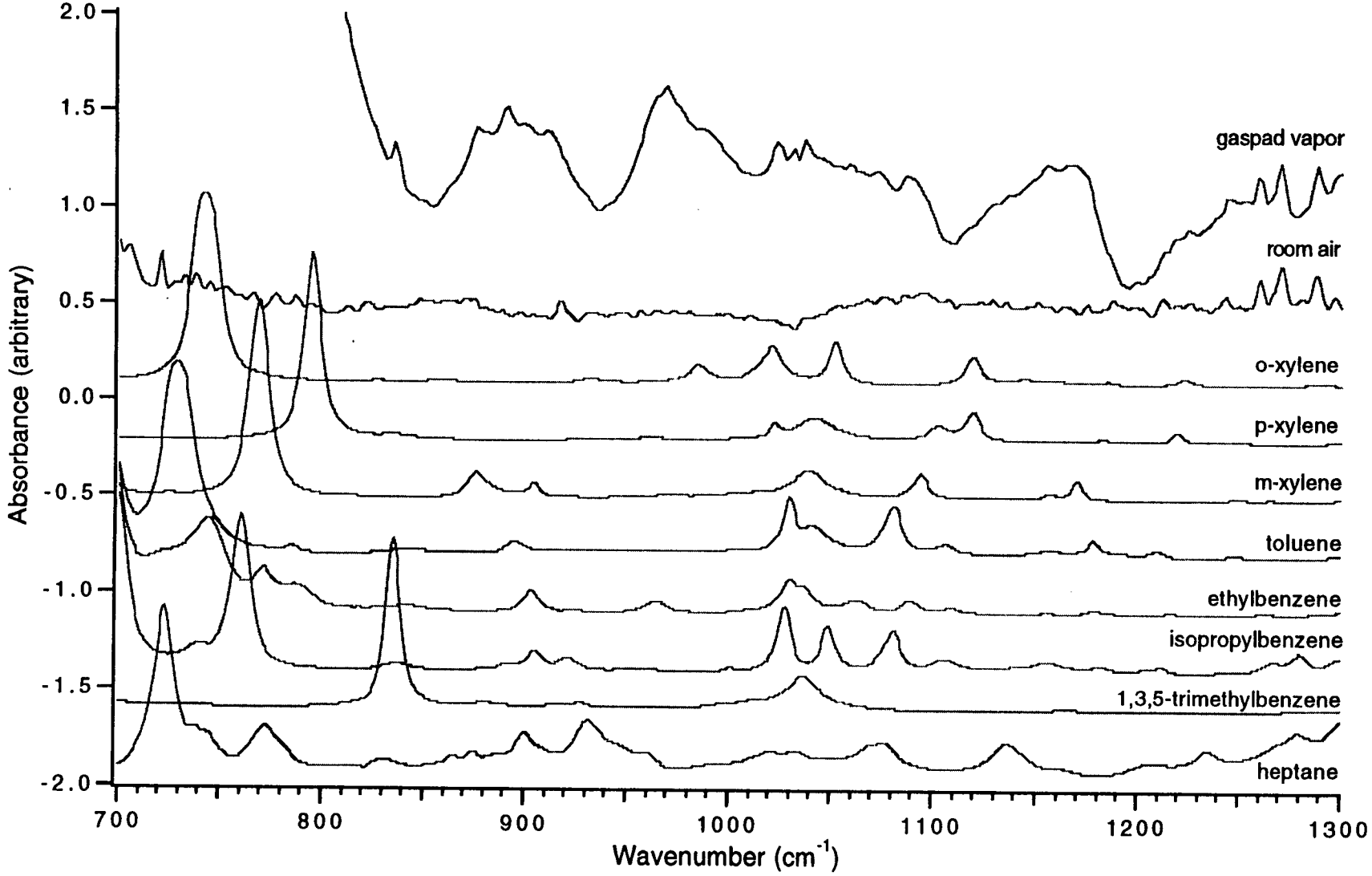

Figure 4. Comparison of the vapor effluent in the fingerprint region with library reference compounds. The absorptivity of the effluent vapor spectrum is so low that it was magnified in this figure to show its spectral characteristics. The reference spectra are displayed at arbitrary intensities so that comparisons can be made more easily.

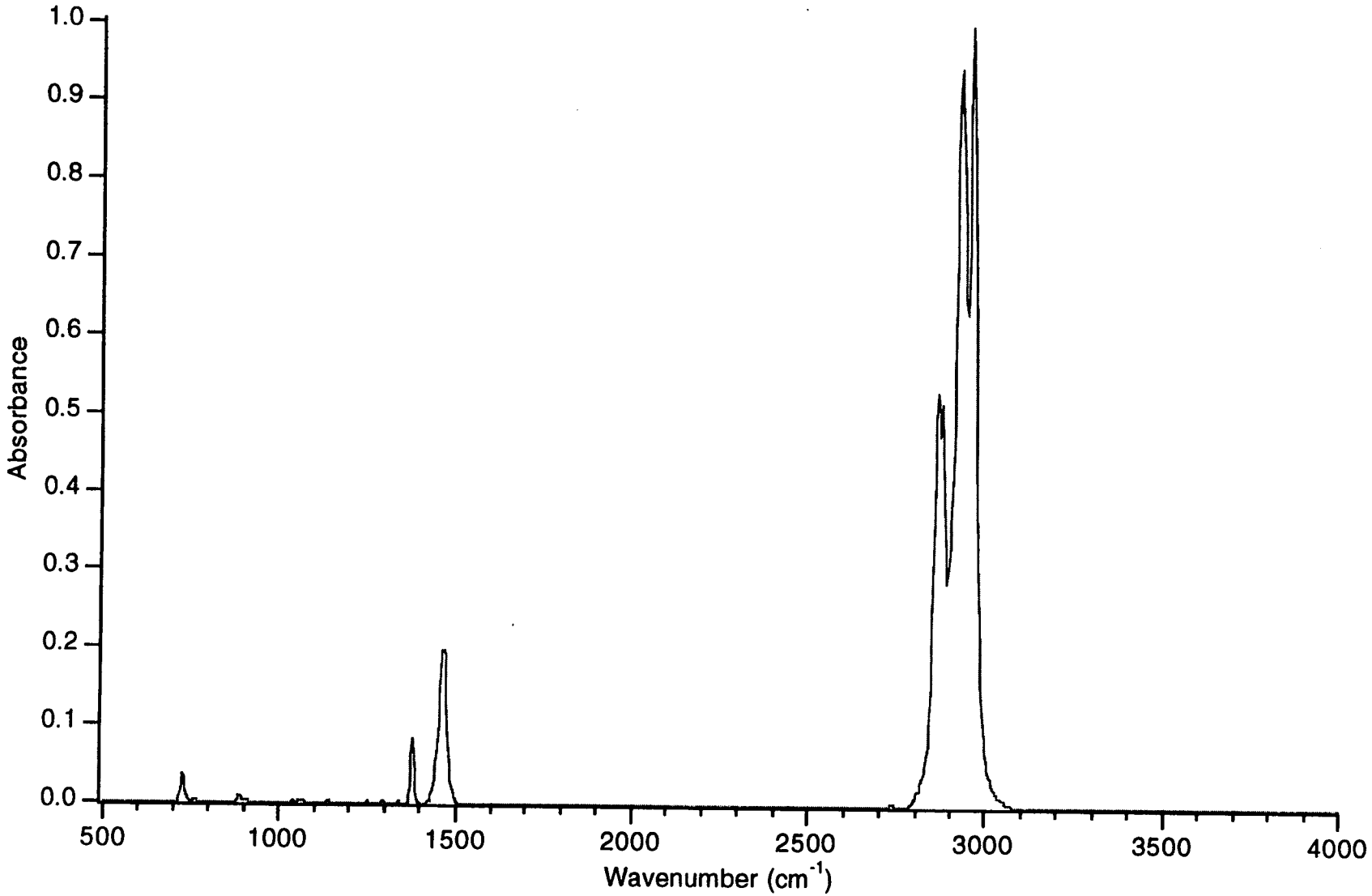

Figure 5.1.1. Infrared spectrum of liquid hexane at 4 cm^{-1} resolution. Hexane is a typical alkane and exhibits a relatively simple spectrum. A comparison of the infrared spectra for the homologous alkane series of C5 to C8 compounds indicates that infrared spectroscopy cannot easily be used to differentiate these alkane components in a mixture.

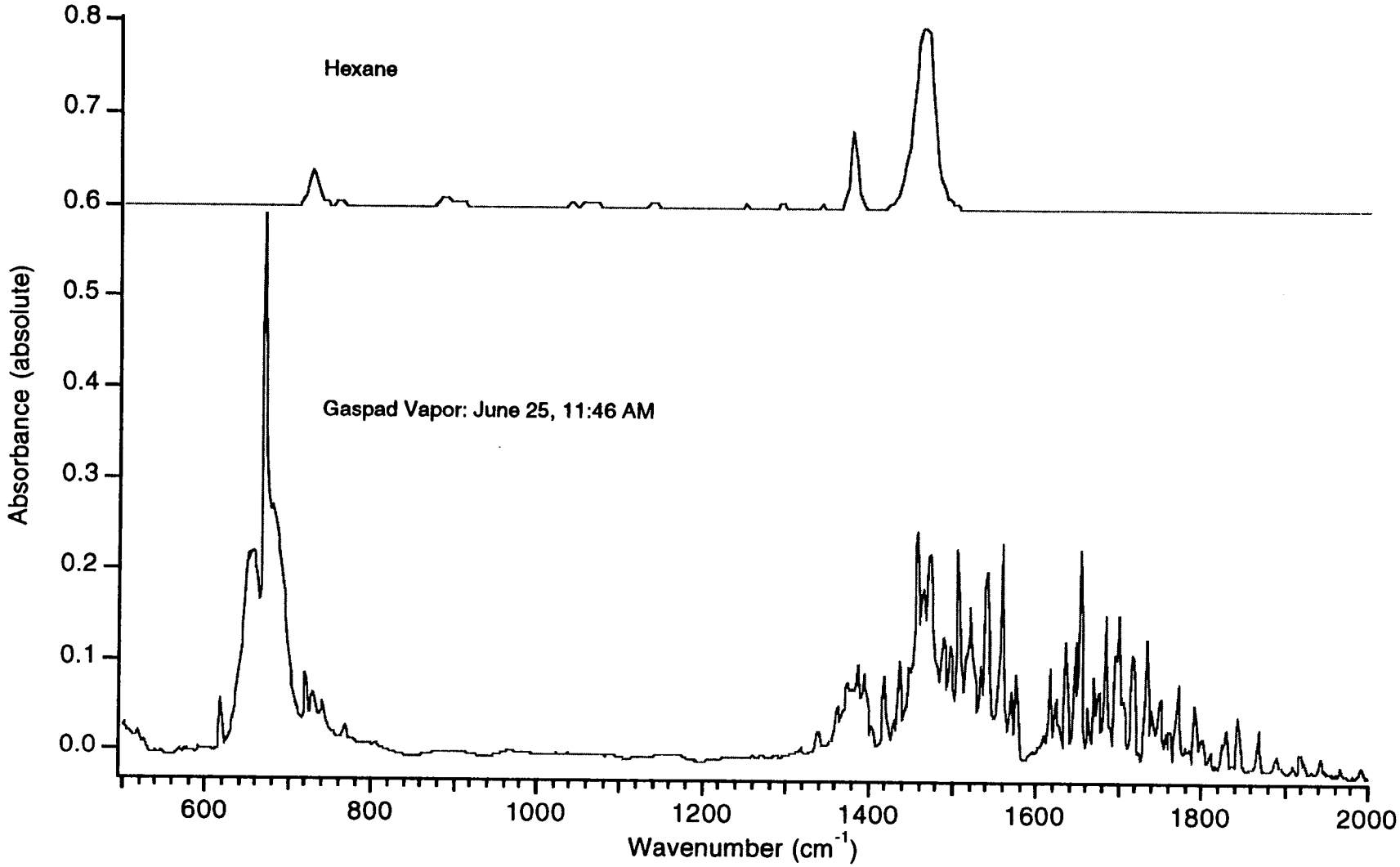

Figure 5.1.2. The infrared fingerprint region of liquid hexane and the gaspad vapor effluent is shown. The alkane C-H bending absorbances in this region are noticeably less intense than the C-H stretching vibrations centered around 2950 cm^{-1}. The most prominent feature of the gaspad effluent in this region is the CO_2 bending mode at 667 cm^{-1}. Unless noted otherwise, the spectra for each compound in this series are expanded only in the energy dimension so that the absorbance intensities remain proportionate.

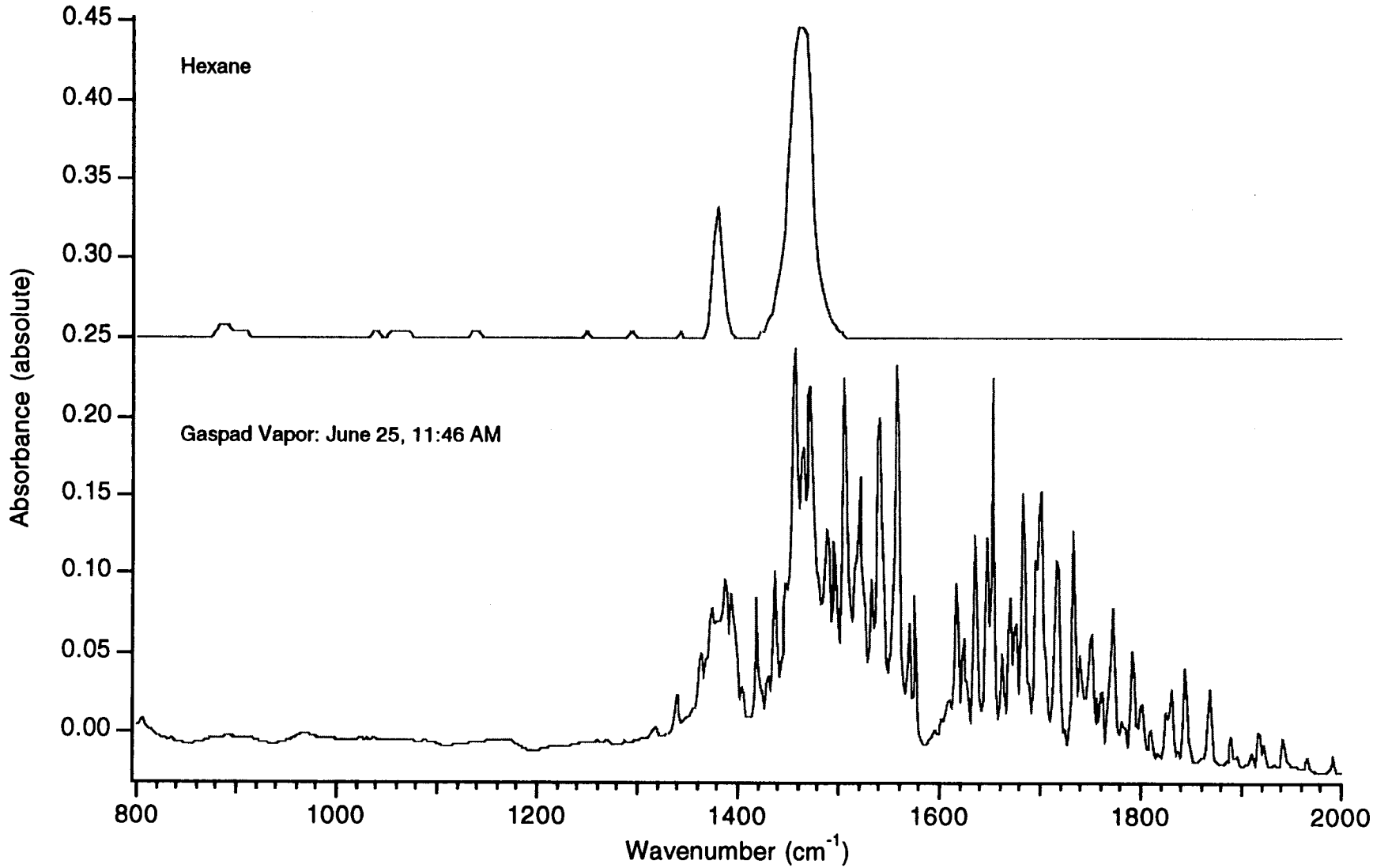

Figure 5.1.3. The view of the fingerprint region of liquid hexane and the gaspad vapor effluent is expanded to more clearly show the contribution of the C-H bending absorbances within the water envelop.

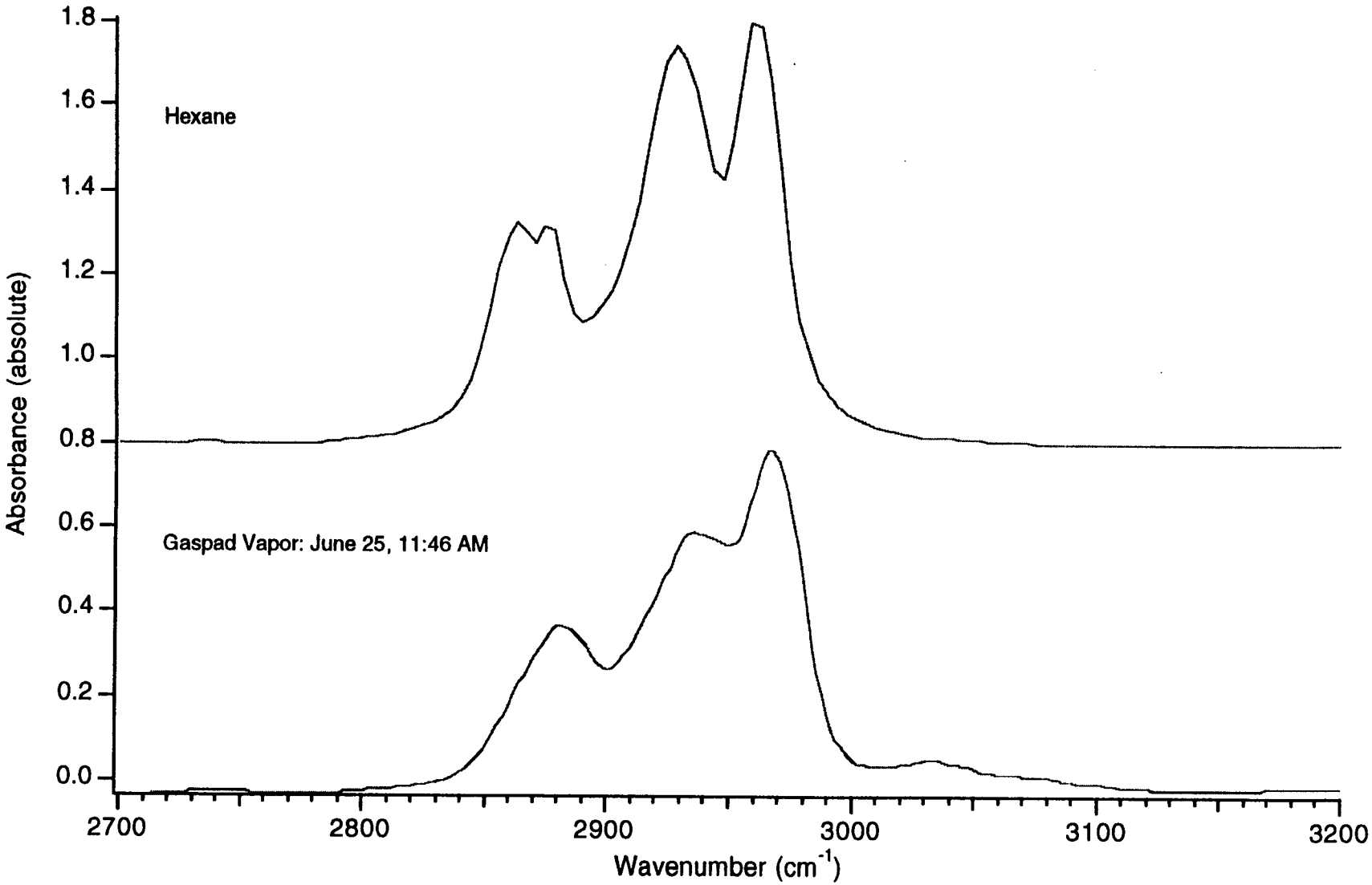

Figure 5.1.4. A magnified view of the C-H stretching region of liquid hexane and the gaspad vapor effluent. The hump at 3300 cm^{-1} may be indicative of aromatic components in the gaspad effluent.

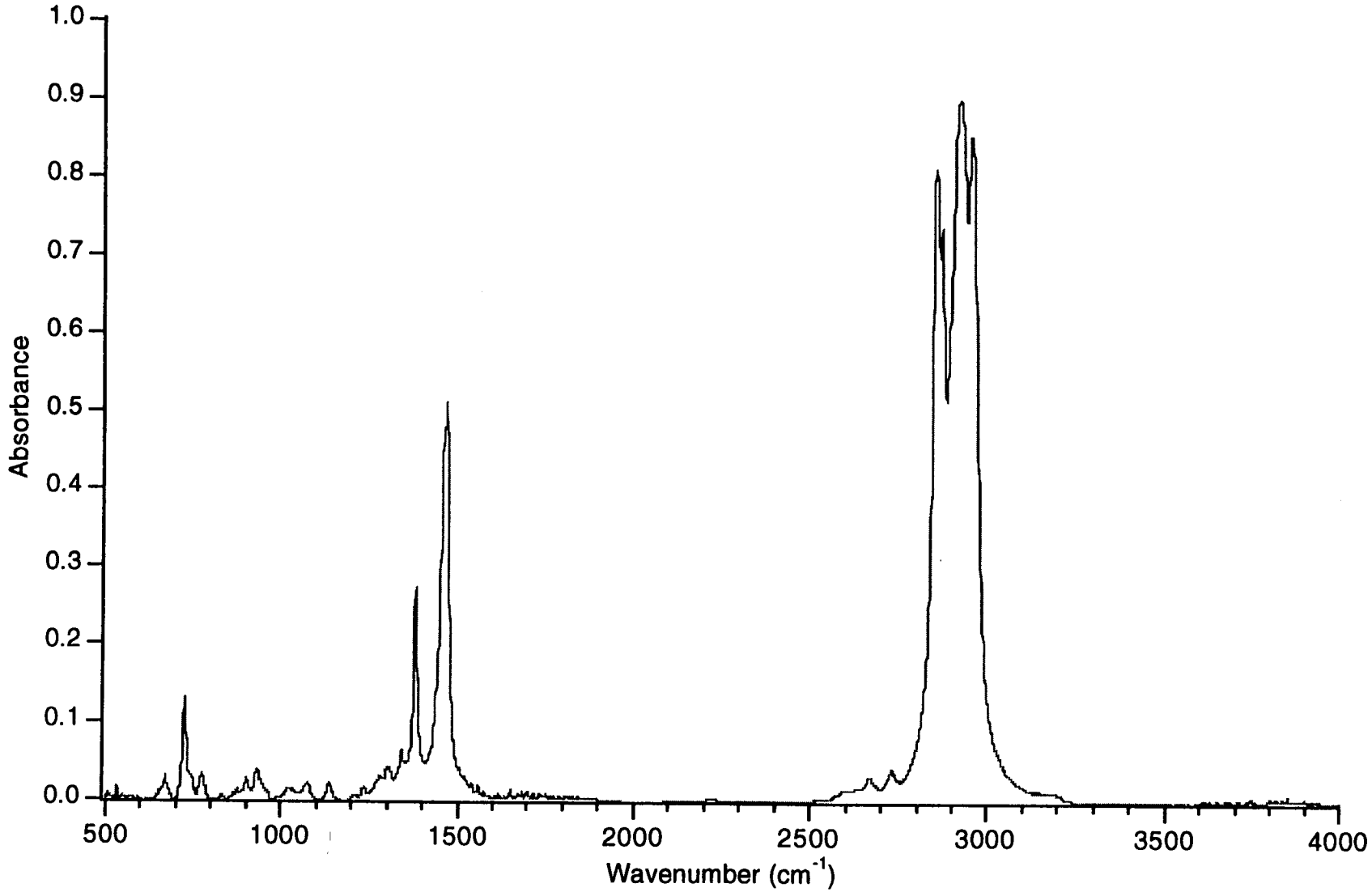

Figure 5.2.1. Infrared spectrum of liquid heptane at 4 cm^{-1} resolution. Note the similarity to the spectrum of hexane.

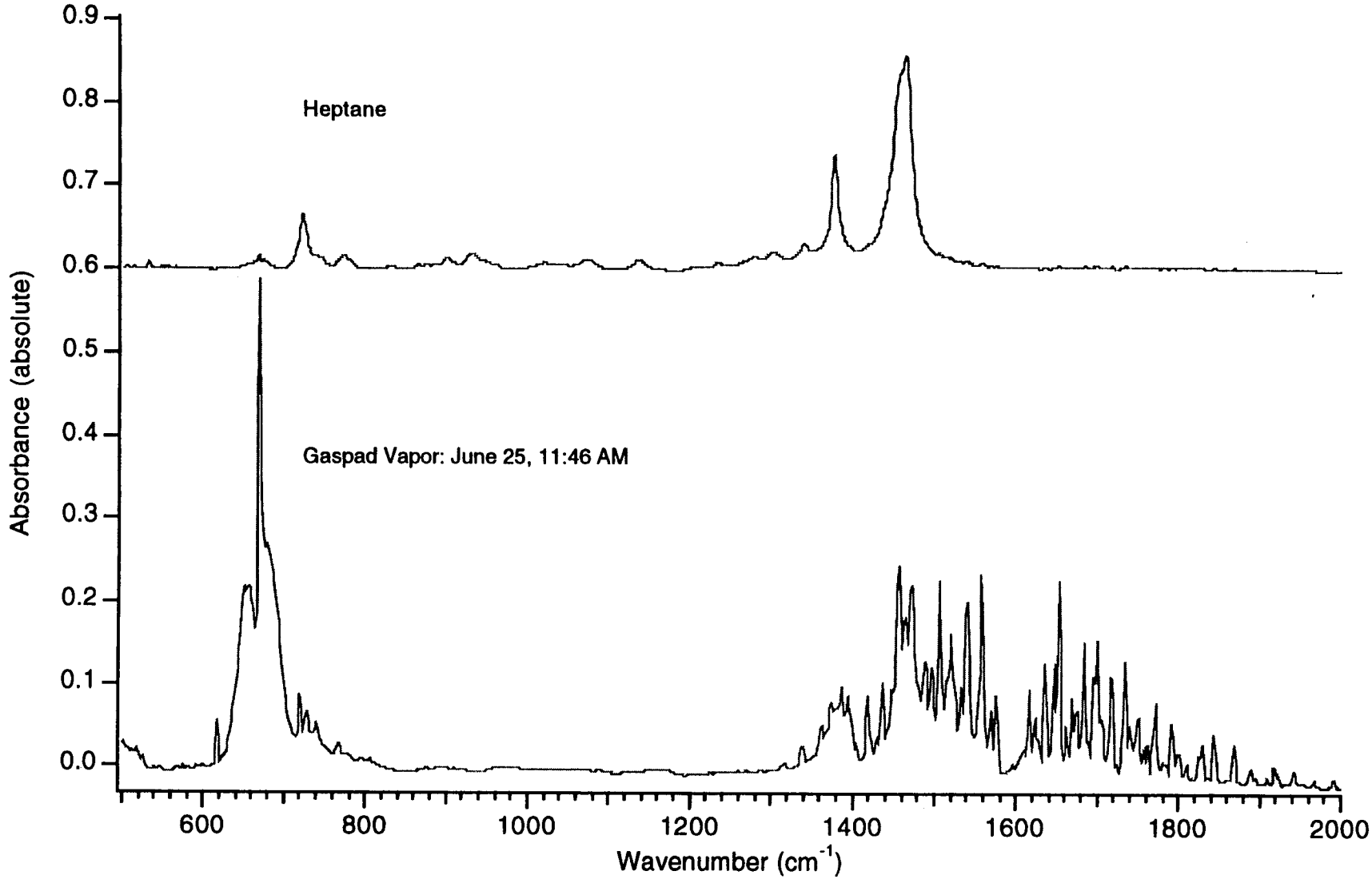

Figure 5.2.2. A view of the infrared fingerprint region of liquid heptane and the gaspad vapor effluent.

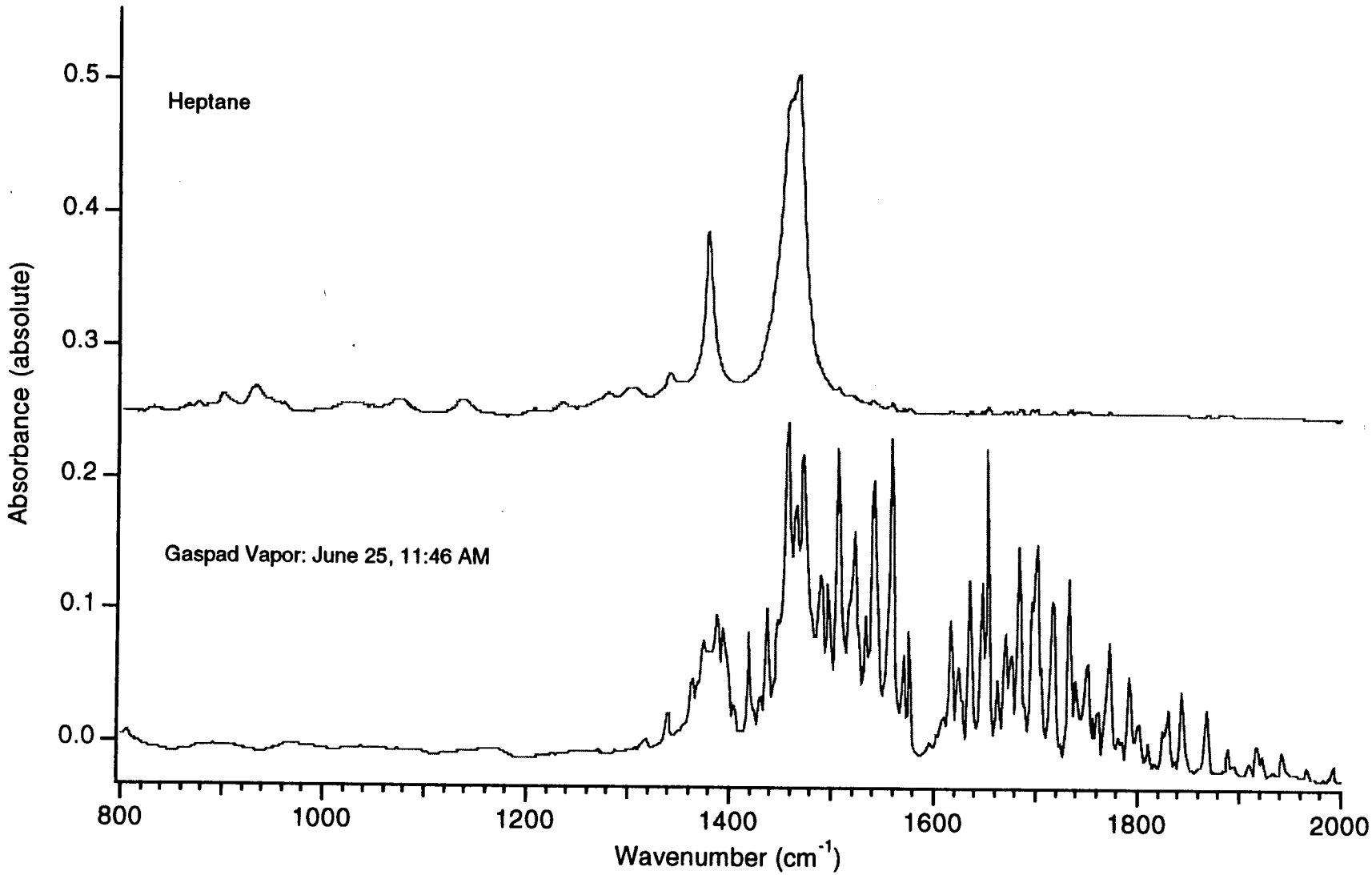

Figure 5.2.3 An expanded view of the fingerprint region to show overlap of C-H modes of heptane with the water enveloped of the gaspad vapor.

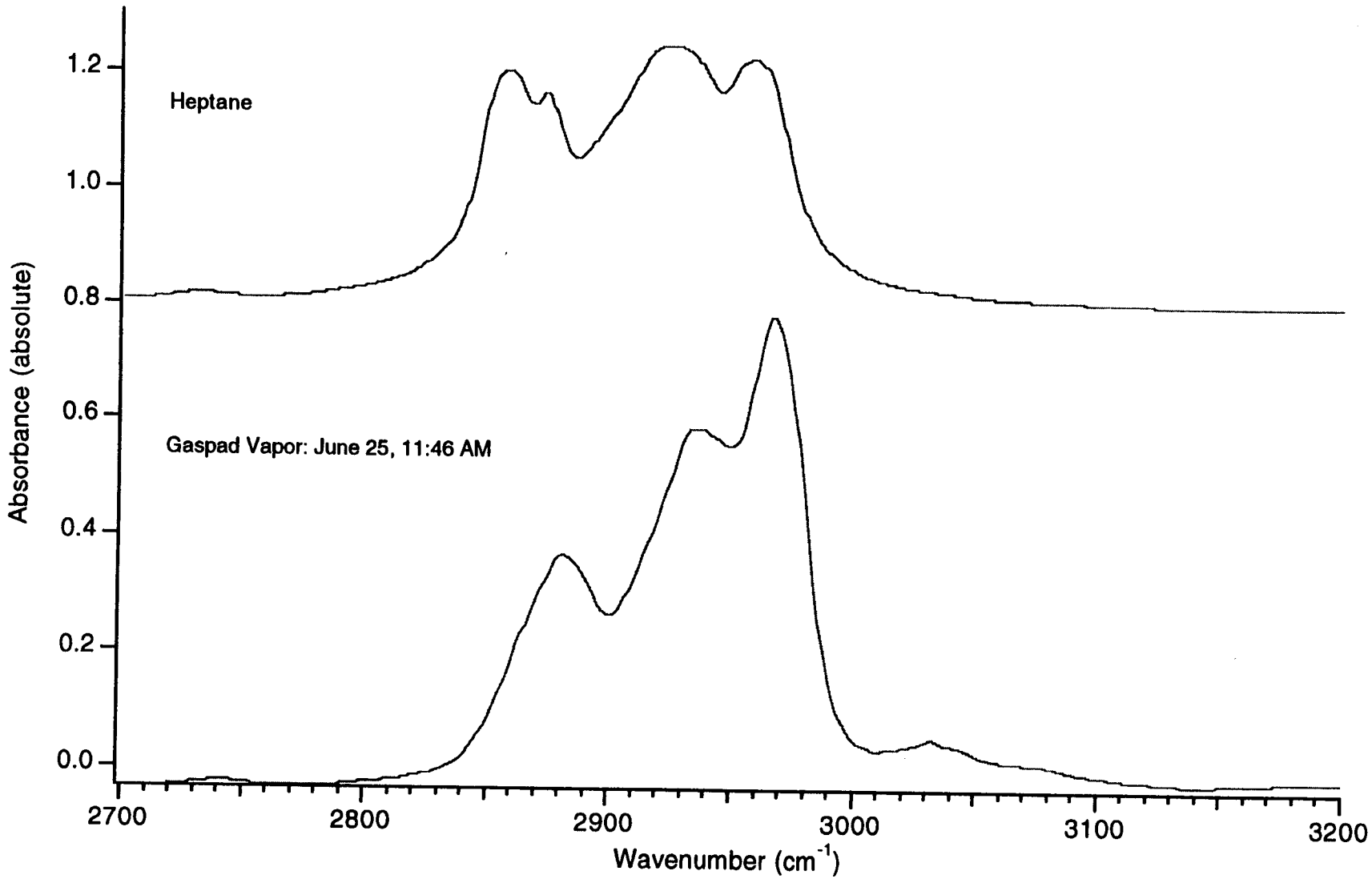

Figure 5.2.4. A magnified view of the C-H stretching region of liquid heptane and the gaspad vapor effluent.

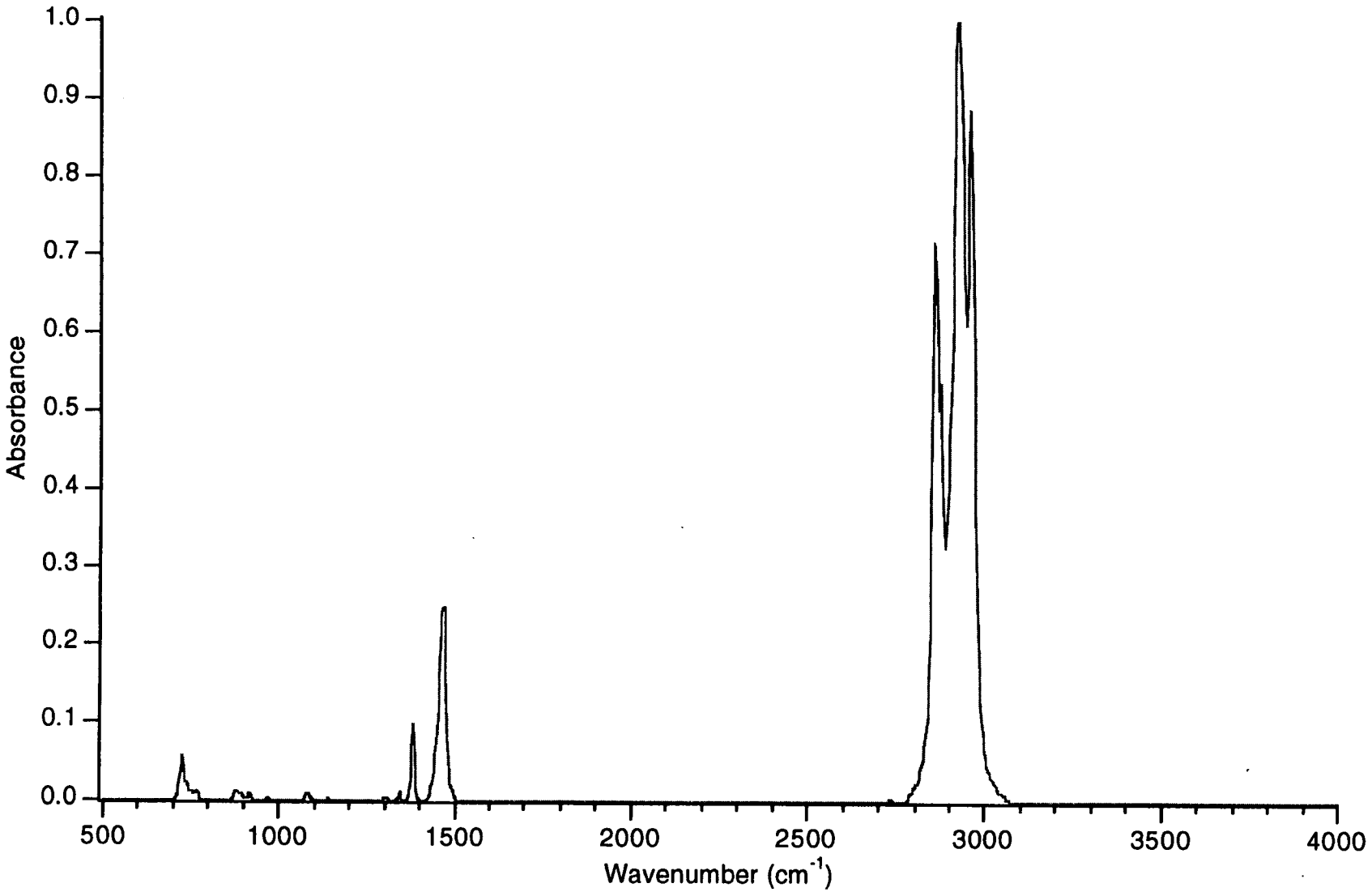

Figure 5.3.1. Infrared spectrum of liquid octane at 4 cm^{-1} resolution. Note the similarity of this spectrum to those of hexane and heptane.

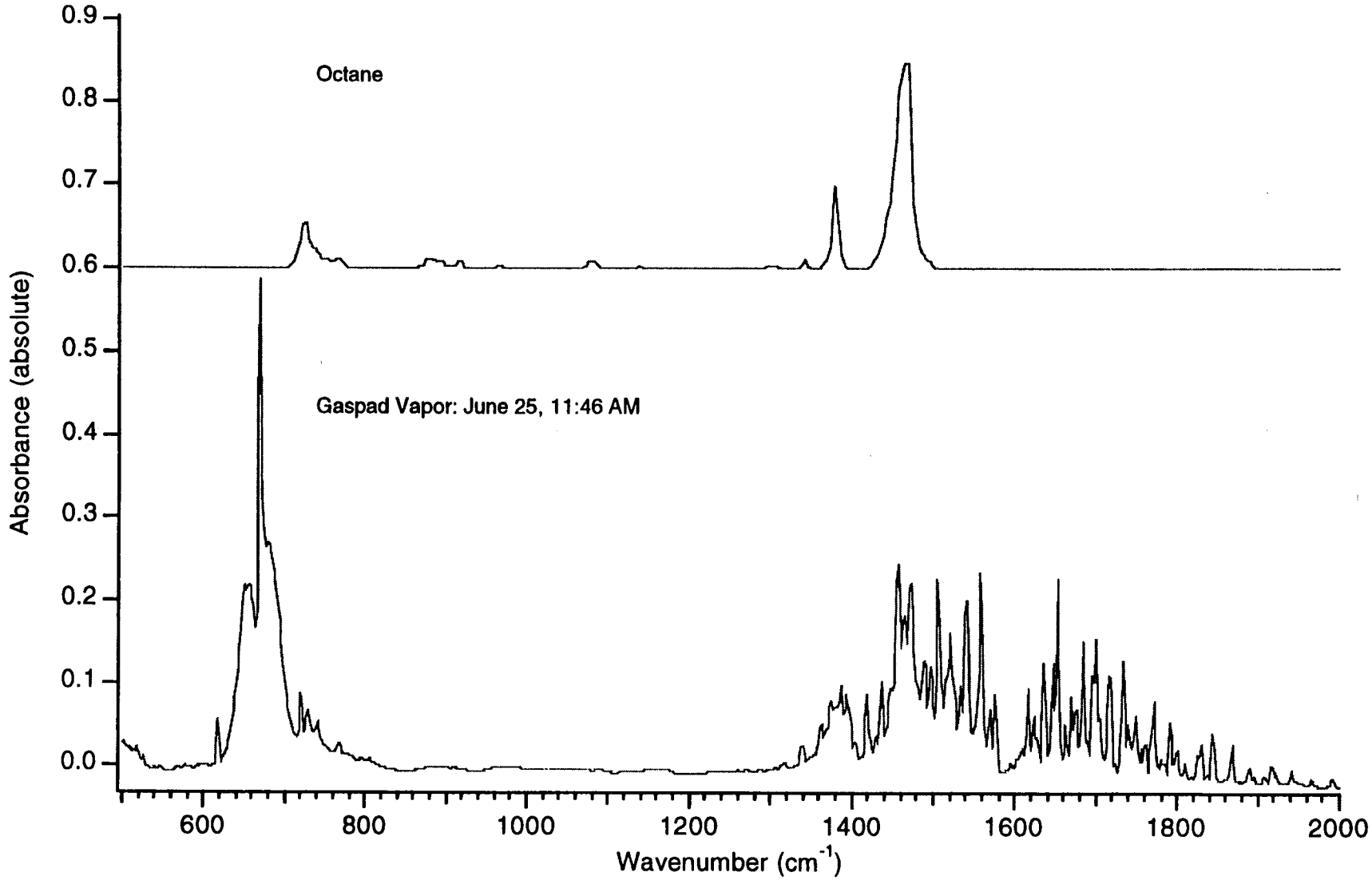

Figure 5.3.2. A view of the infrared fingerprint region of liquid octane and the gaspad vapor effluent.

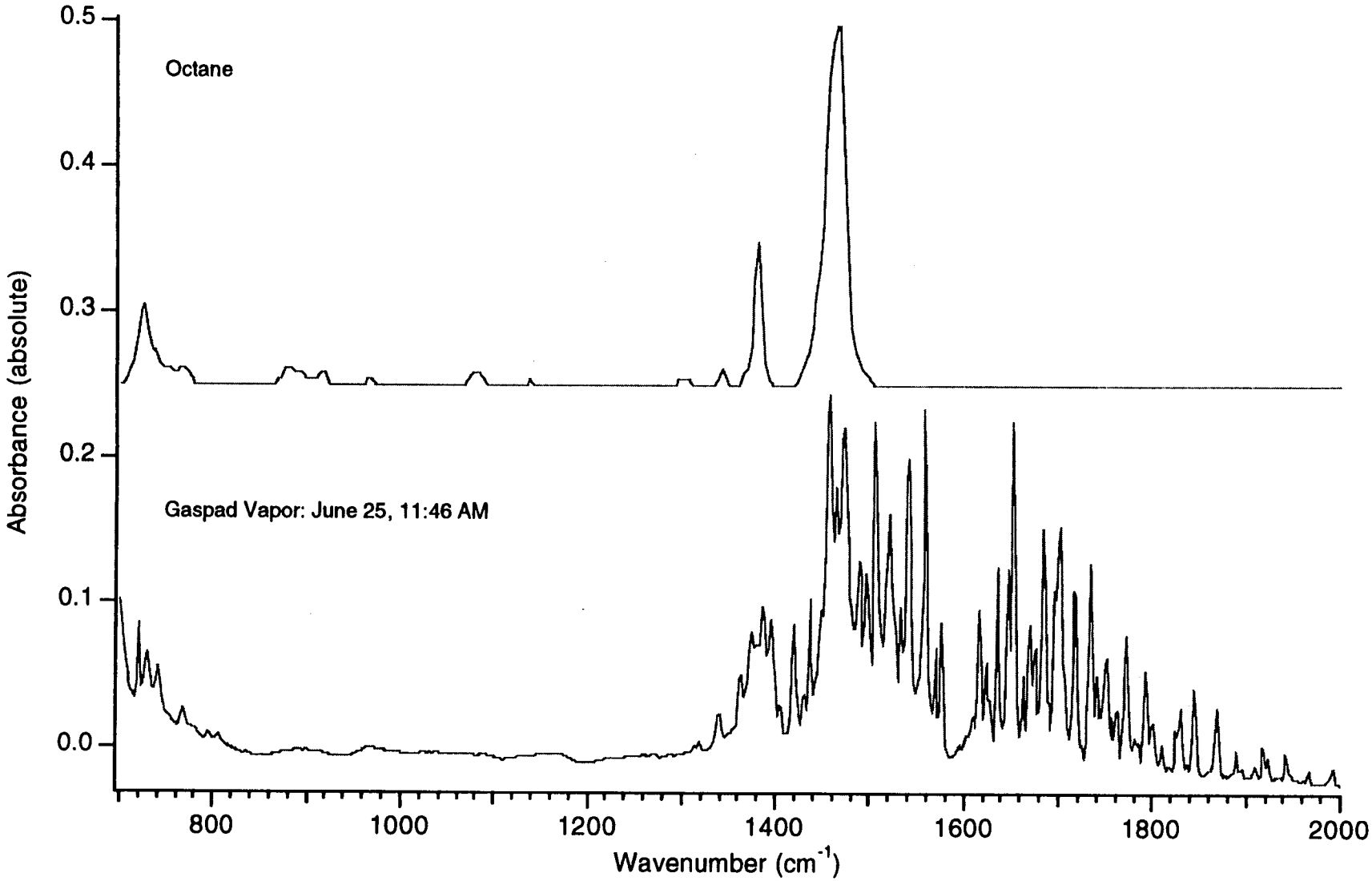

Figure 5.3.3 An expanded view of the fingerprint region to show overlap of C-H modes of octane within the water envelope of the gaspad vapor.

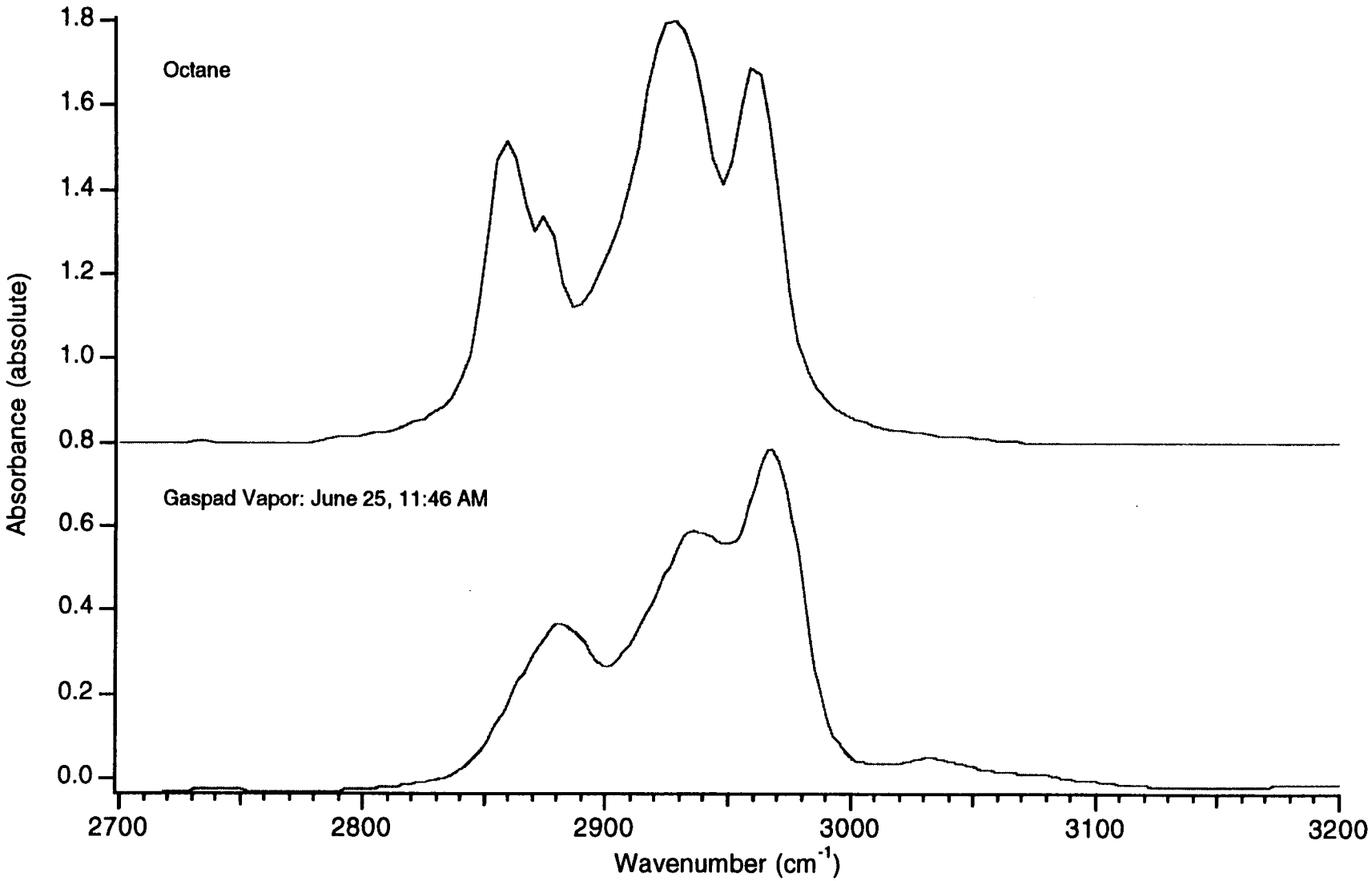

Figure 5.3.4. The region of the C-H stretching modes is expanded to show the similarities between octane and the gaspad vapor.

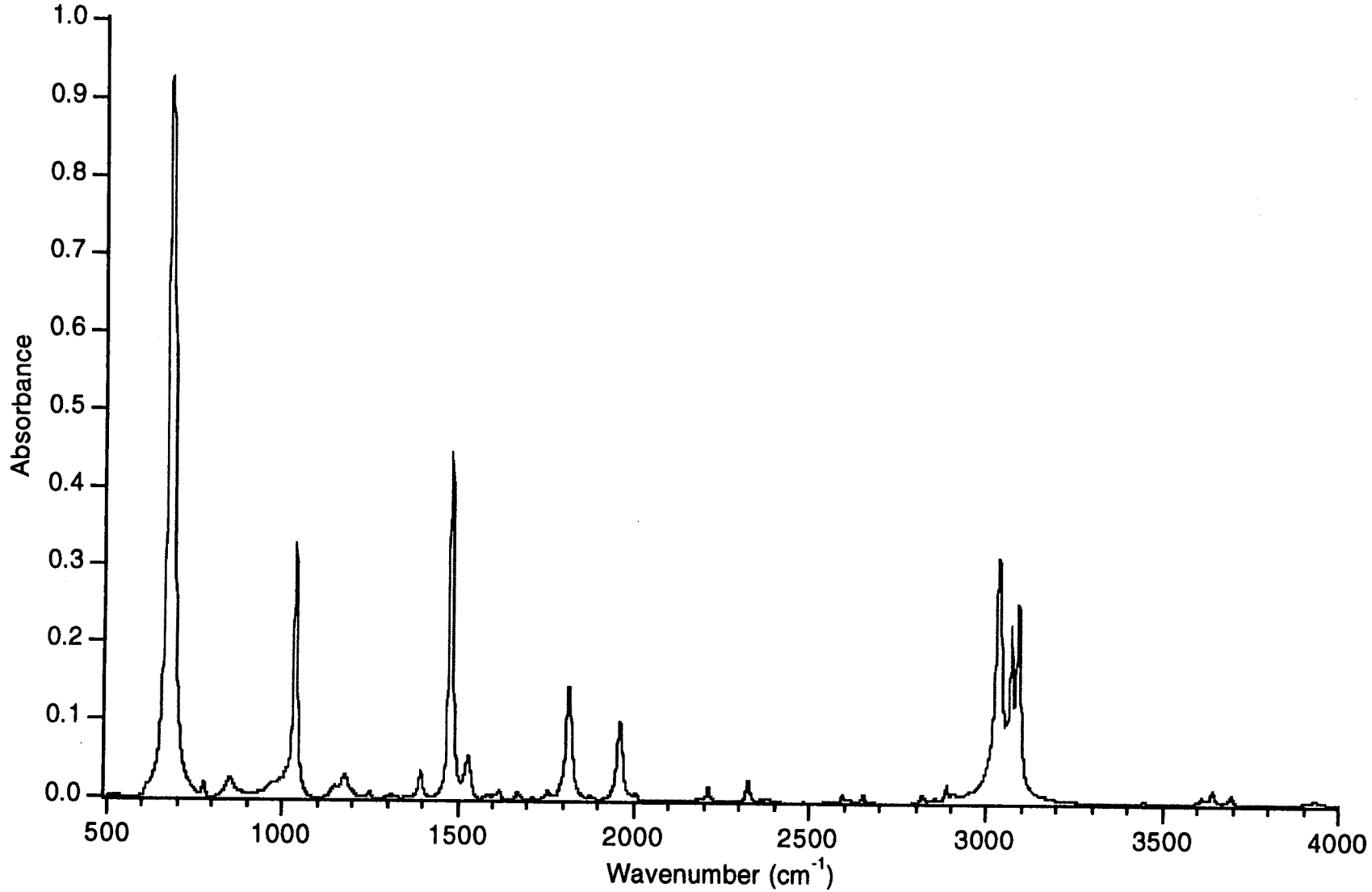

Figure 5.5.1. Infrared spectrum of liquid benzene collected at 4 cm^{-1} resolution.

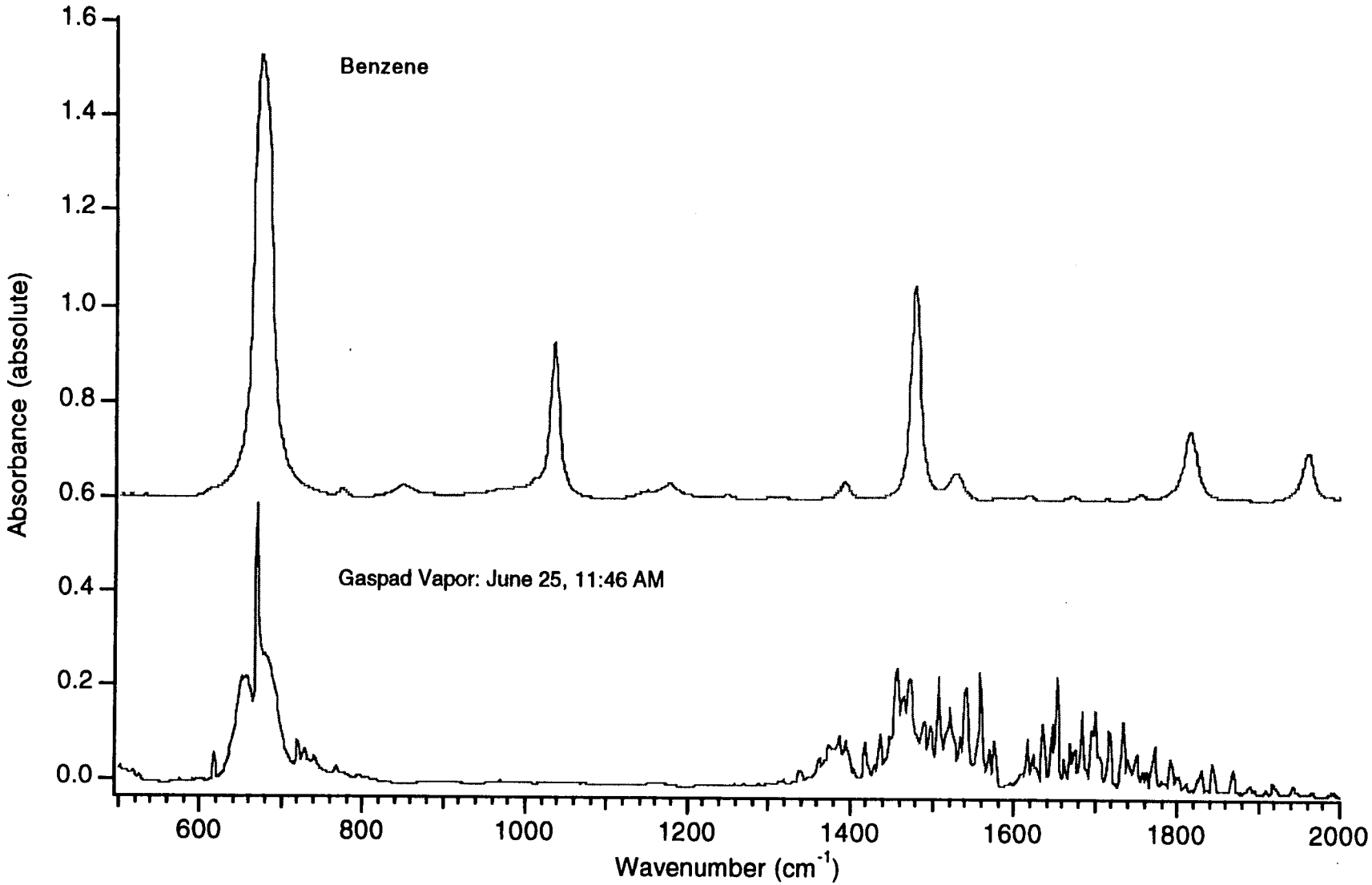

Figure 5.5.2. An expand view of the infrared spectra shows the fingerprint region of liquid benzene and the gaspad vapor effluent. Note that there is a clear spectral window between 800 and 1300 cm^{-1} that can be monitored to detect benzene.

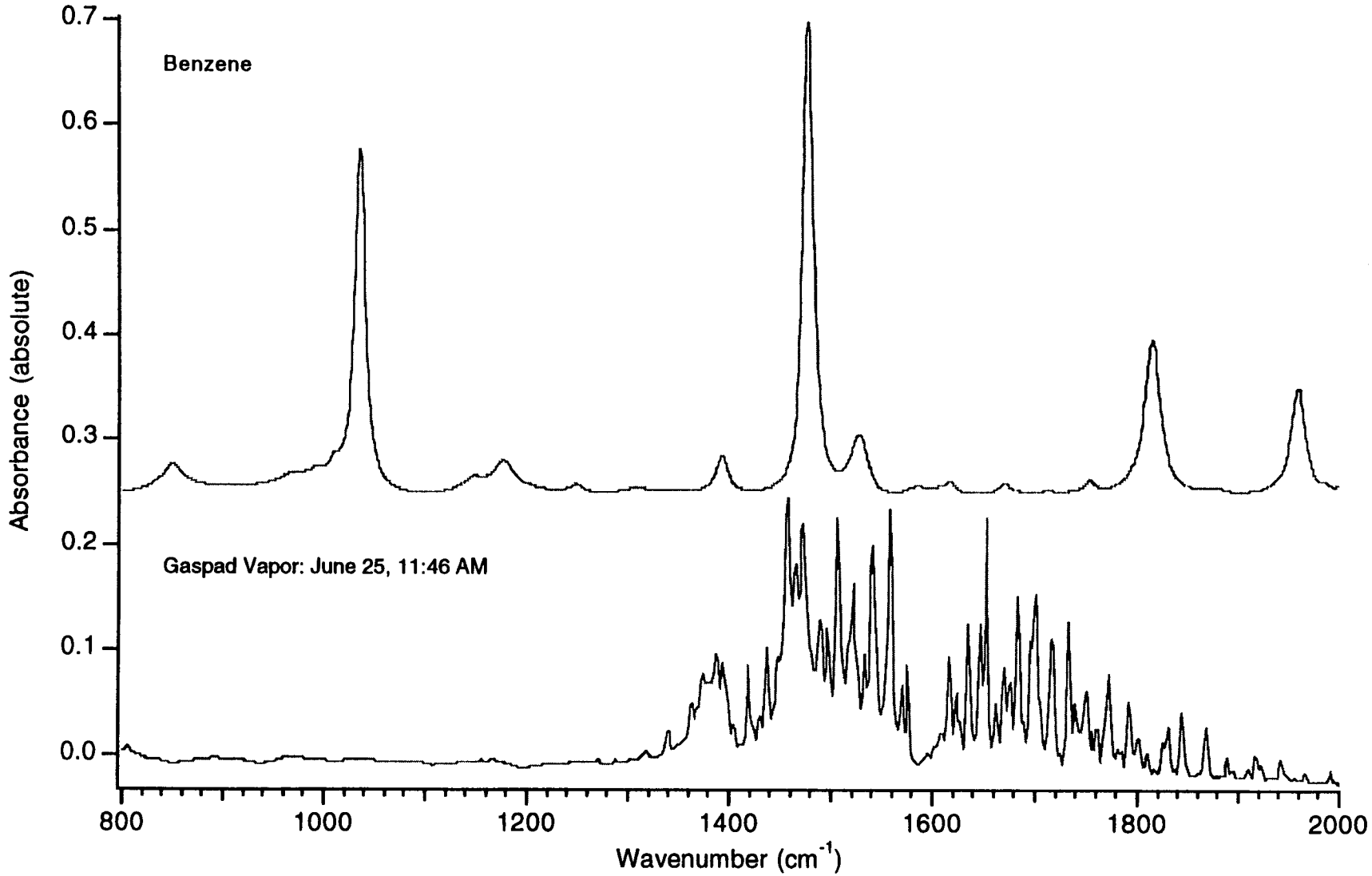

Figure 5.5.3. Expanded view of the fingerprint region of liquid benzene and the gaspad vapor effluent. Some benzene absorbances appear in uncluttered portions of the vapor spectra to enable benzene detection.

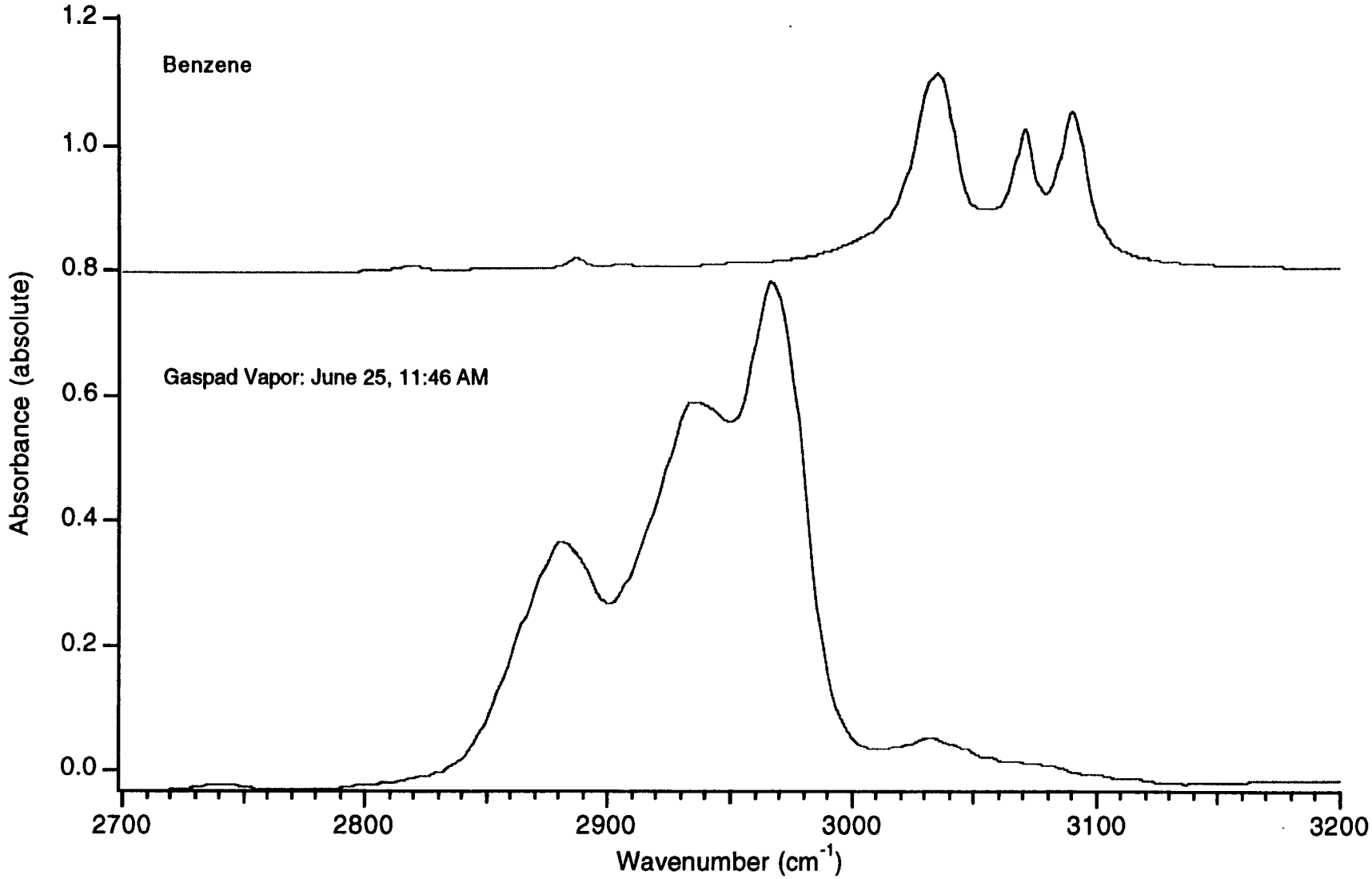

Figure 5.5.4. A magnified view of the C-H stretching region of liquid benzene and the gaspad vapor effluent. The aromatic stretching bands of the C-H absorbances are higher energy vibrations than those related to the alkanes and appear as distinct absorbances.

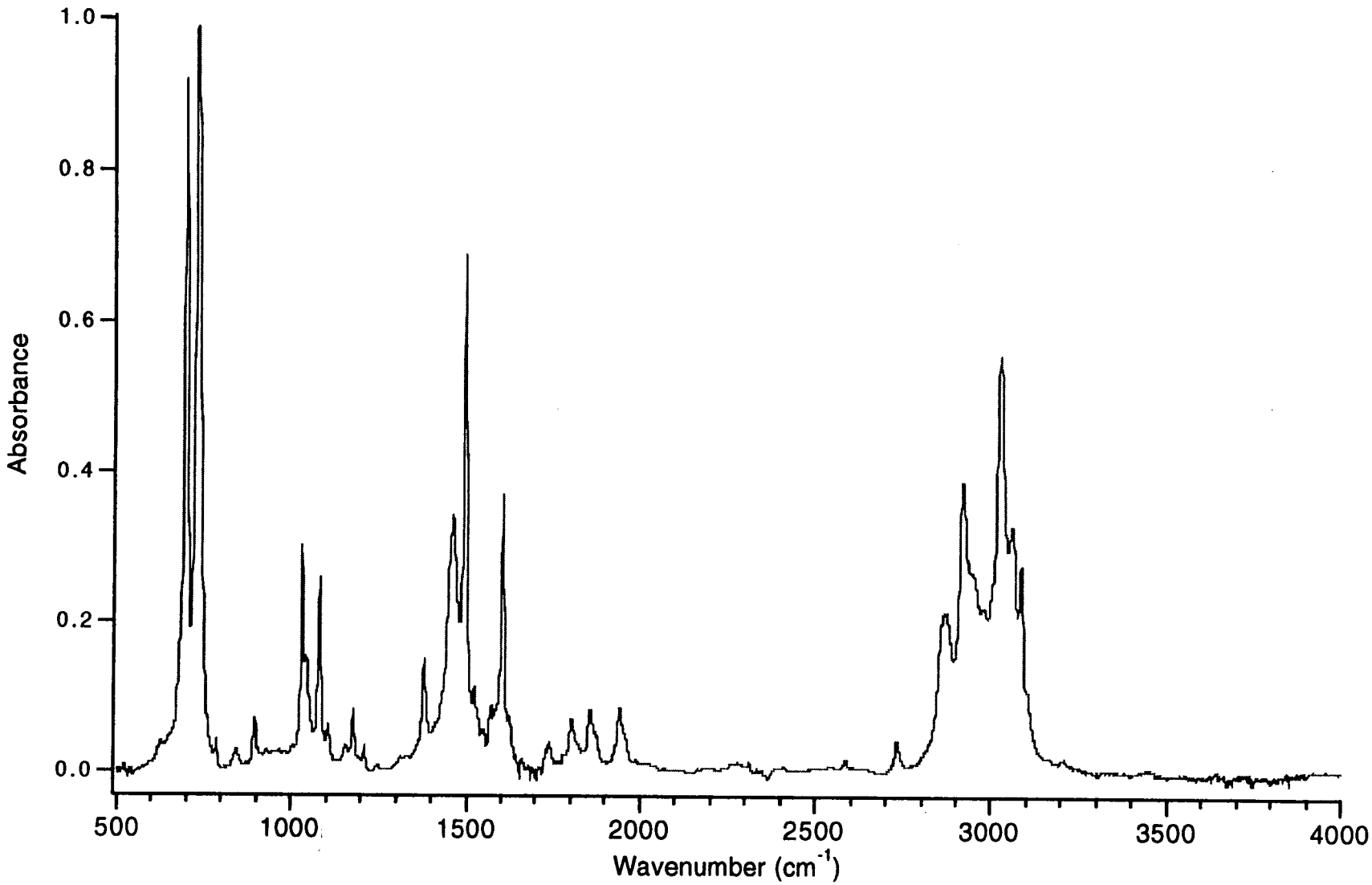

Figure 5.6.1. Infrared spectrum of liquid toluene collected at 4 cm^{-1} resolution. The aromatic ring bending modes are the strongest features of aromatic compounds.

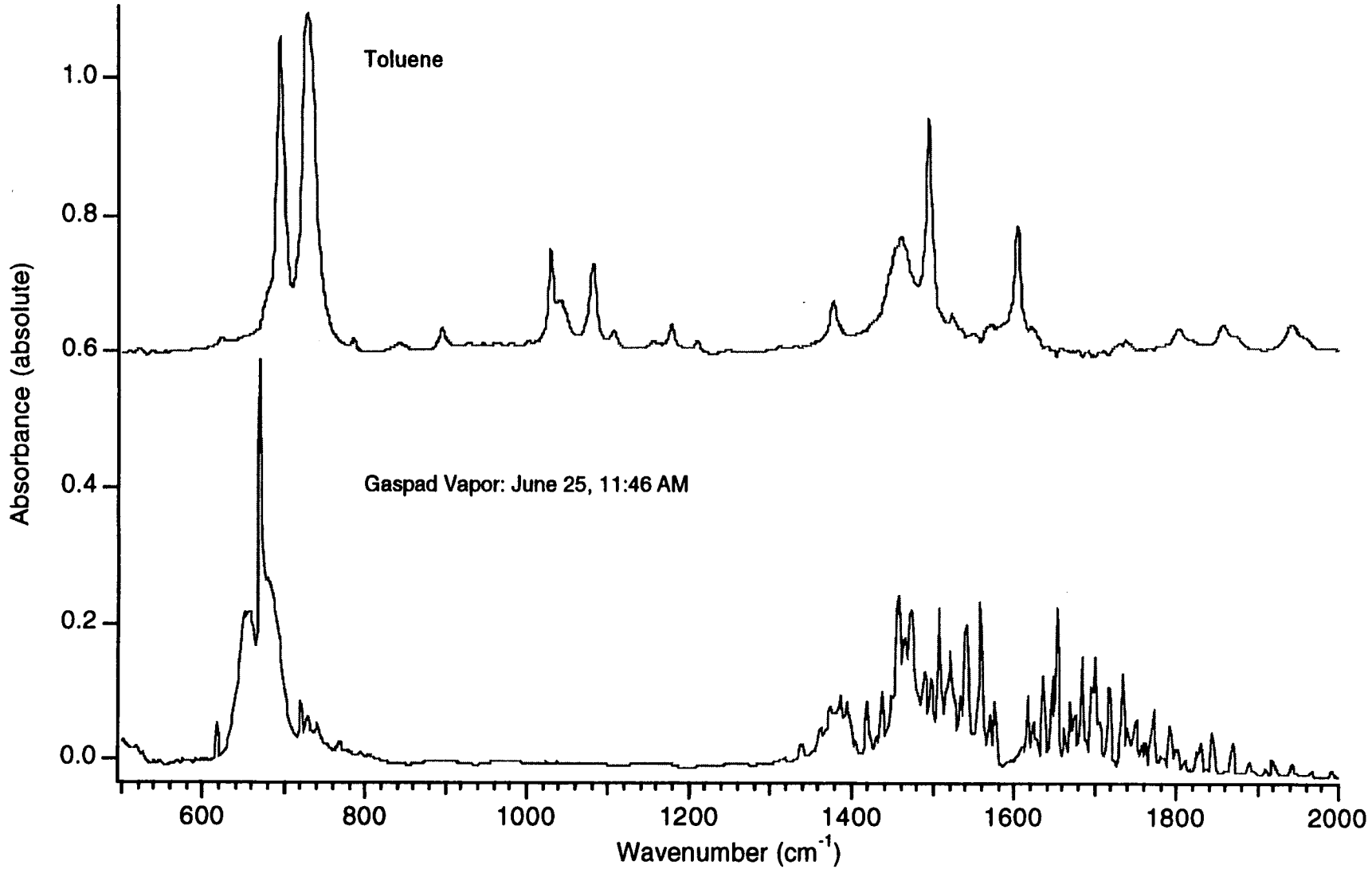

Figure 5.6.2. The fingerprint region of the spectra shows the strong ring C-H bending modes characteristic of toluene at 695 and 730 cm-1. Unfortunately, CO_2 overwhelms this region in the gaspad vapor spectrum.

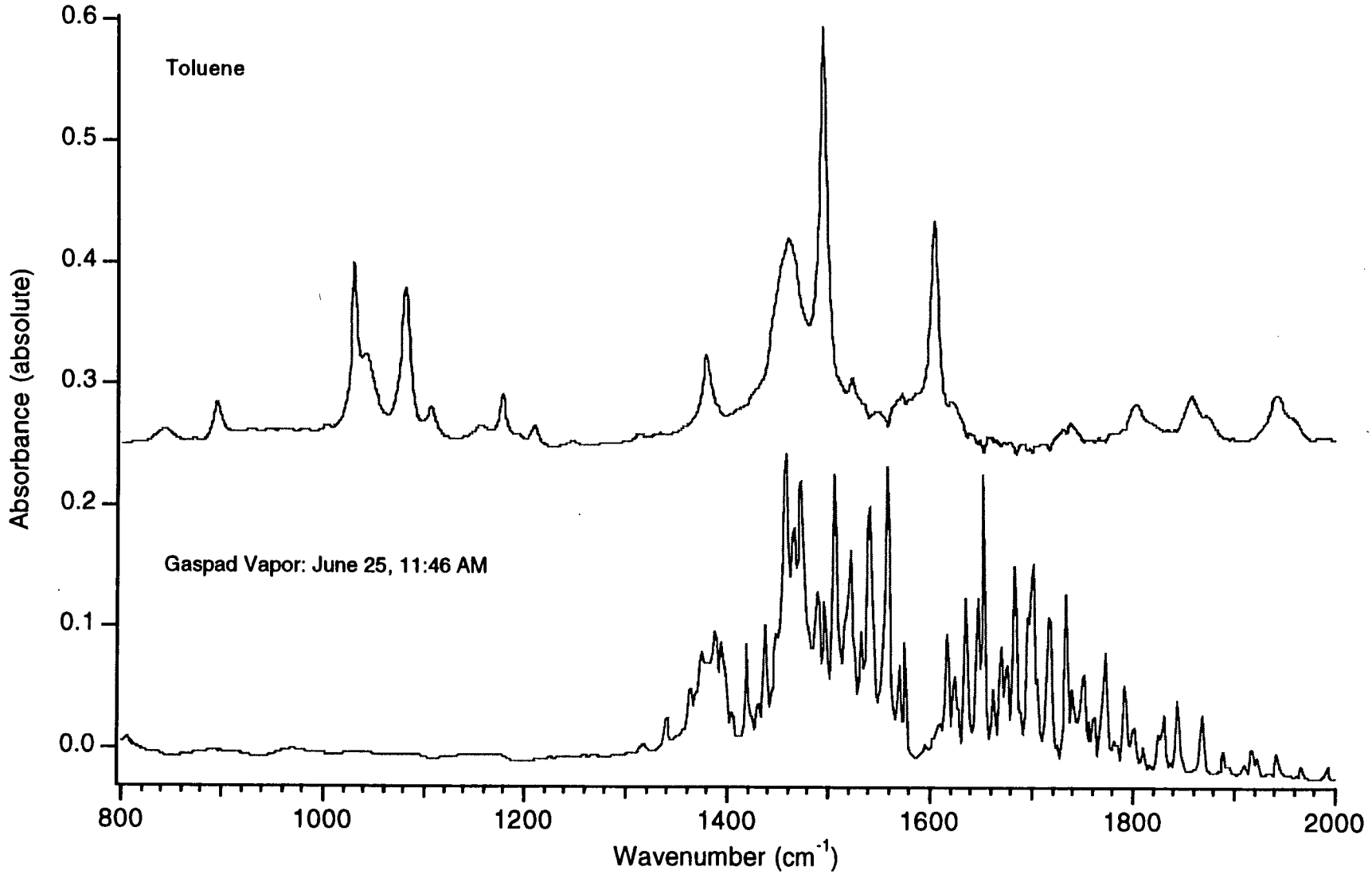

Figure 5.6.3. Expanded view of the fingerprint region of liquid toluene and the gaspad vapor effluent. Some aromatic toluene vibrations have absorbances in the window of the gaspad spectra. The characteristic alkane C-H bending modes of toluene's methyl group are evident at 1385 and 1440 cm-1.

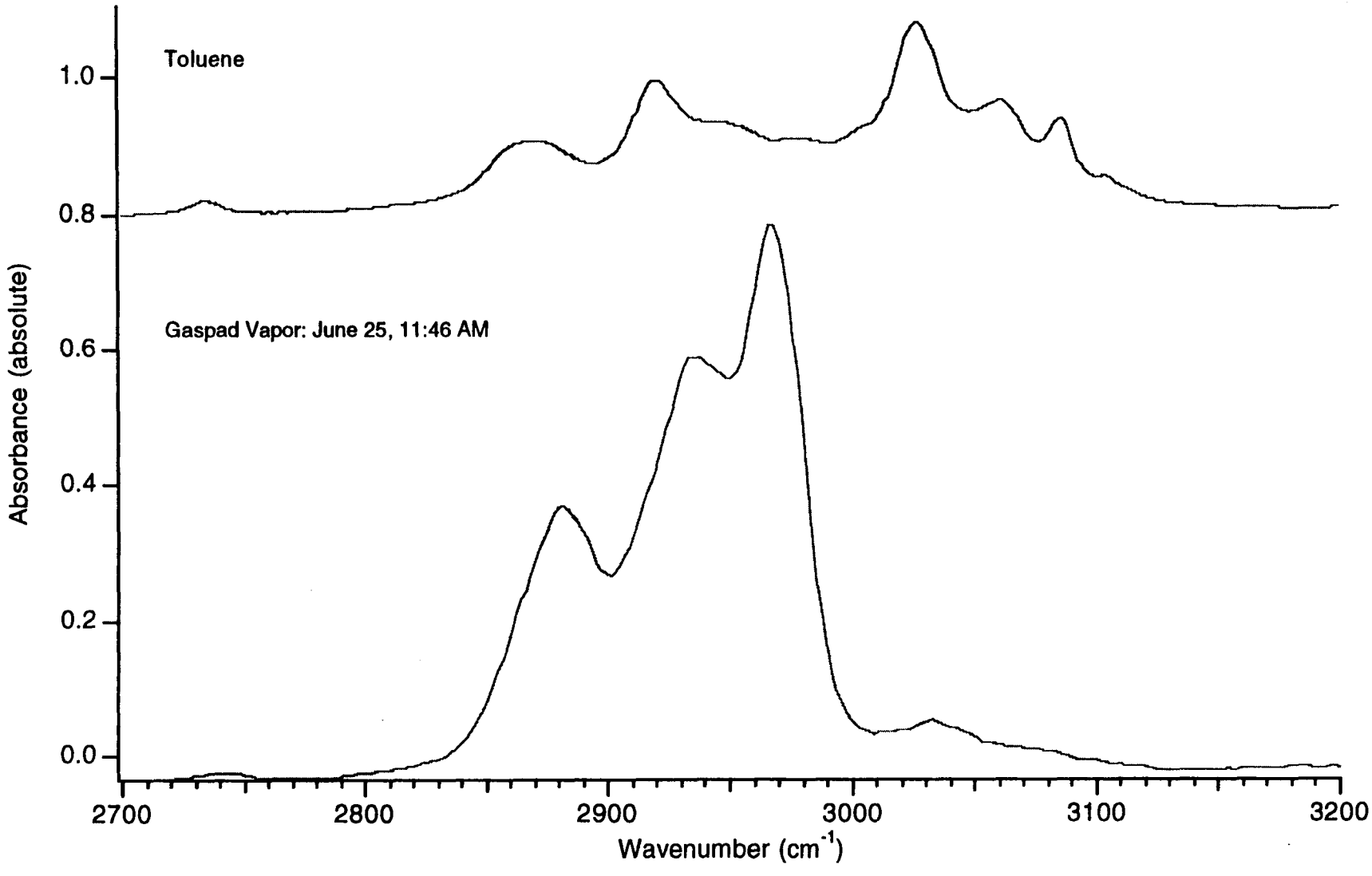

Figure 5.6.4. A magnified view of the C-H stretching region of liquid toluene and the gaspad vapor effluent. The aromatic stretching bands of the C-H absorbances are higher energy vibrations than those related to the alkanes and appear as distinct absorbances. The two different modes are displayed in the spectrum of toluene.

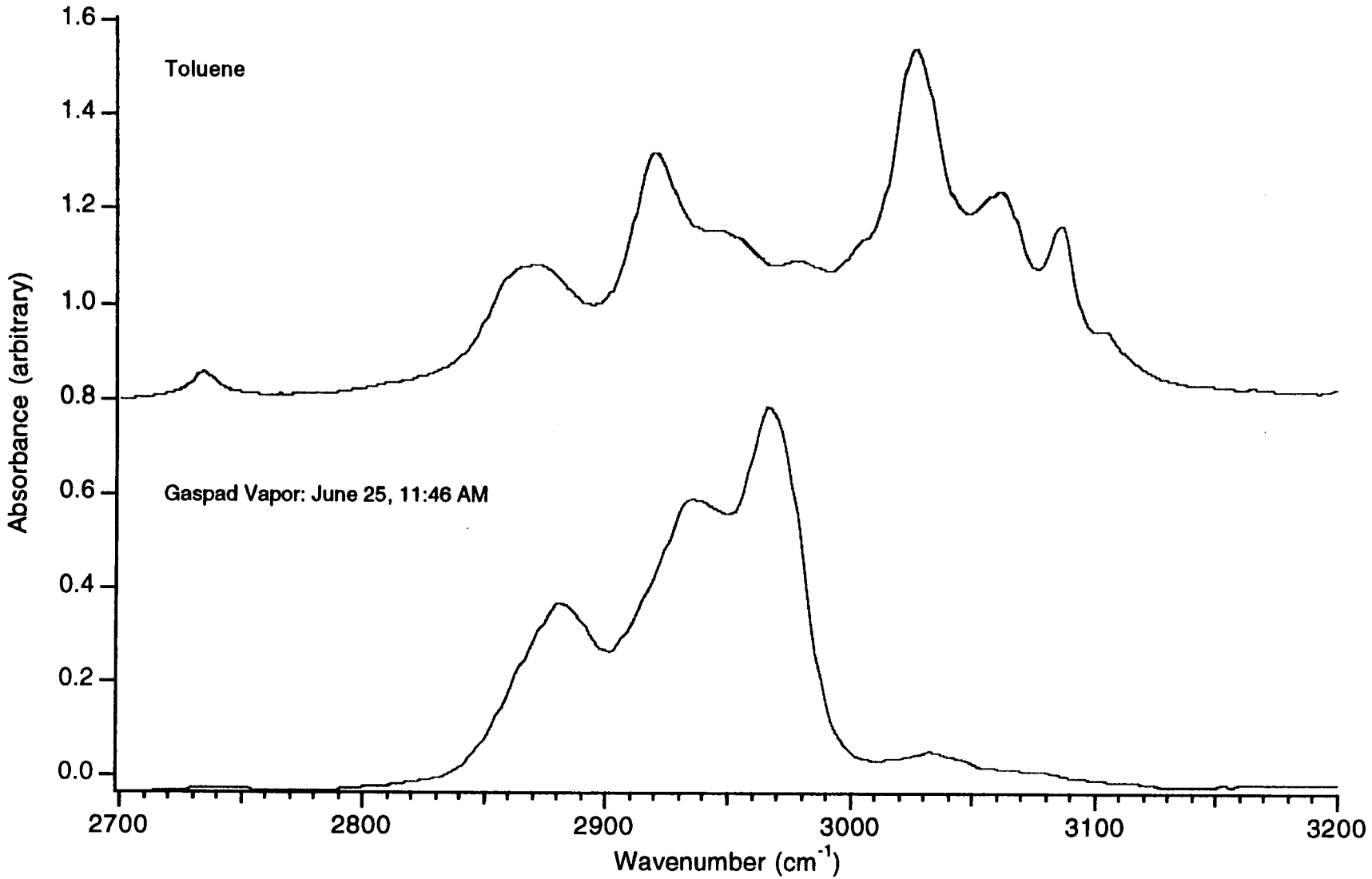

Figure 5.6.5. The spectrum of toluene is enhanced in this graph to more clearly show the band structure for the C-H stretching region.

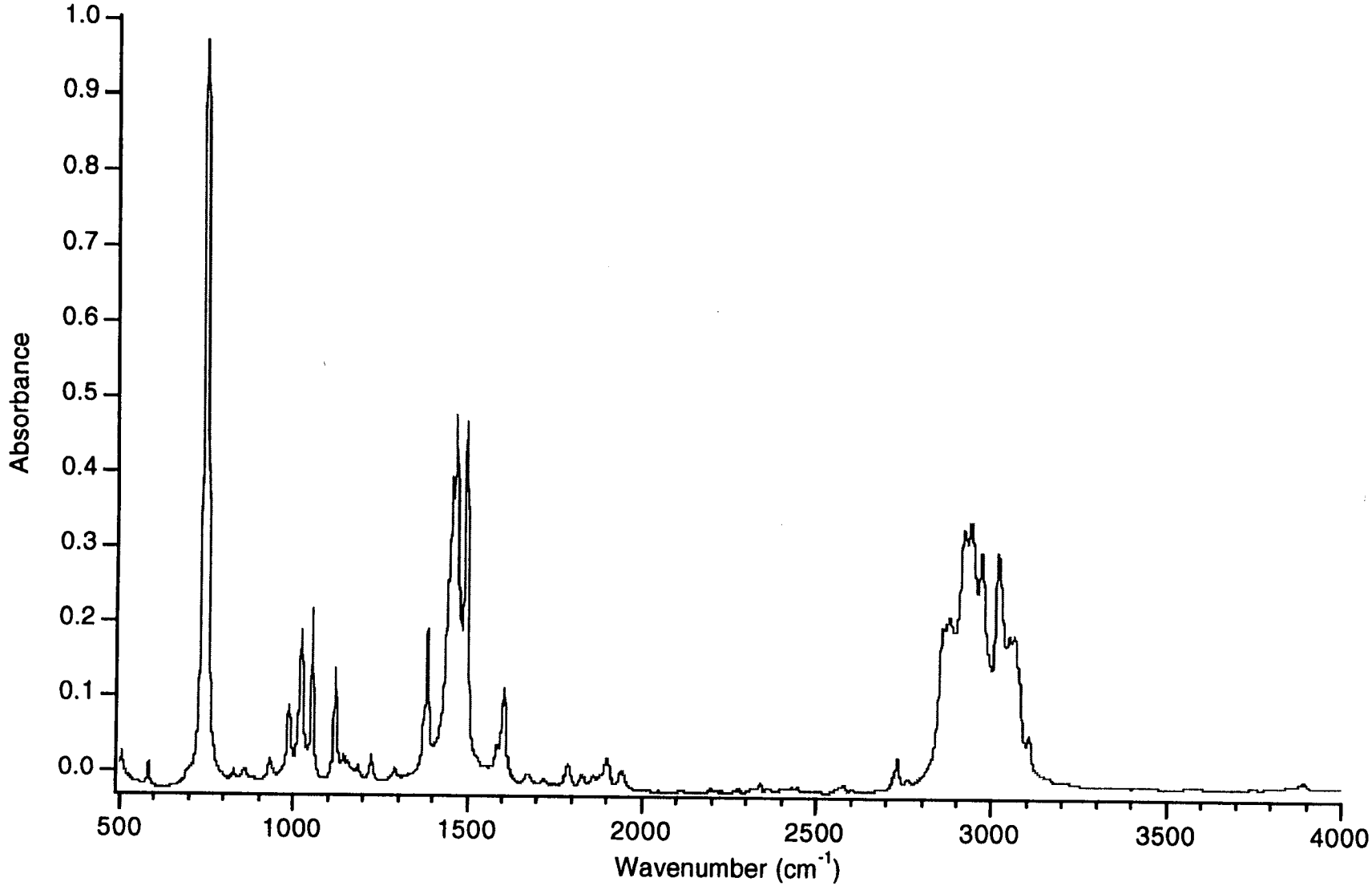

Figure 5.7.1. Infrared spectrum of liquid *o*-xylene collected at 4 cm^{-1} resolution. The aromatic ring bending modes are the strongest features of aromatic compounds.

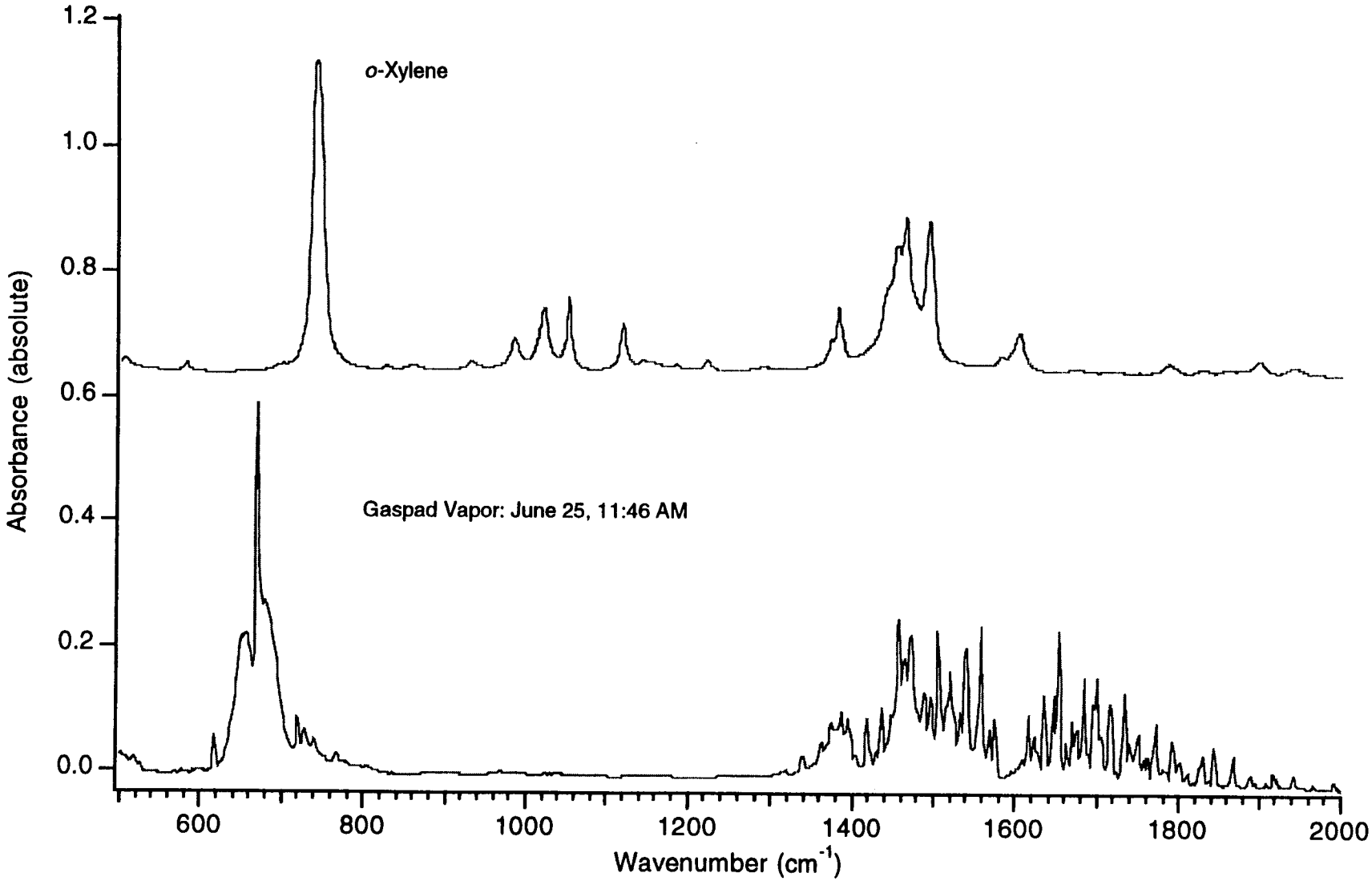

Figure 5.7.2. The fingerprint region of the spectra shows the strong ring C-H bending mode characteristic of *o*-xylene at 742 cm^{-1}. This intense band is quite distinct from the CO_2 bending vibration in the gaspad vapor spectrum.

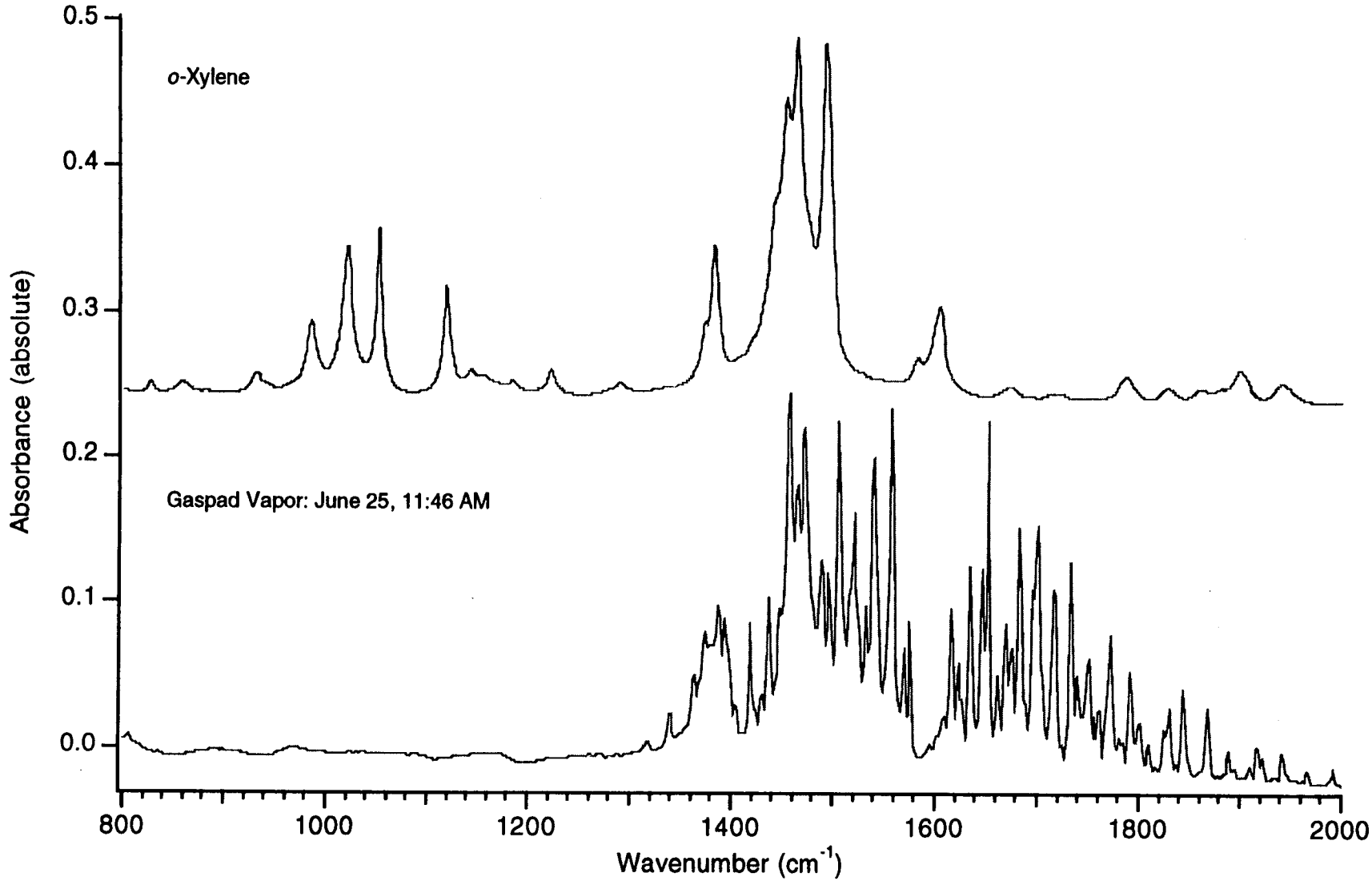

Figure 5.7.3. Expanded view of the fingerprint region showing condensed phase *o*-xylene and gaspad vapor effluent. Several aromatic *o*-xylene vibrations have absorbances in the window of the gaspad spectrum. The alkane C-H bending modes of the methyl groups are evident in *o*-xylene's spectrum at 1385 and 1440 cm-1.

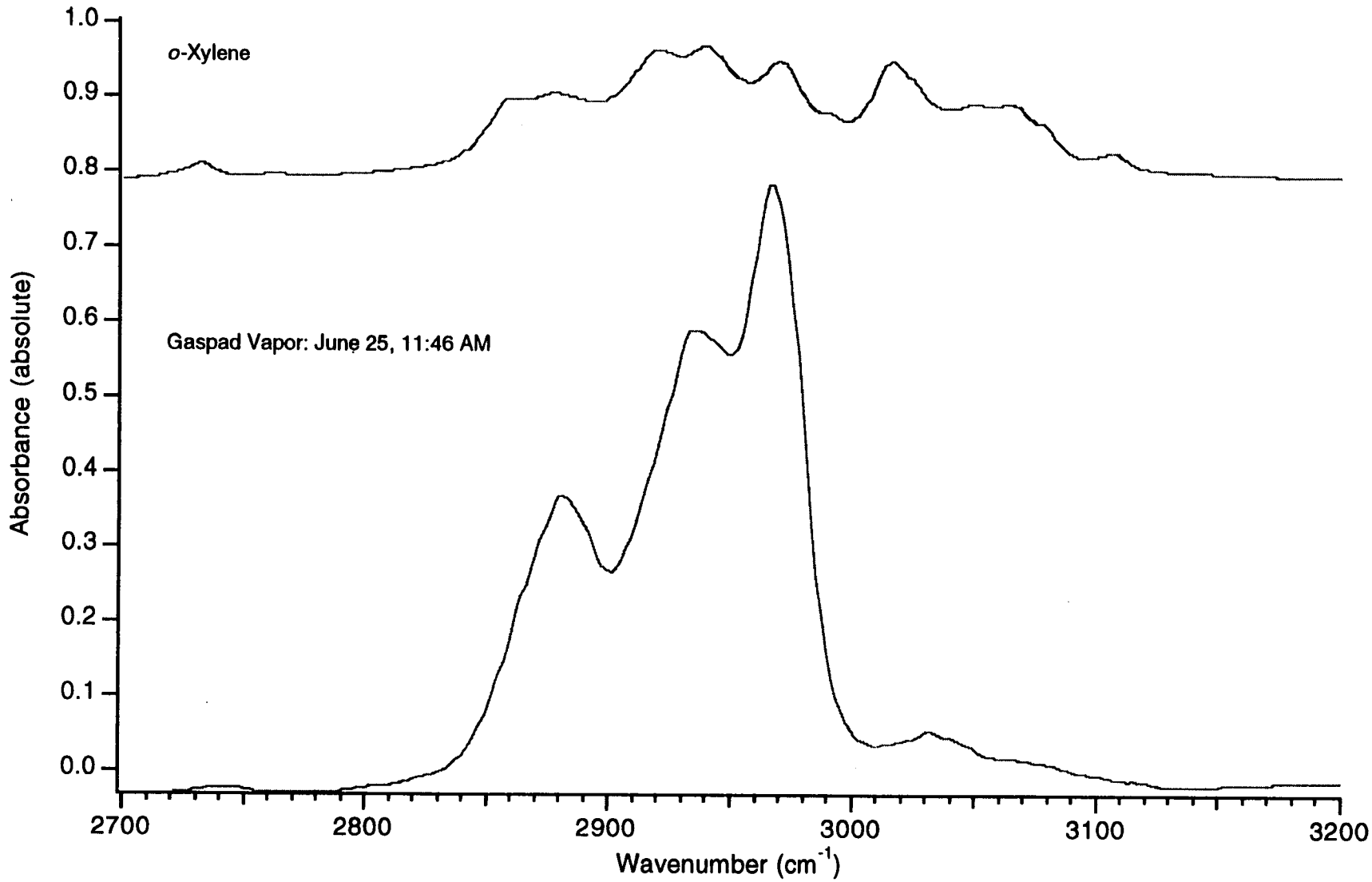

Figure 5.7.4. A magnified view is displayed of the C-H stretching region of liquid *o*-xylene and the gaspad vapor effluent. The aromatic stretching bands of the C-H absorbances are higher energy vibrations than those related to the alkanes and appear as distinct absorbances. The two different modes are displayed in the spectrum of toluene.

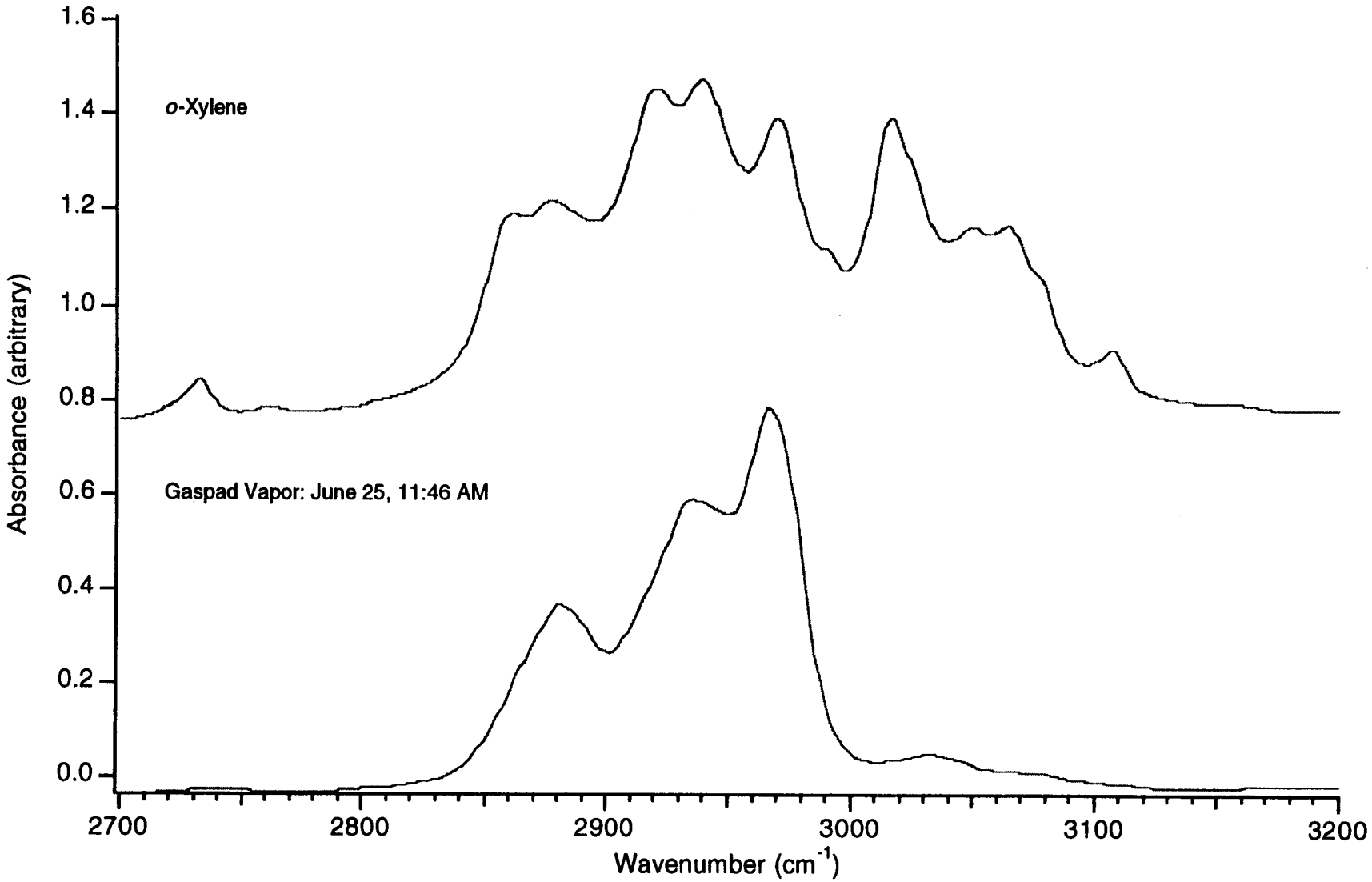

Figure 5.7.5. The spectrum of *o*-xylene is enhanced in this graph to more clearly show the band structure for the C-H stretching region.

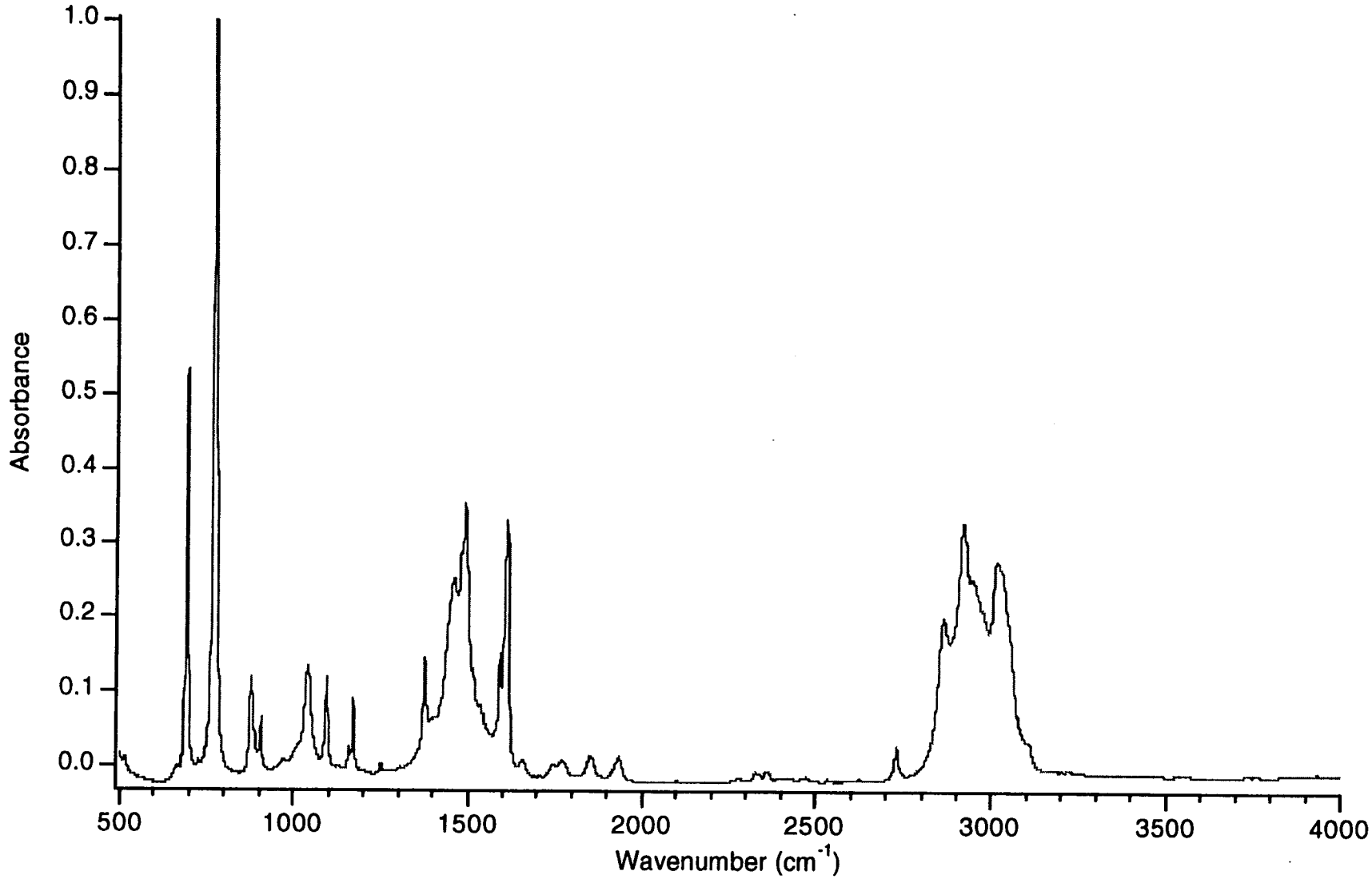

Figure 5.8.1. Infrared spectrum of liquid *m*-xylene collected at 4 cm^{-1} resolution. The aromatic ring bending modes are the strongest features of this aromatic compound although the methyl C-H stretching and bending modes are of significant intensity.

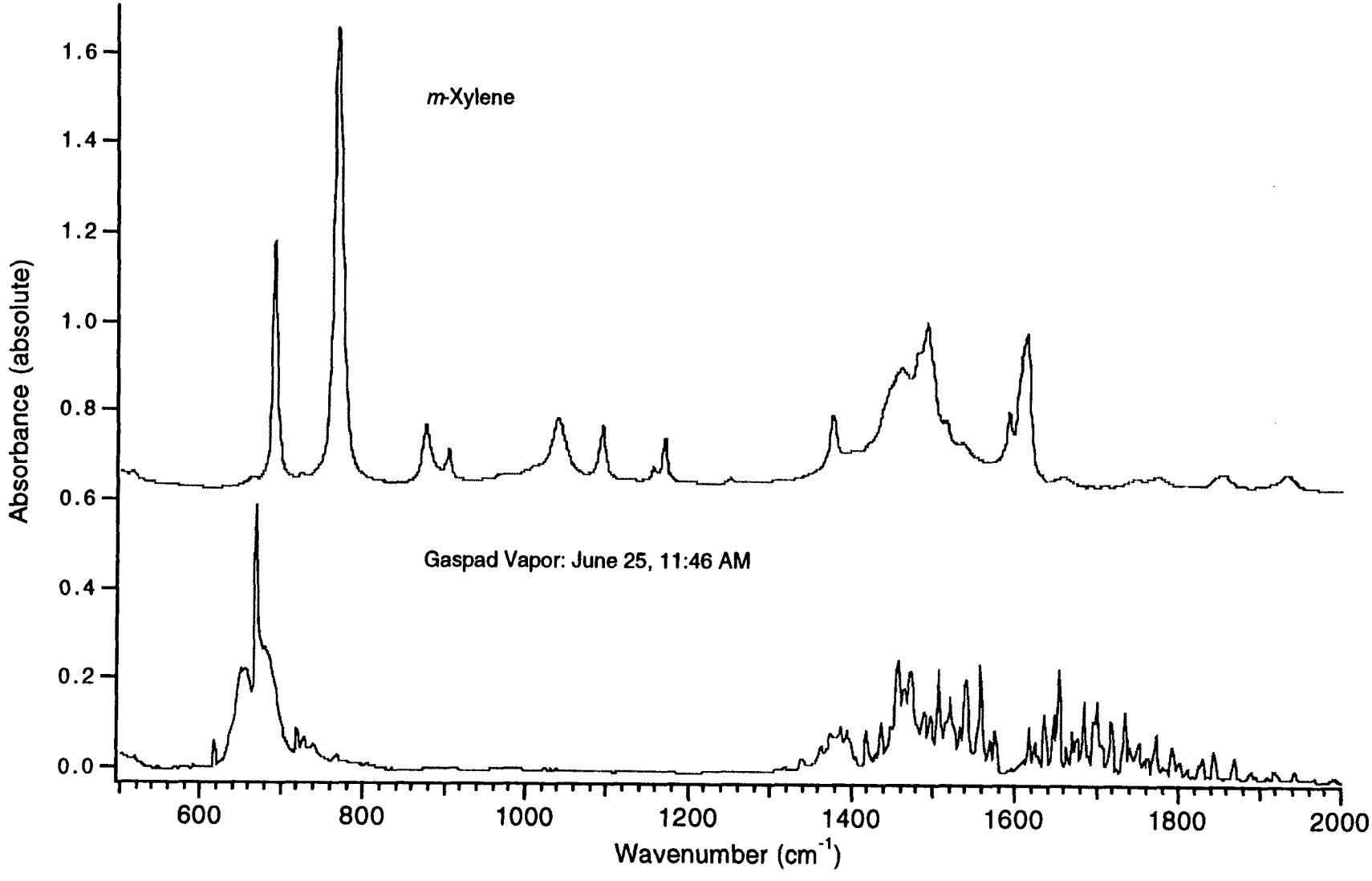

Figure 5.8.2. The fingerprint region of the *m*-xylene spectrum shows the strong ring C-H bending modes characteristic of aromatic compounds at 691 and 770 cm^{-1}. The CO_2 of the gaspad vapor spectrum appears sufficiently displaced to observe at least the 770 cm-1 band.

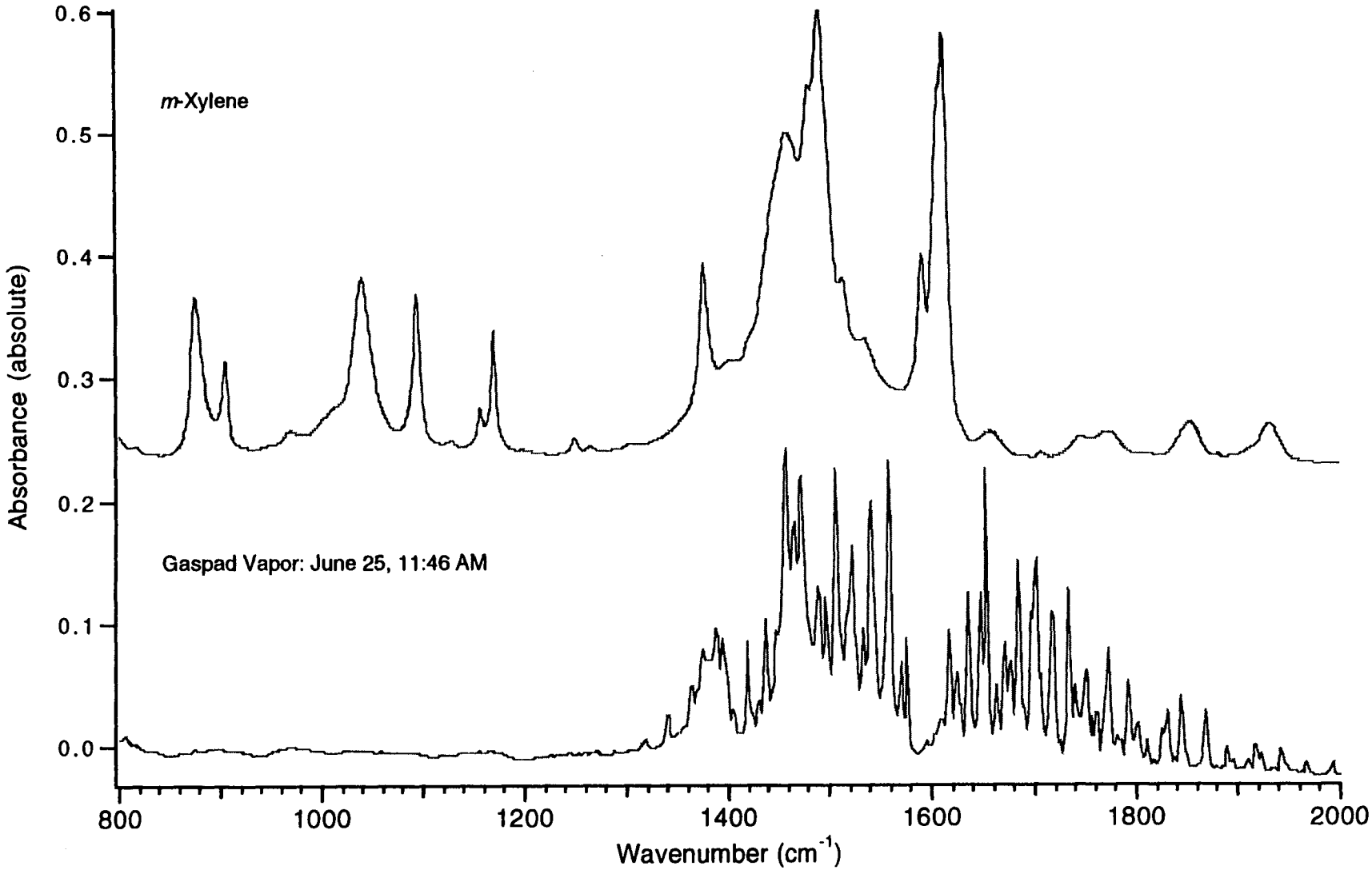

Figure 5.8.3. Expanded view of the fingerprint region of condensed phase *m*-xylene and the gaspad vapor effluent. Many aromatic vibrations characteristic of *m*-xylene have absorbances in the window of the gaspad spectra. One of the characteristic alkane C-H bending modes of the peripheral methyl groups is evident at 1385, while the other alkane C-H bending mode at 1440 cm^{-1} is mixed in with various C-H ring vibrations.

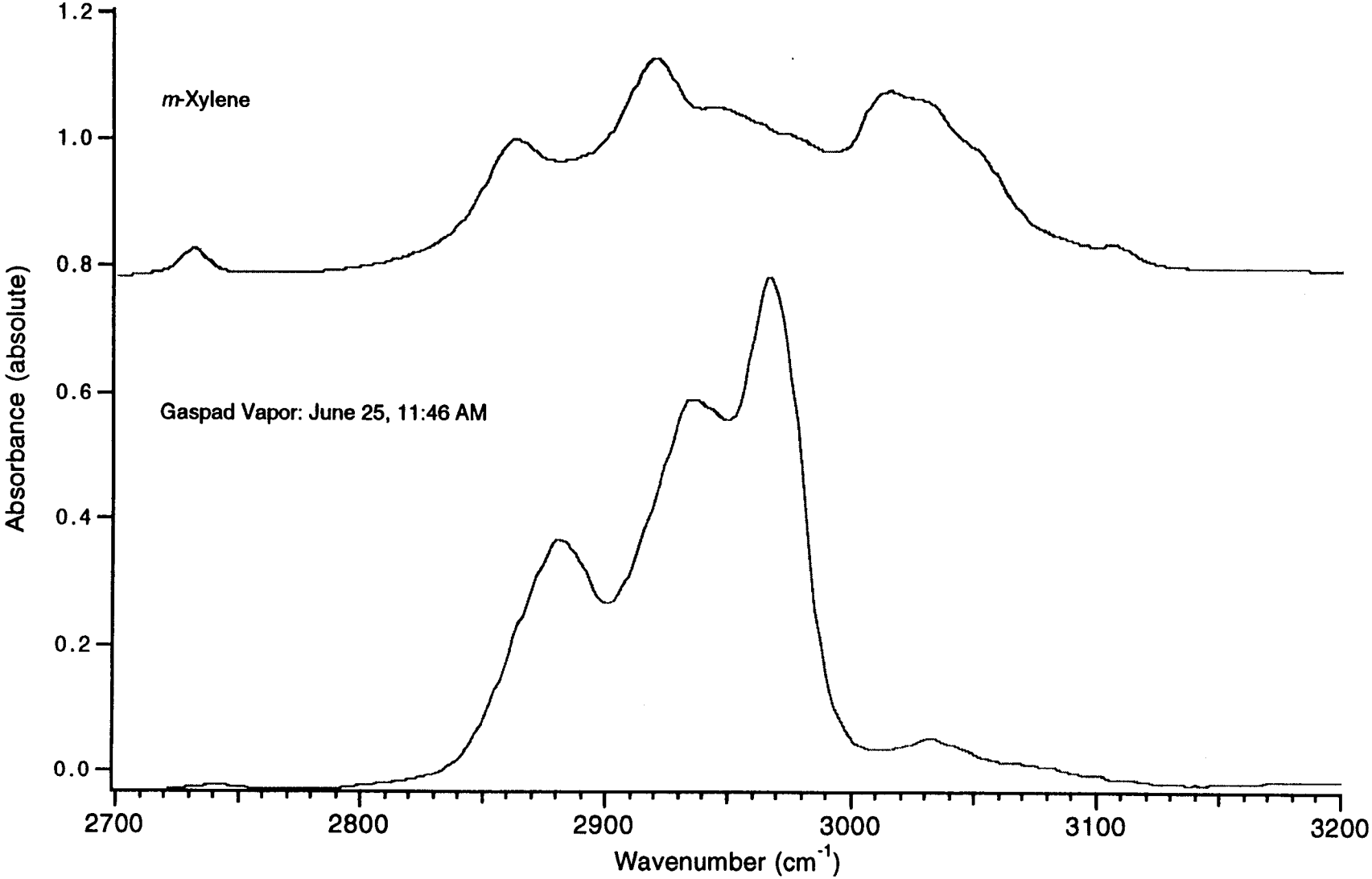

Figure 5.8.4. A magnified view of the C-H stretching region of liquid *m*-xylene and the gaspad vapor effluent. The aromatic stretching bands of the C-H absorbances are higher energy vibrations than those related to the alkanes and appear as distinct absorbances above 3000 cm^{-1}. The two different modes are displayed in this spectrum of *m*-xylene.

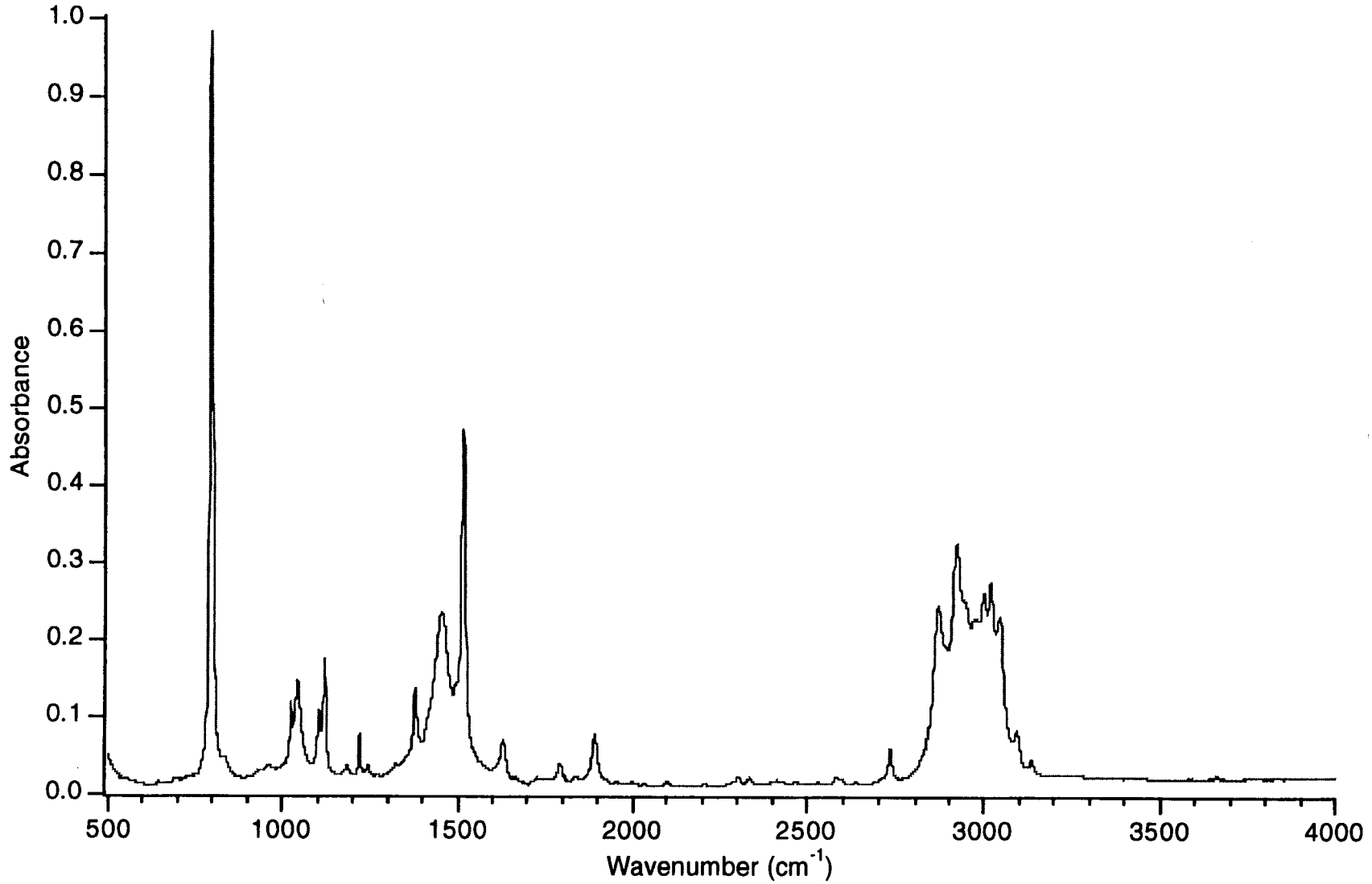

Figure 5.9.1. Infrared spectrum of liquid *p*-xylene collected at 4 cm^{-1} resolution.

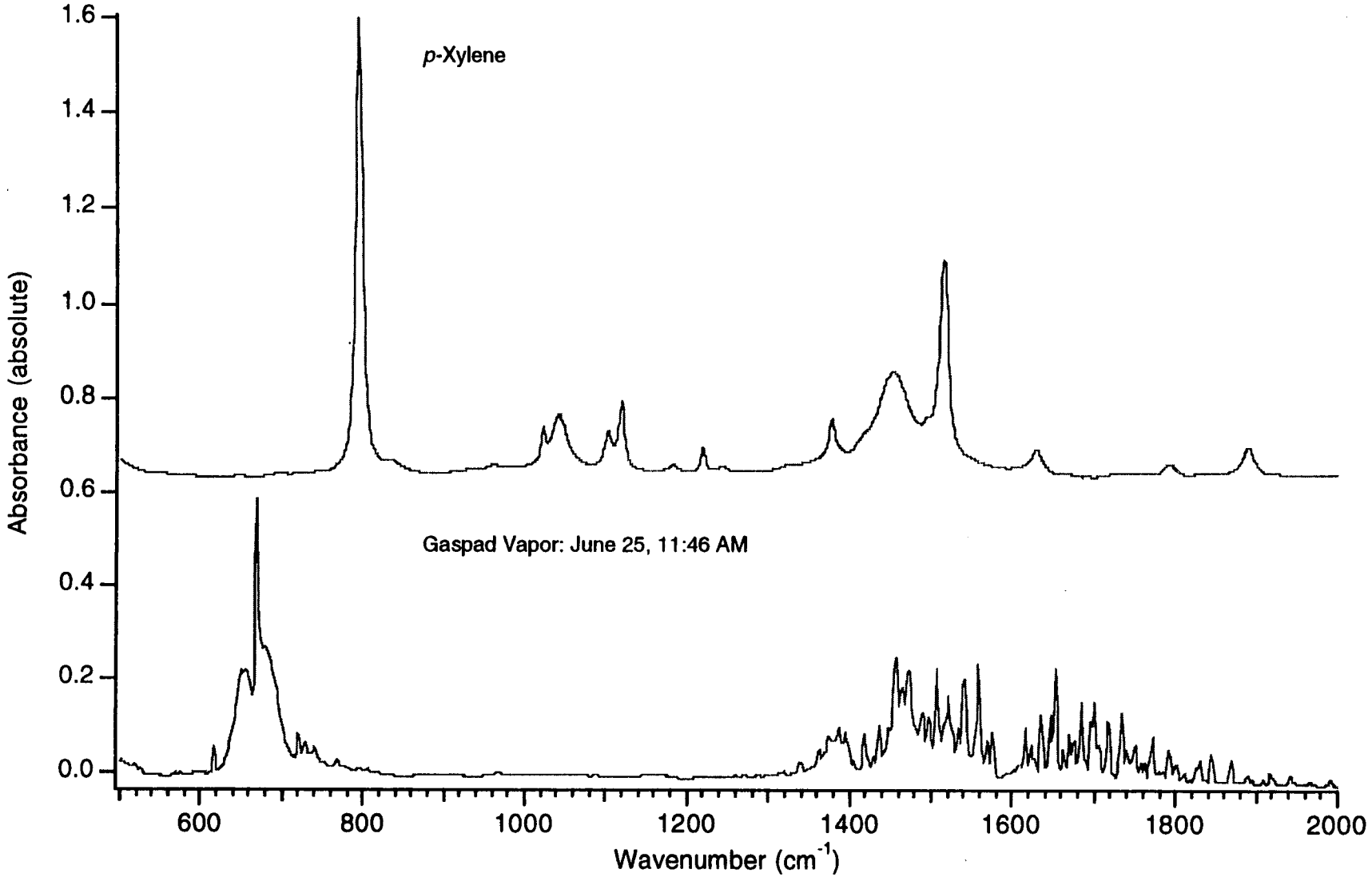

Figure 5.9.2. The fingerprint region of the spectra shows the strong ring C-H bending mode characteristic of *p*-xylene at 794 cm^{-1}, unobstructed by the gaspad CO_2 spectrum.

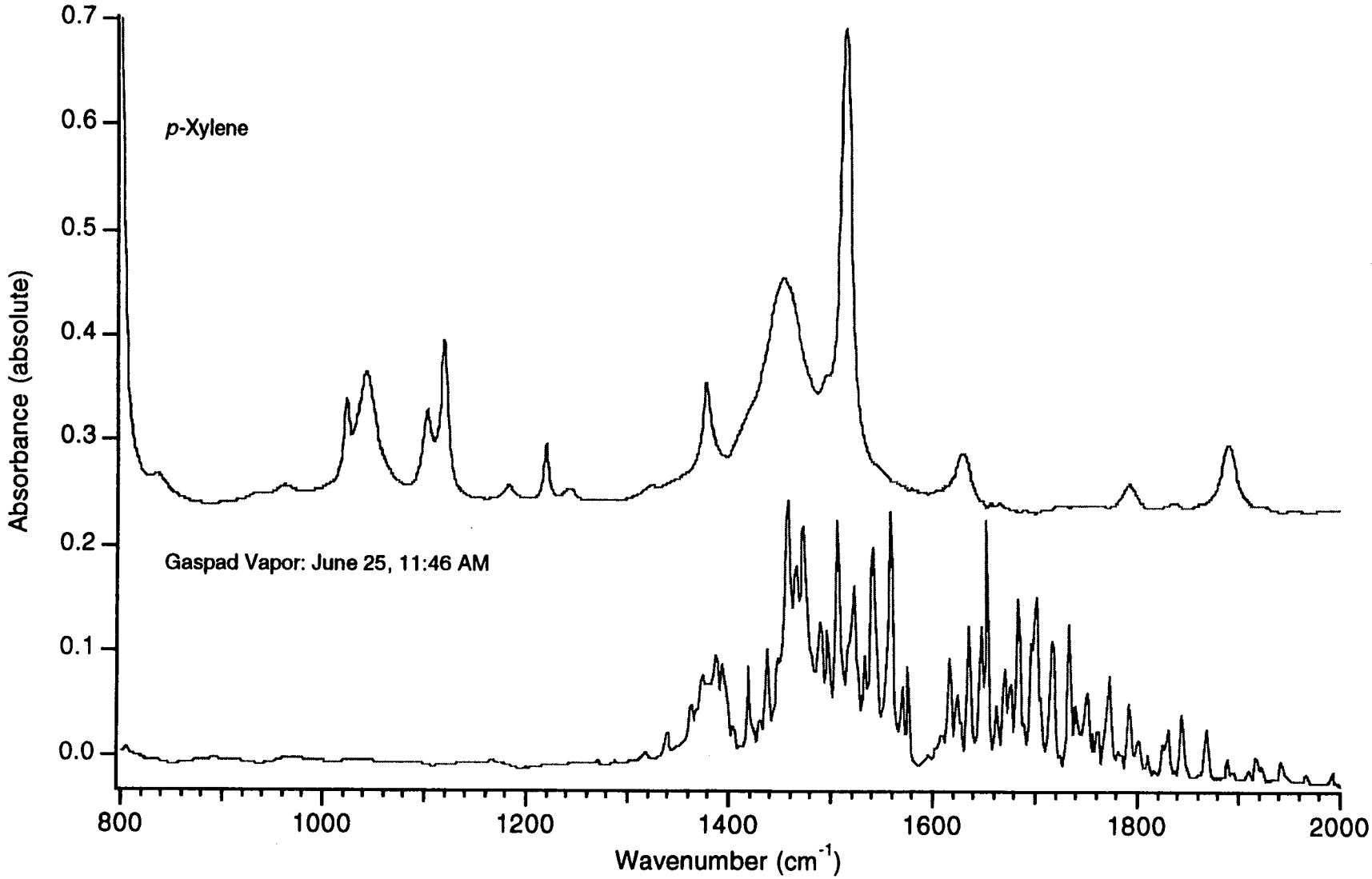

Figure 5.9.3. Expanded view of the fingerprint region of liquid toluene and the gaspad vapor effluent. Some aromatic ring vibrations have absorbances in the window of the gaspad spectra. The characteristic alkane C-H bending modes of the methyl groups are evident at 1370 and 1450 cm^{-1}.

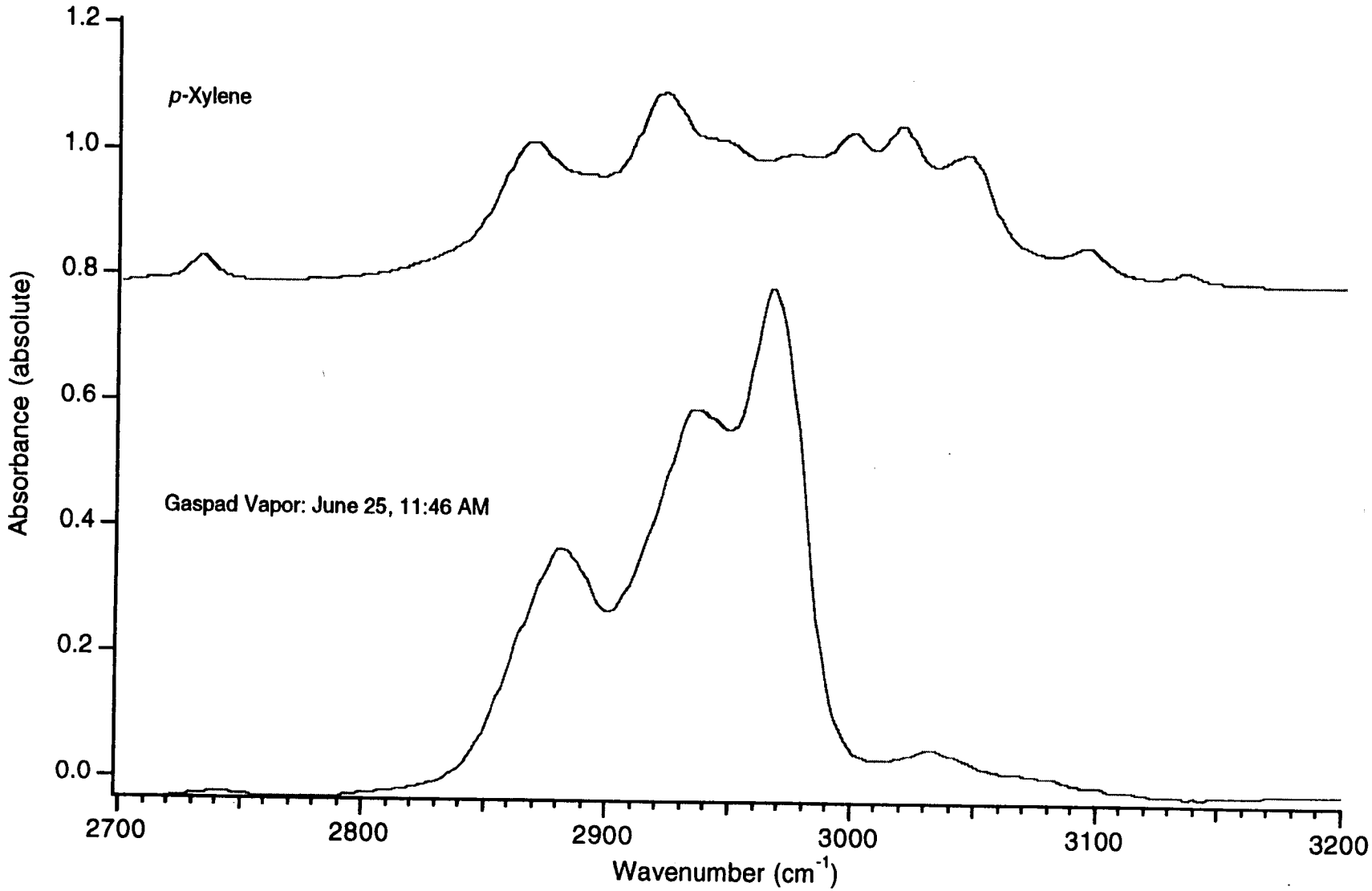

Figure 5.9.4. A magnified view of the C-H stretching region of liquid *p*-xylene and the gaspad vapor effluent. The aromatic stretching bands of the C-H absorbances are higher energy vibrations than those related to the alkanes and appear as distinct absorbances above 3000 cm^{-1}.

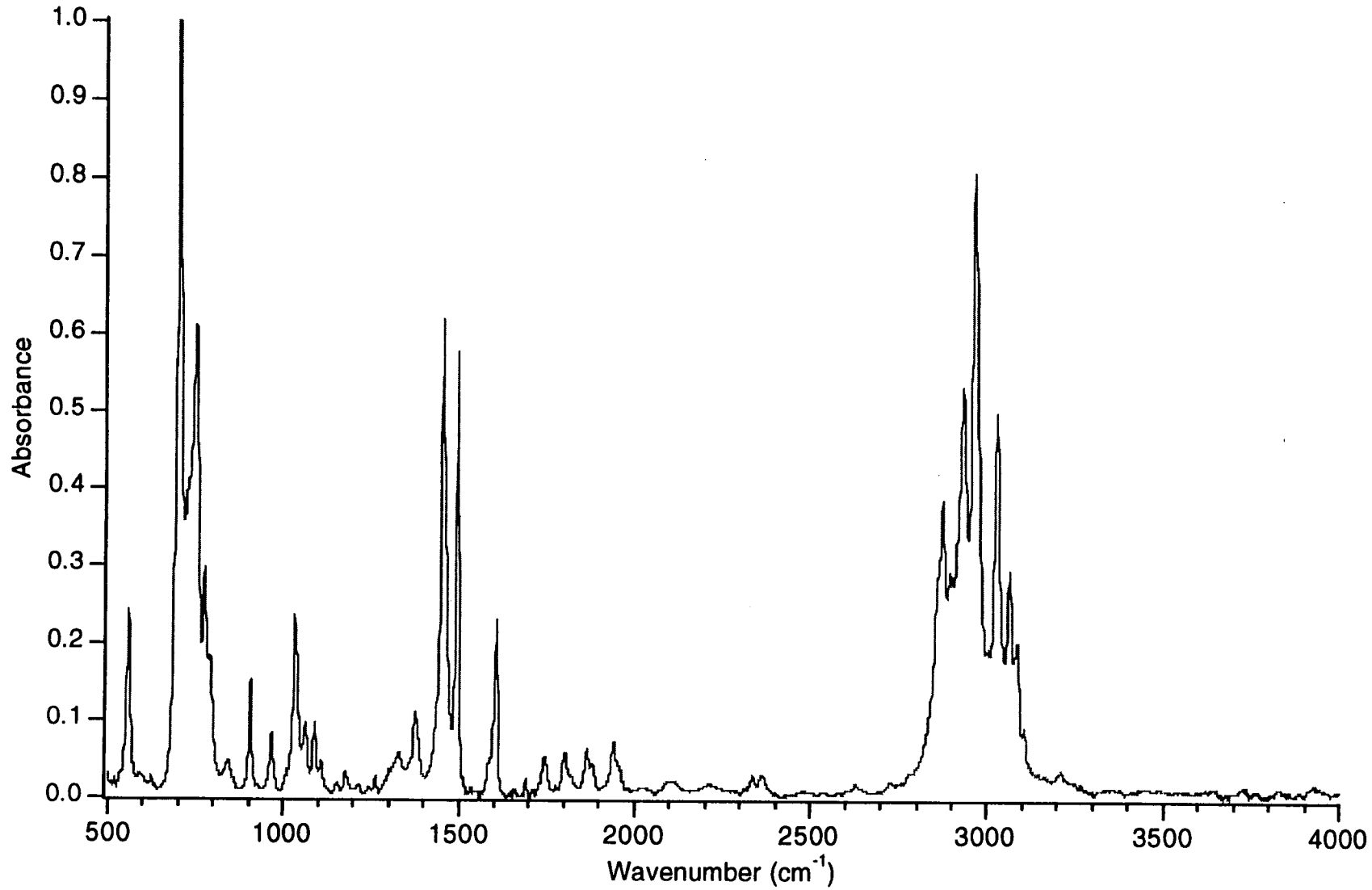

Figure 5.10.1. Infrared spectrum of liquid ethylbenzene collected at 4 cm^{-1} resolution. The four low intensity bands between 1700 and 2000 cm^{-1} are characteristic of monosubstituted benzene rings.

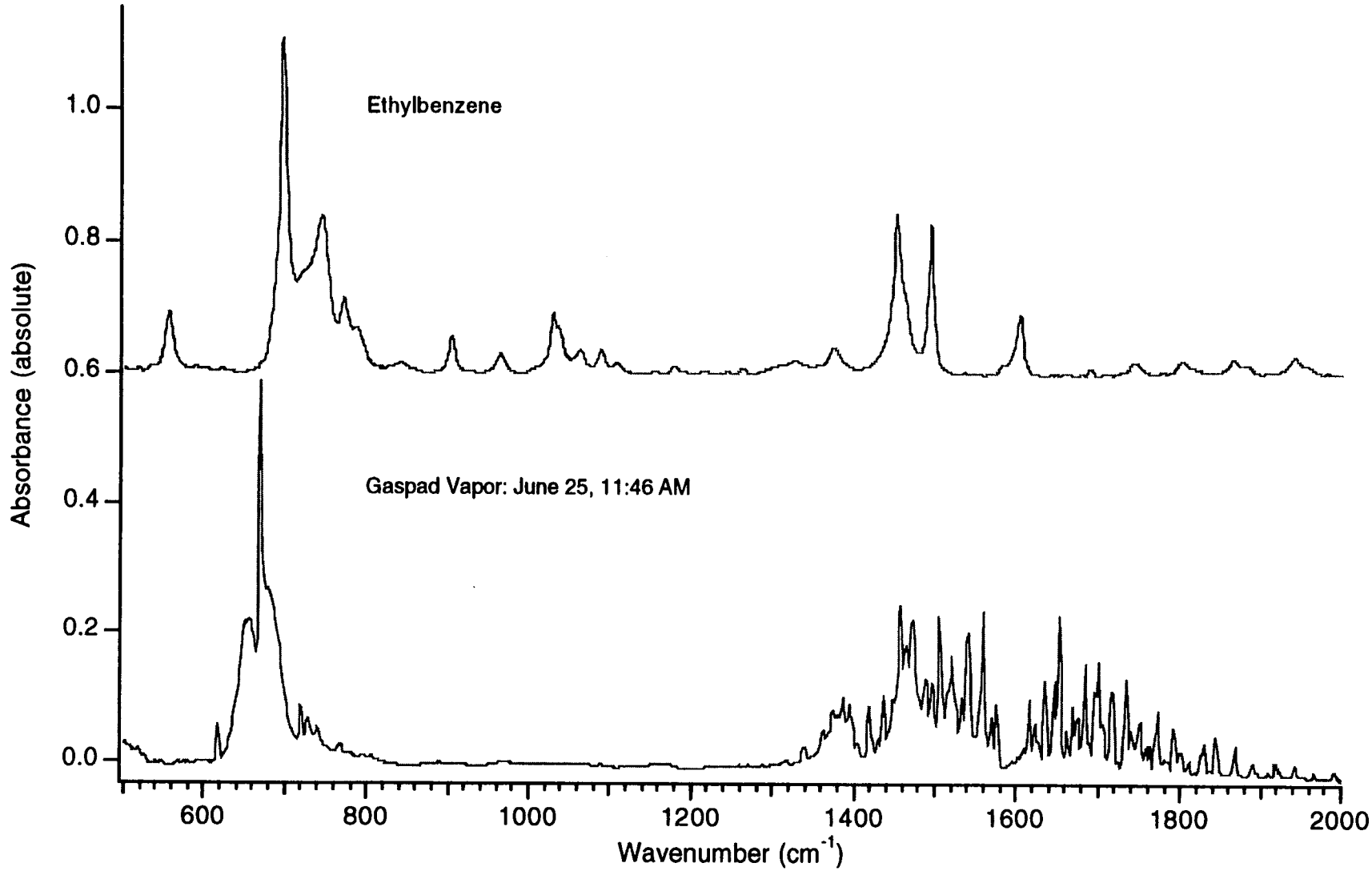

Figure 5.10.2. The fingerprint region of the spectra shows the strong ring C-H bending mode of ethylbenzene at 697 cm^{-1}.

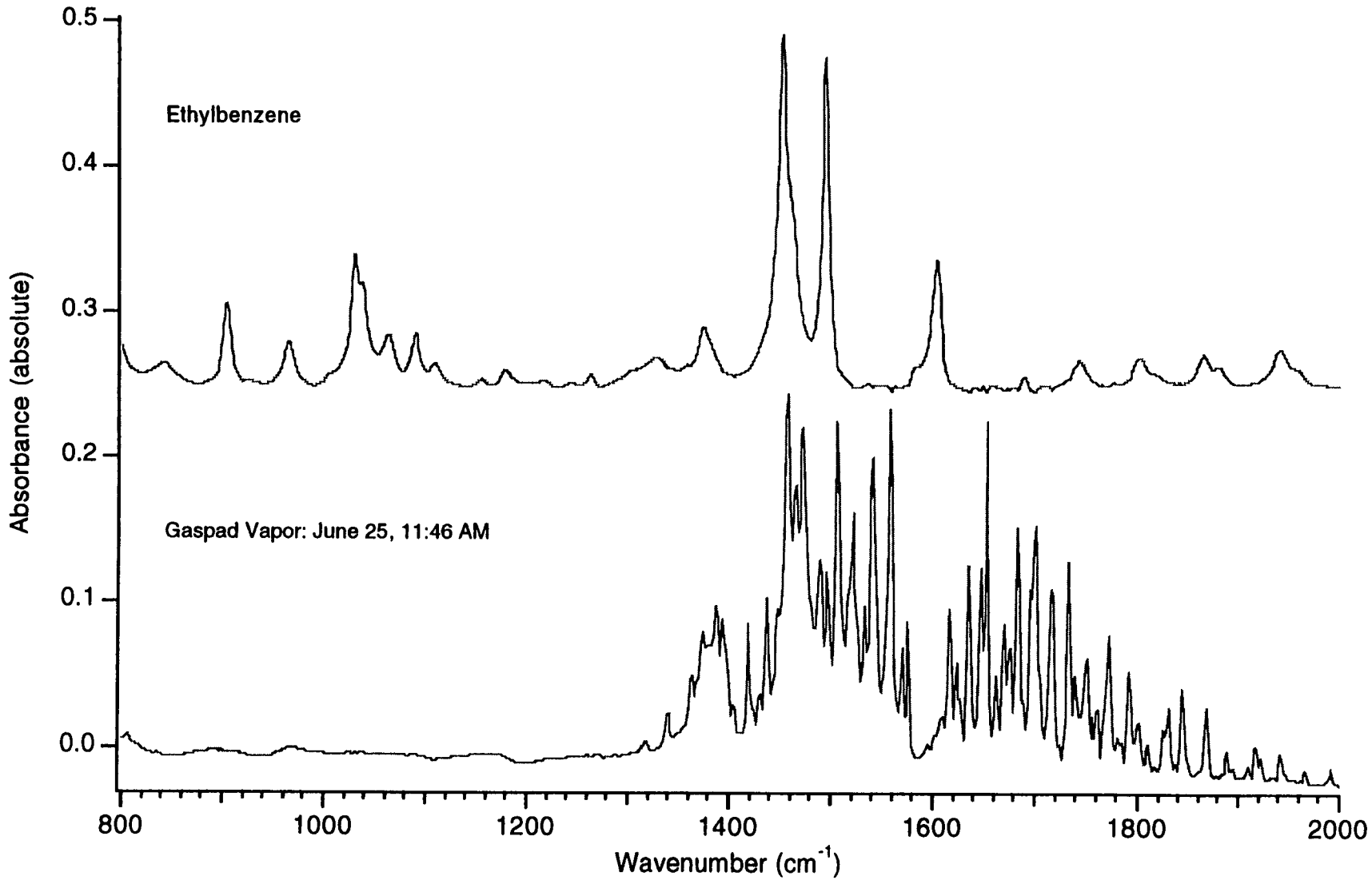

Figure 5.10.3. Expanded view of the fingerprint region of liquid ethylbenzene and the gaspad vapor effluent.

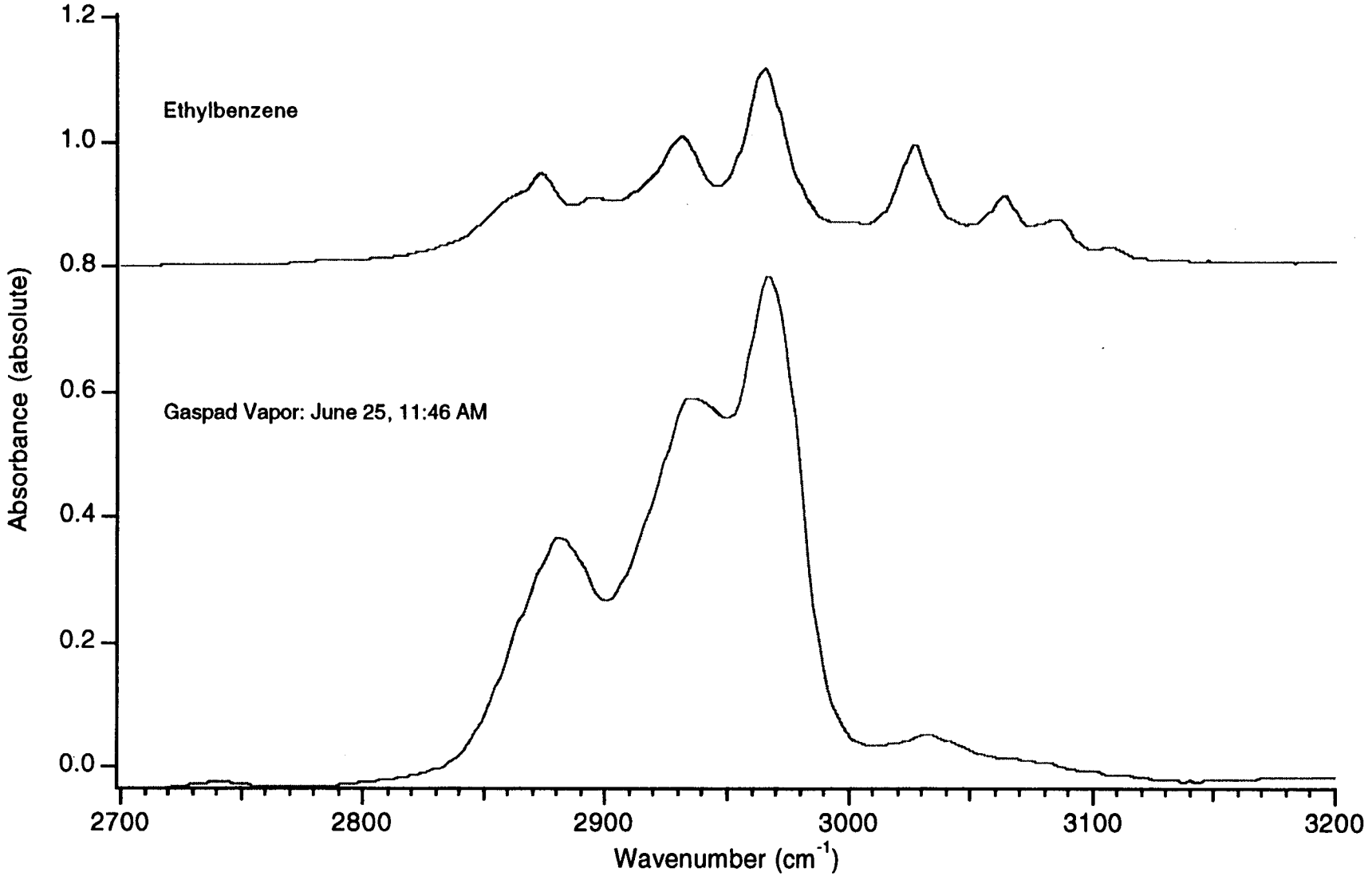

Figure 5.10.4. A magnified view of the C-H stretching region of liquid ethylbenzene and the gaspad effluent. The aromatic stretching bands of the C-H absorbances are higher energy vibrations than those related to the alkanes and appear as distinct absorbances. The two different modes are clearly displayed in this spectrum of ethylbenzene.

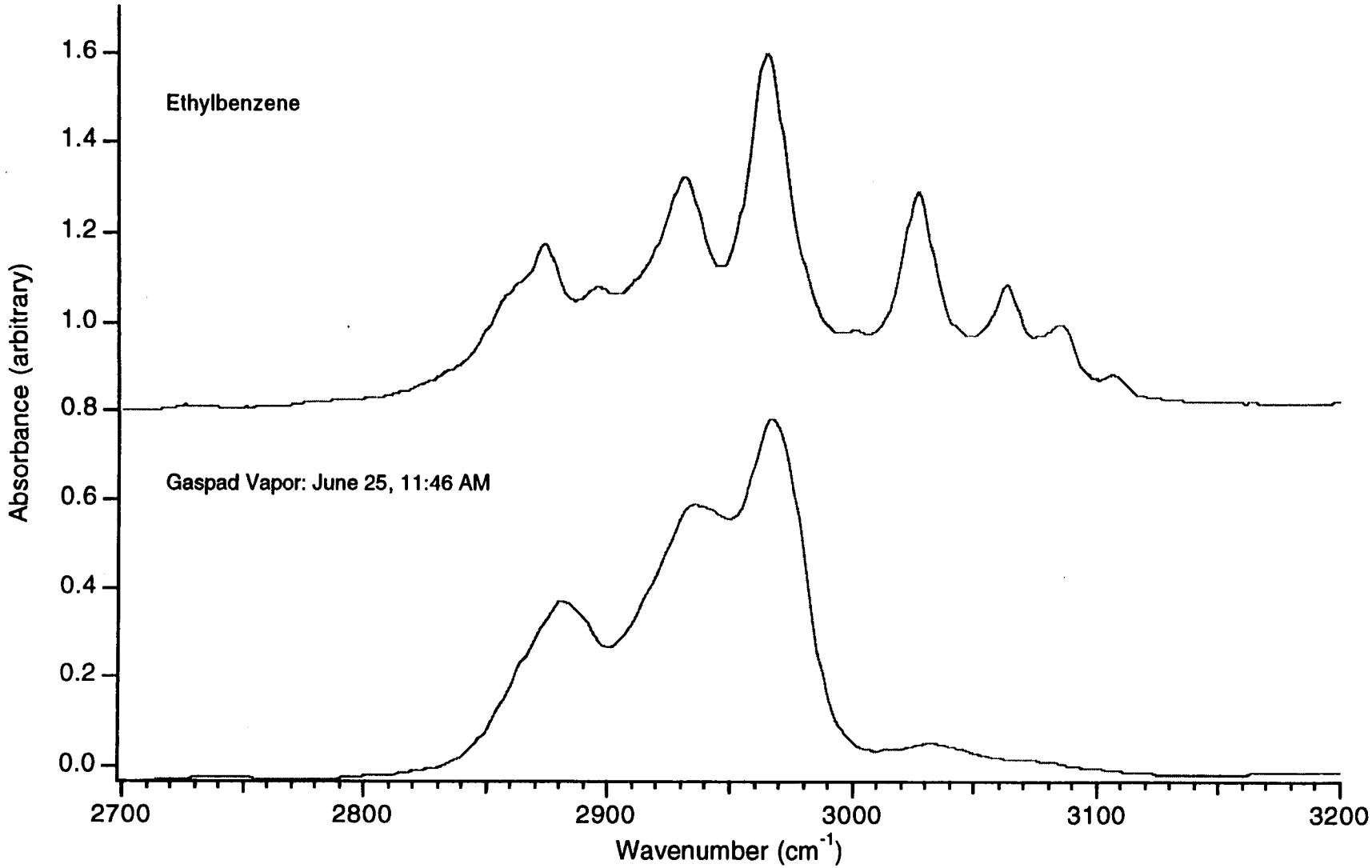

Figure 5.10.5. The spectrum of ethylbenzene is enhanced in this graph to more clearly show the band structure for the C-H stretching region.

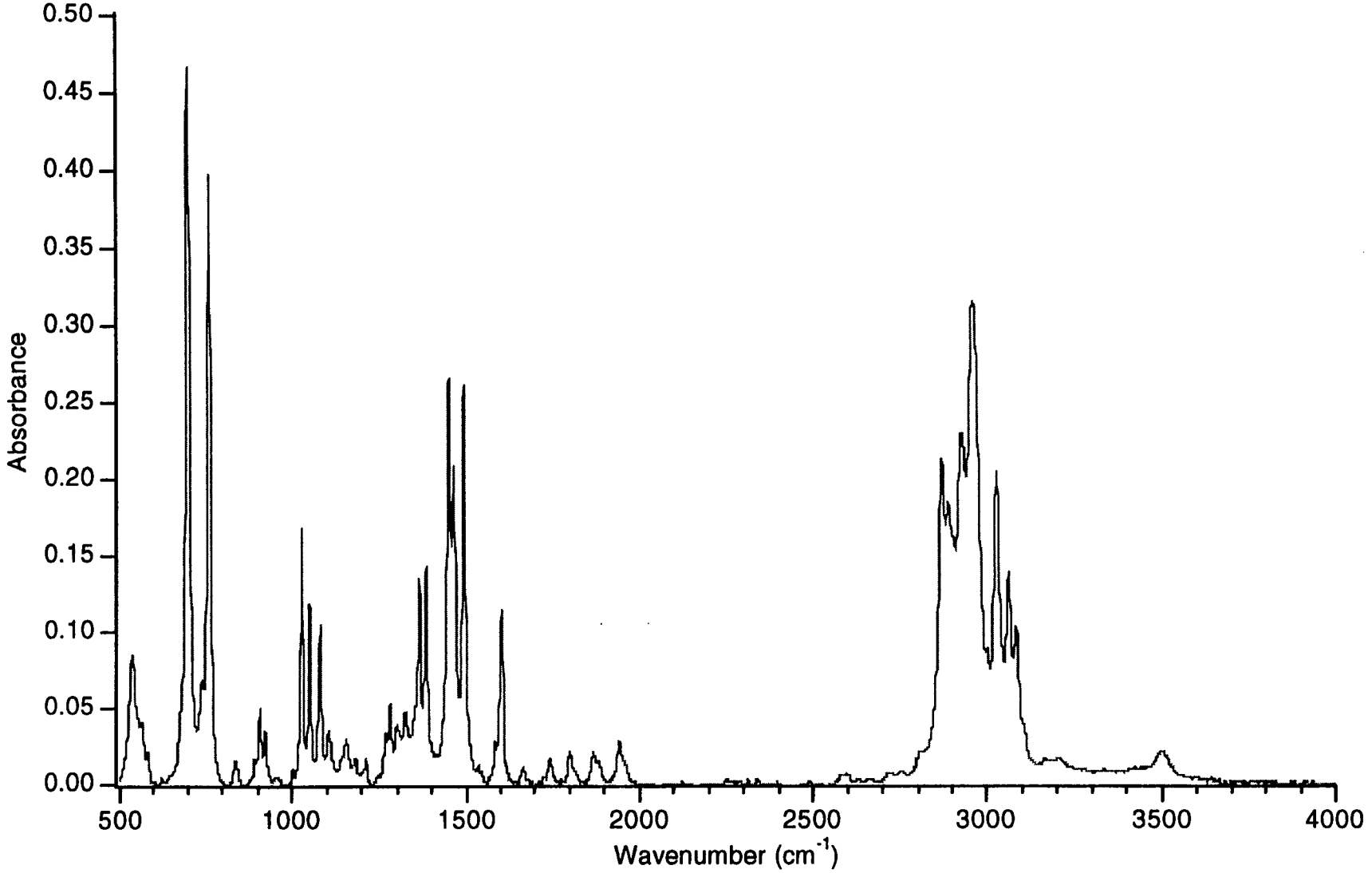

Figure 5.11.1. Infrared spectrum of liquid *iso*-propylbenzene collected at 4 cm^{-1} resolution. The four low intensity bands between 1650 cm^{-1} and 2000 cm^{-1} are characteristic of monosubstituted benzene rings.

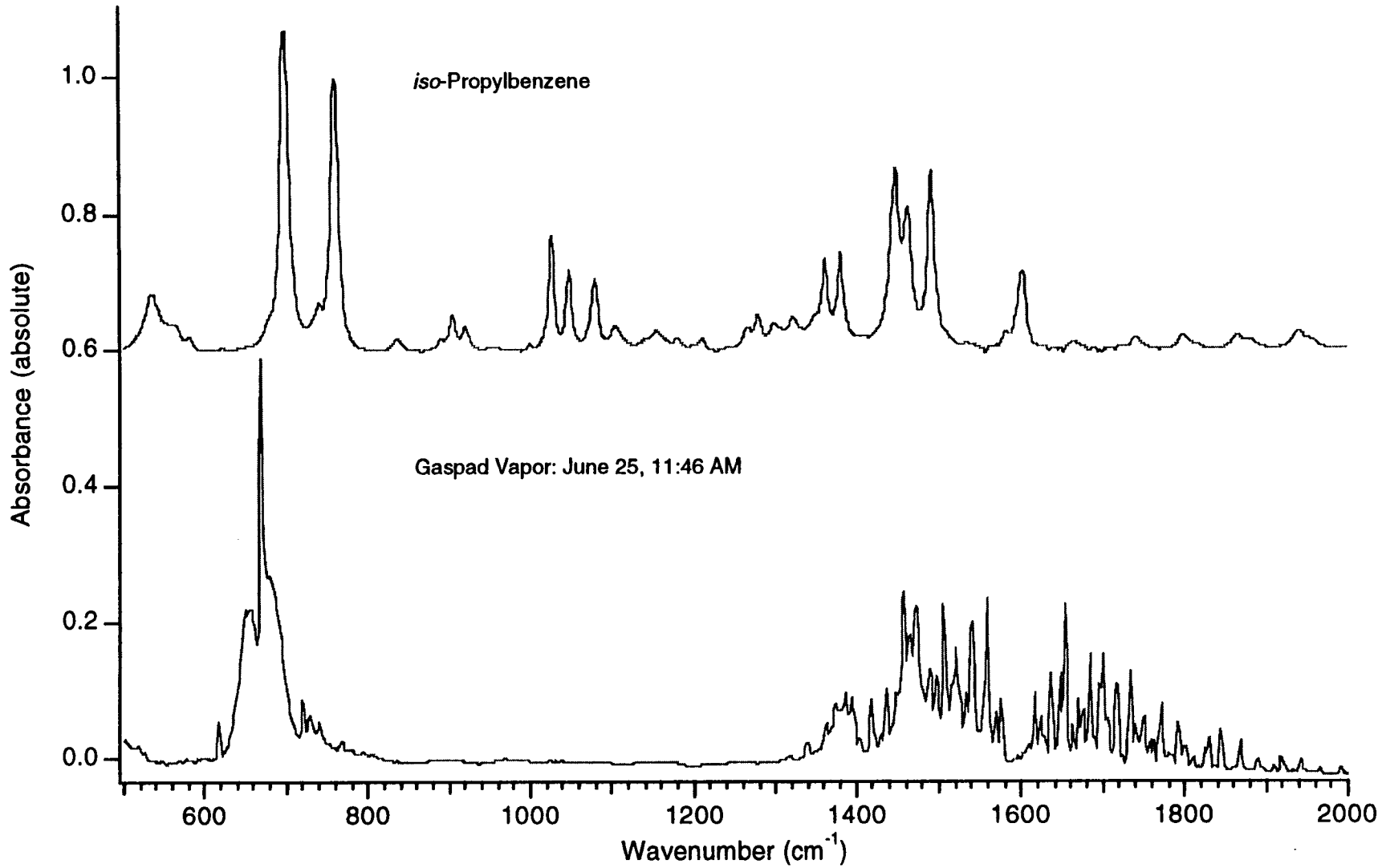

Figure 5.11.2. The fingerprint region of this spectrum shows the strong ring C-H bending modes characteristic of *iso*-propylbenzene at 700 cm^{-1} and 760 cm^{-1}.

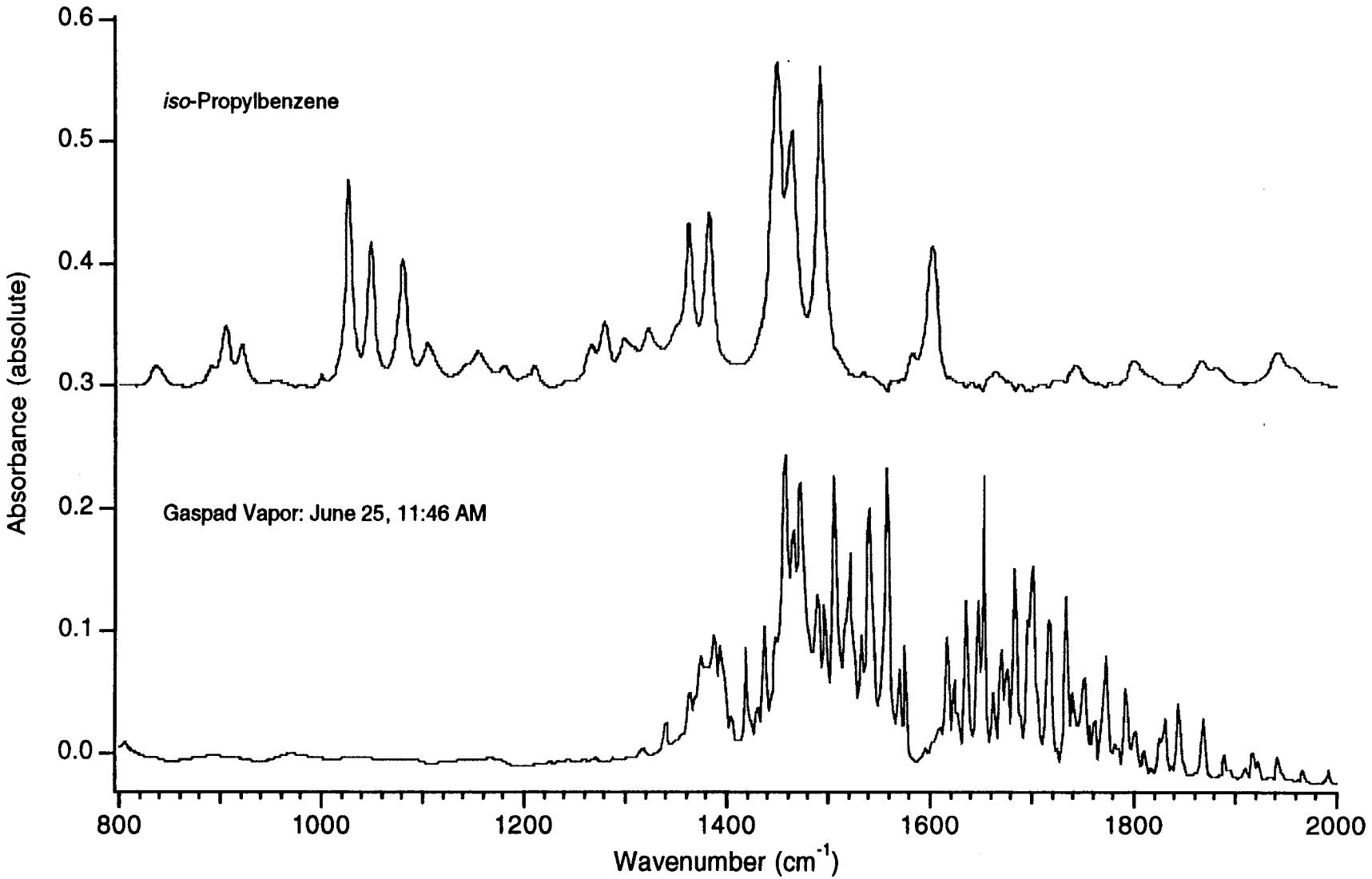

Figure 5.11.3. Expanded view of the fingerprint region of liquid *iso*-propylbenzene and the gaspad vapor effluent. Some aromatic *iso*-propylbenzene vibrations have absorbances in the window of the gaspad spectra. The characteristic alkane C-H bending modes of two methyl groups are evident near 1385 cm^{-1} and 1440 cm^{-1}.

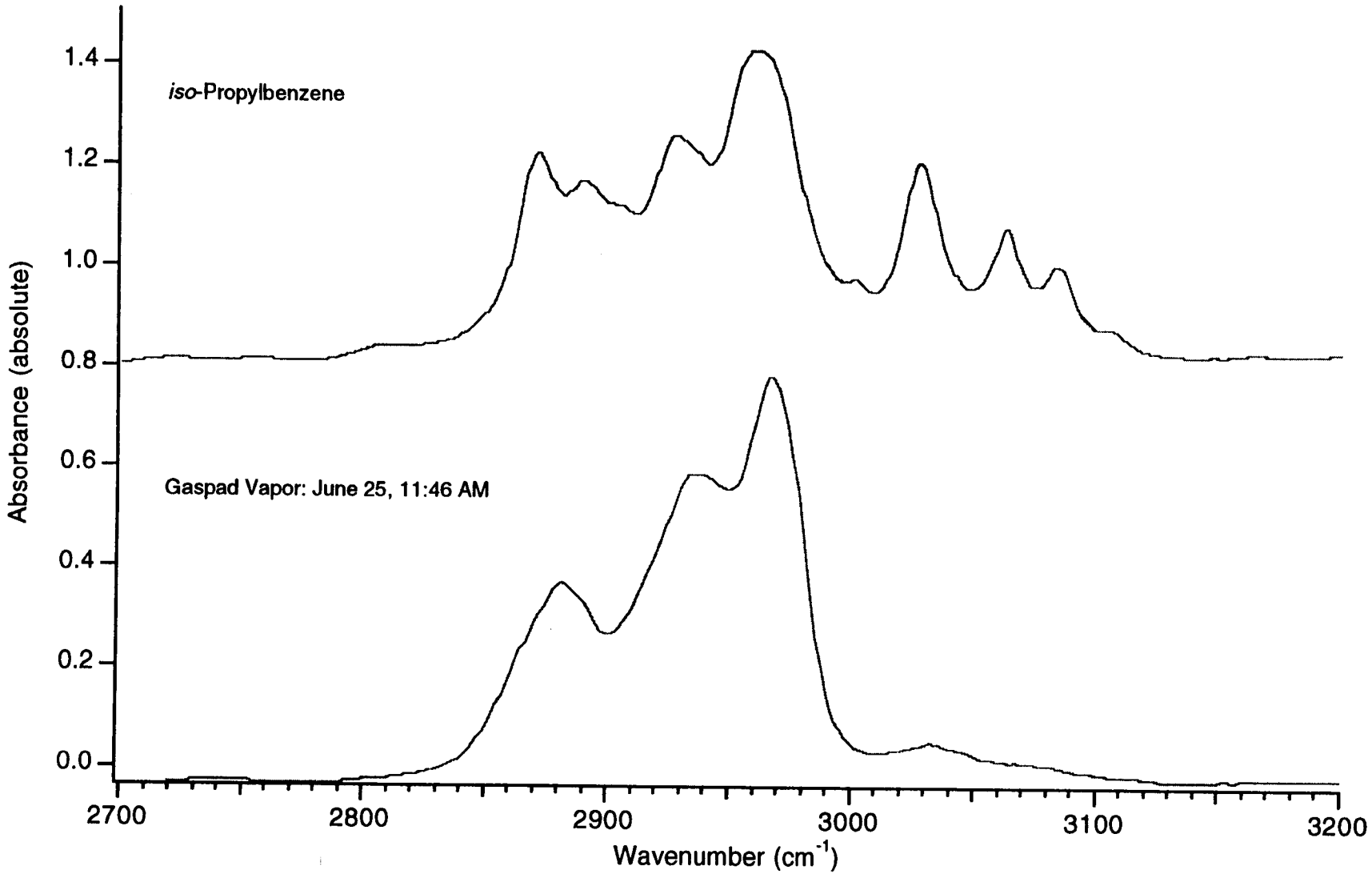

Figure 5.11.4. A magnified view of the C-H stretching region of liquid *iso*-propylbenzene and the gaspad vapor effluent. The aromatic stretching bands of the C-H absorbances are higher energy vibrations than those related to the alkanes and appear as distinct absorbances.

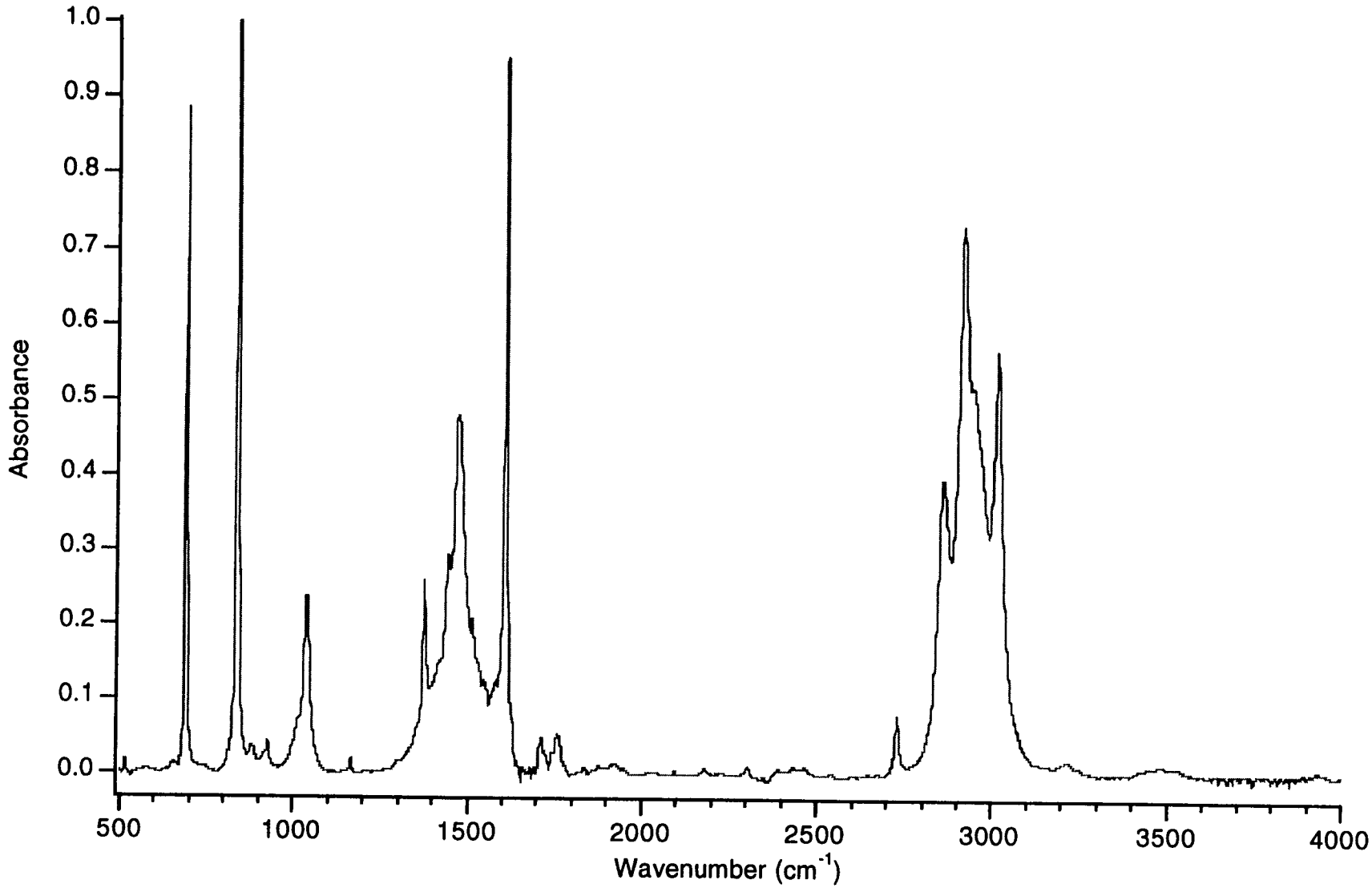

Figure 5.12.1. Infrared spectrum of liquid 1,3,5-trimethylbenzene collected at 4 cm^{-1} resolution.

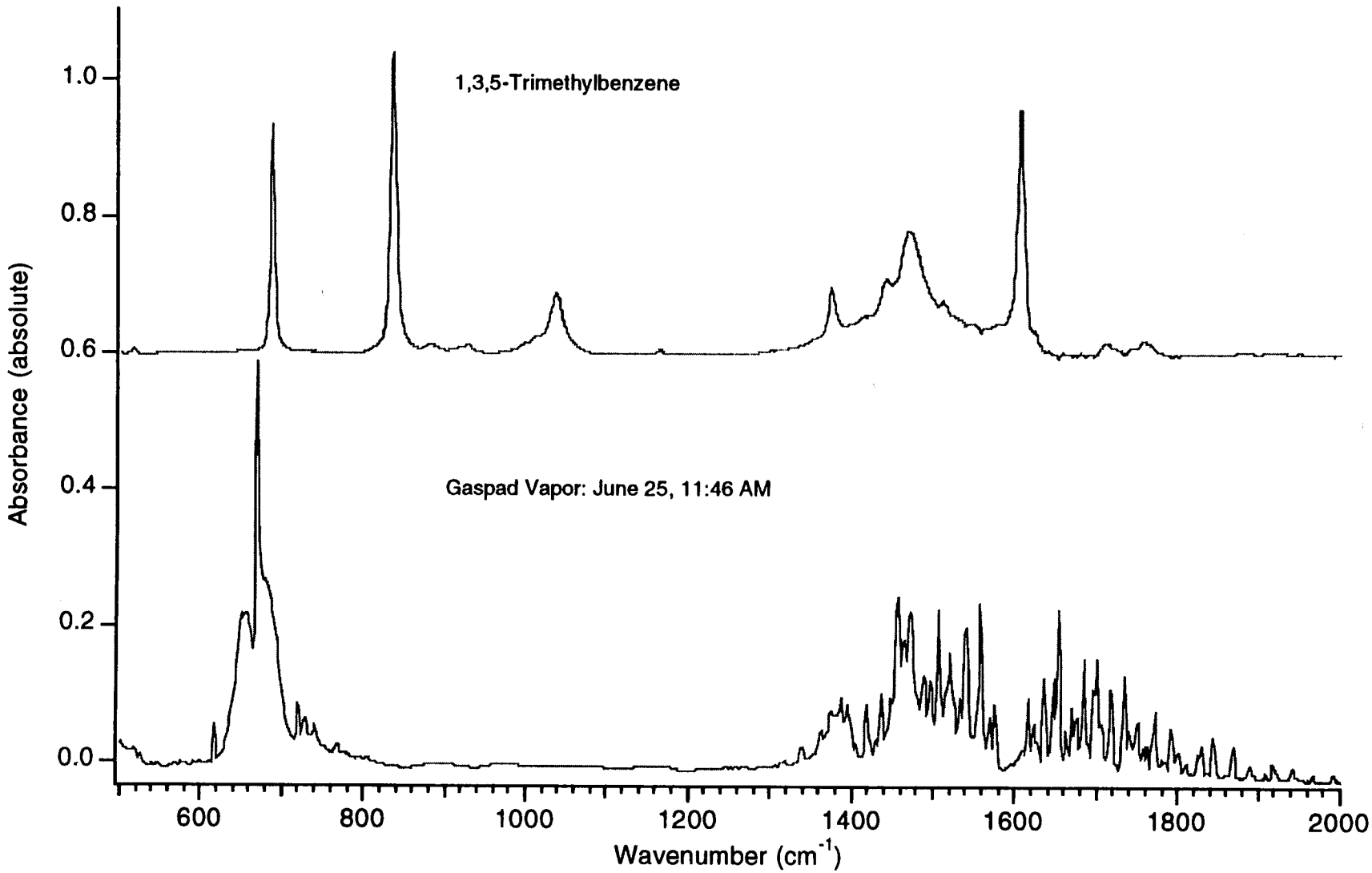

Figure 5.12.2. The fingerprint region of the spectra shows the strong ring C-H bending modes characteristic of 1,3,5-trimethylbenzene at 687 cm^{-1} and 836 cm^{-1}. Intense aromatic C=C ring stretching vibrations resulting from multiple *meta* substitution provide the intense absorbance at 1608 cm^{-1}.

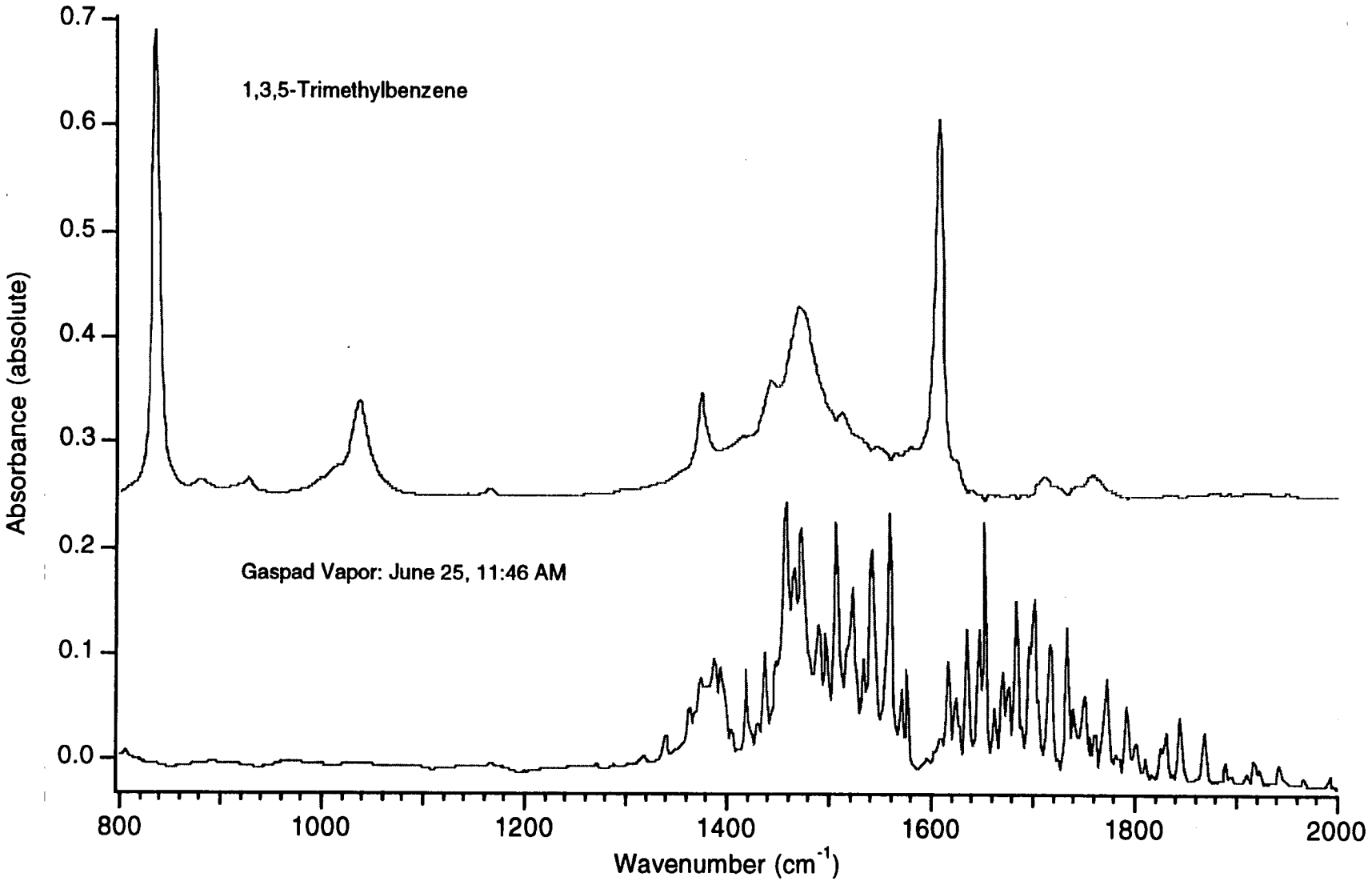

Figure 5.12.3. Expanded view of the fingerprint region of liquid 1,3,5 trimethylbenzene and the gaspad vapor effluent. Some aromatic toluene vibrations have absorbances in the window of the gaspad spectra. The characteristic alkane C-H bending modes of the three ring methyls are evident at 1385 cm^{-1} and 1440 cm^{-1} but the aromatic vibrations at 836 cm^{-1} and 1608 cm^{-1} are the dominant features of this spectrum.

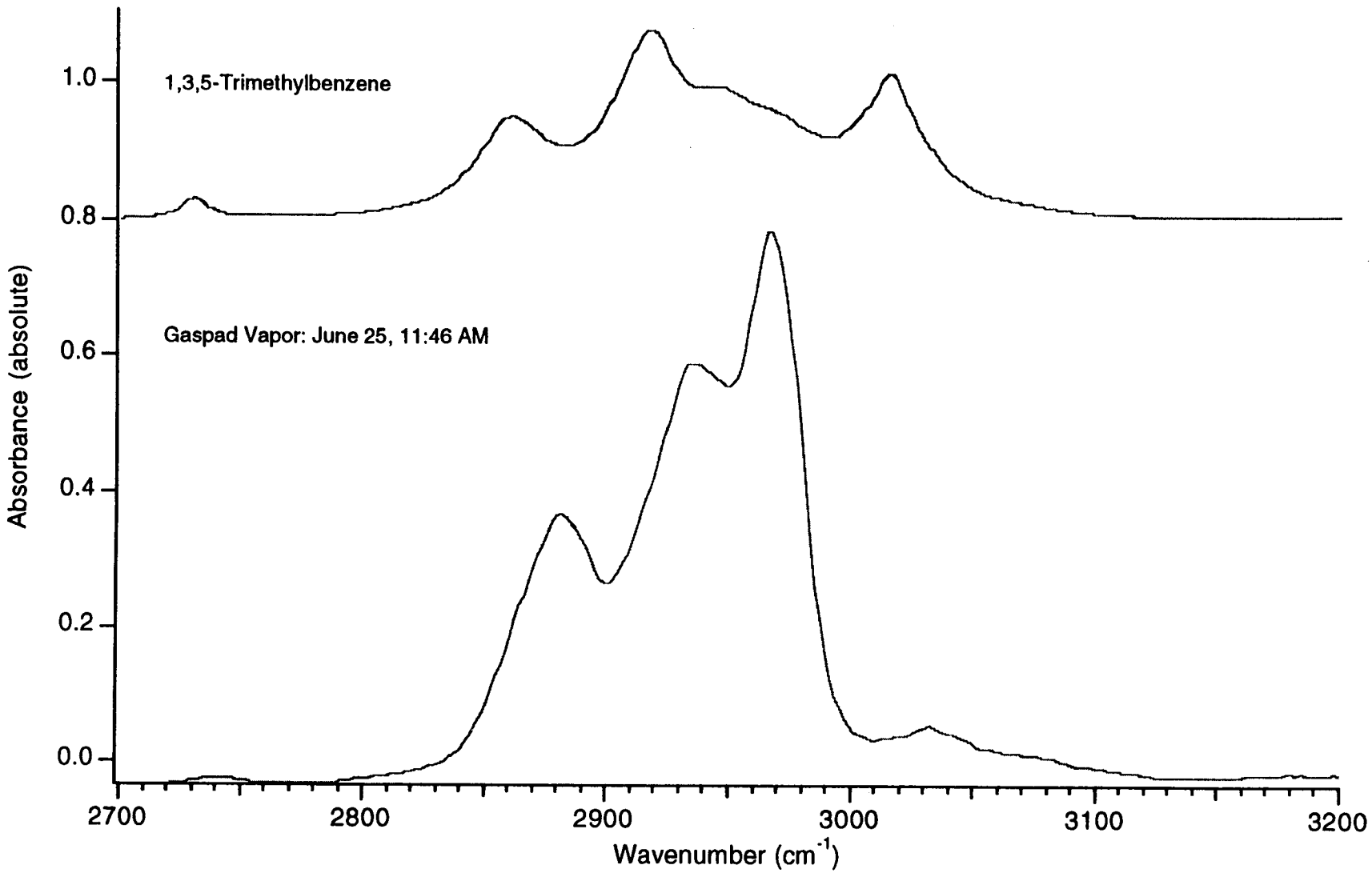

Figure 5.12.4. A magnified view of the C-H stretching region of liquid 1,3,5-trimethylbenzene and the gaspad vapor effluent. The aromatic stretching bands of the C-H absorbances are higher energy vibrations than those related to the alkanes and appear as distinct absorbances. There are nine C-H bonds that belong to the three ring methyl groups and only three aromatic C-H bonds.

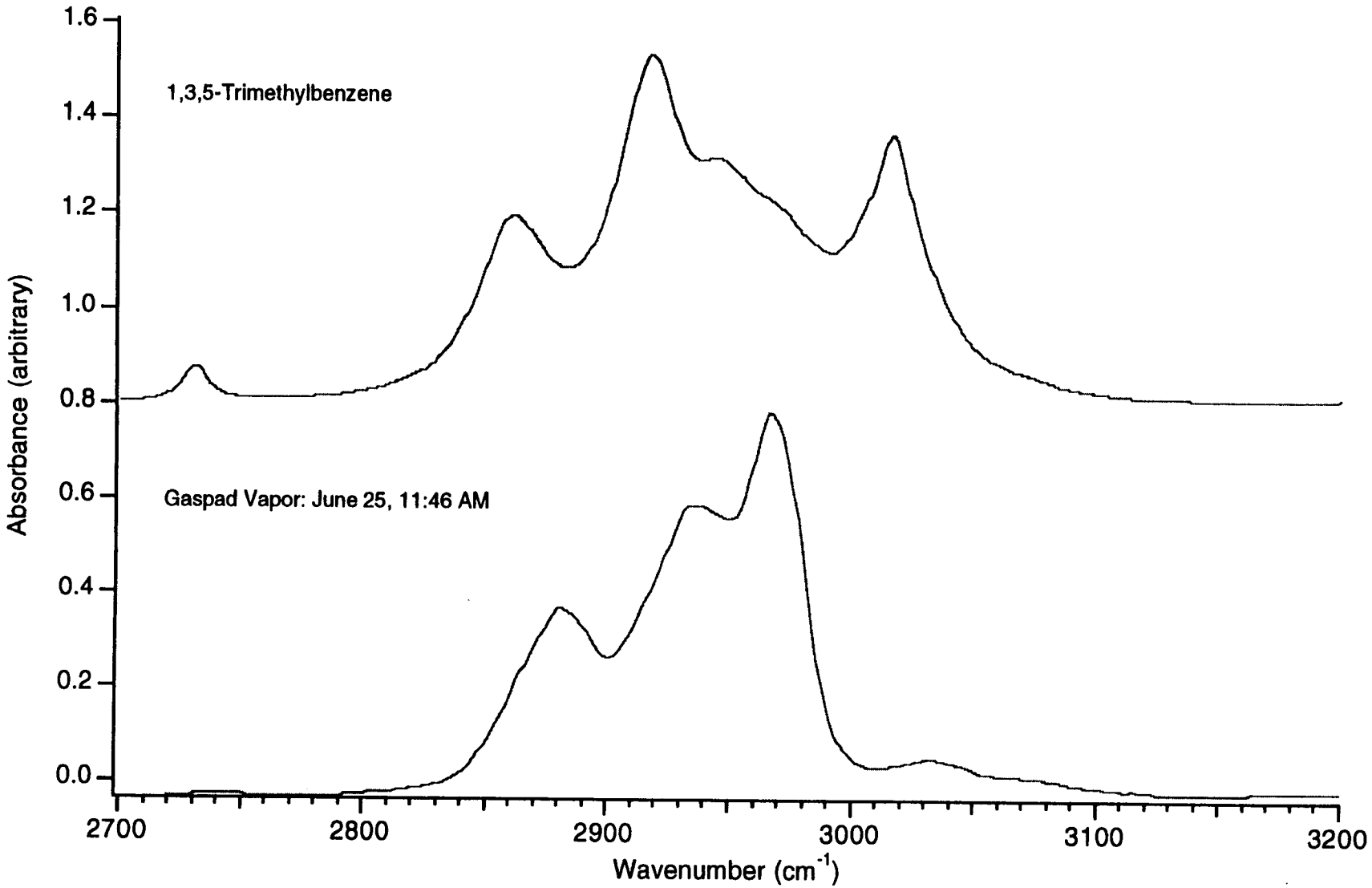

Figure 5.12.5. The spectrum of 1,3,5-trimethylbenzene is enhanced in this graph to more clearly show the band structure of the C-H stretching region.

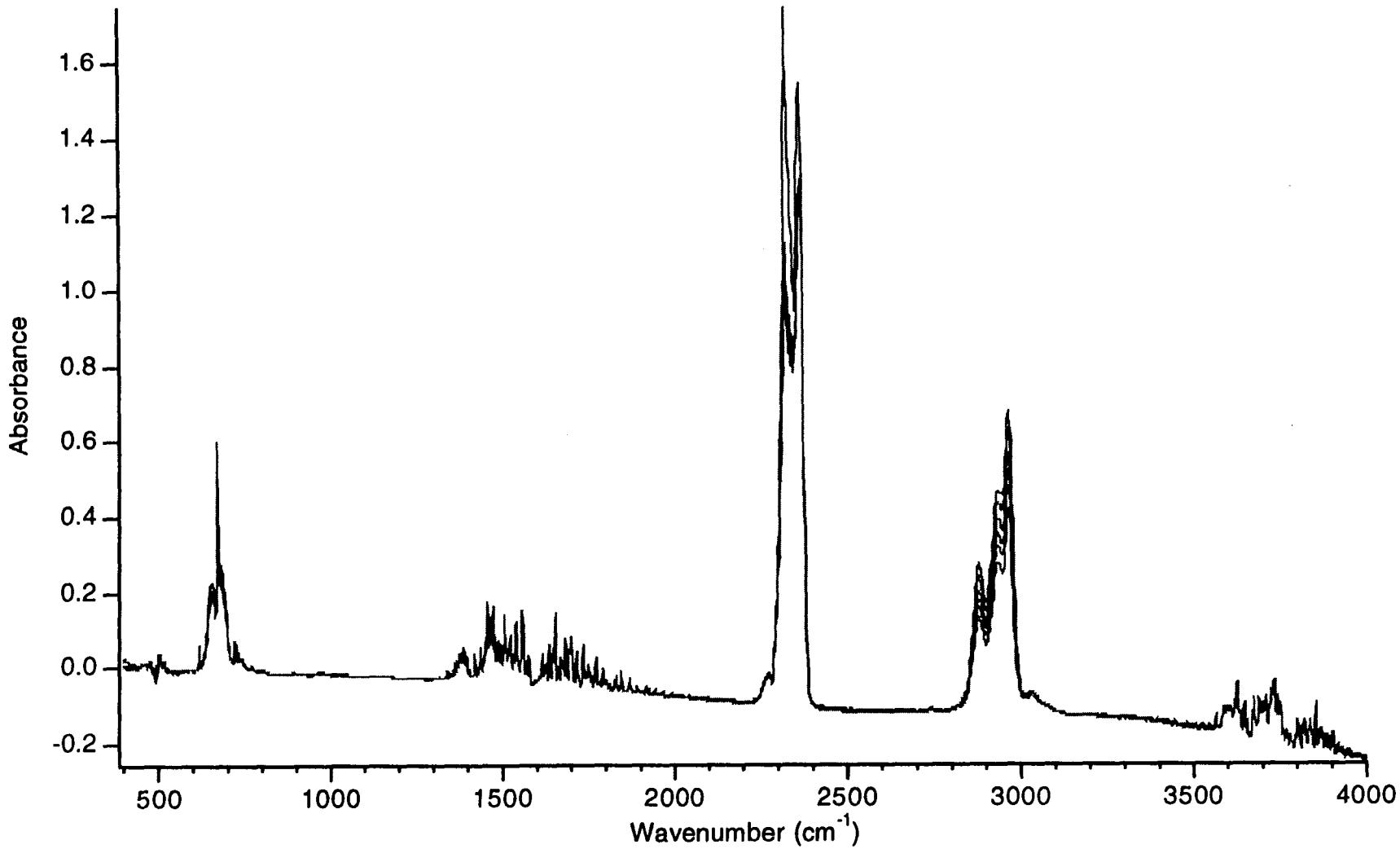

Figure 6.1 Consecutive scans of the gaspad vapor effluent taken between June 27, 11:50 PM and June 28, 1:57 AM at 6 minute intervals are overlaid and displayed without modification of the raw data. The baseline and water region (1600 to 2000 cm^{-1}) are very constant during this time increment while considerable variation exists in the intensity of the alkane and CO_2 bands. Clearly, the concentrations of these components of the gas vapor are changing as the water remains constant, probably at saturation.

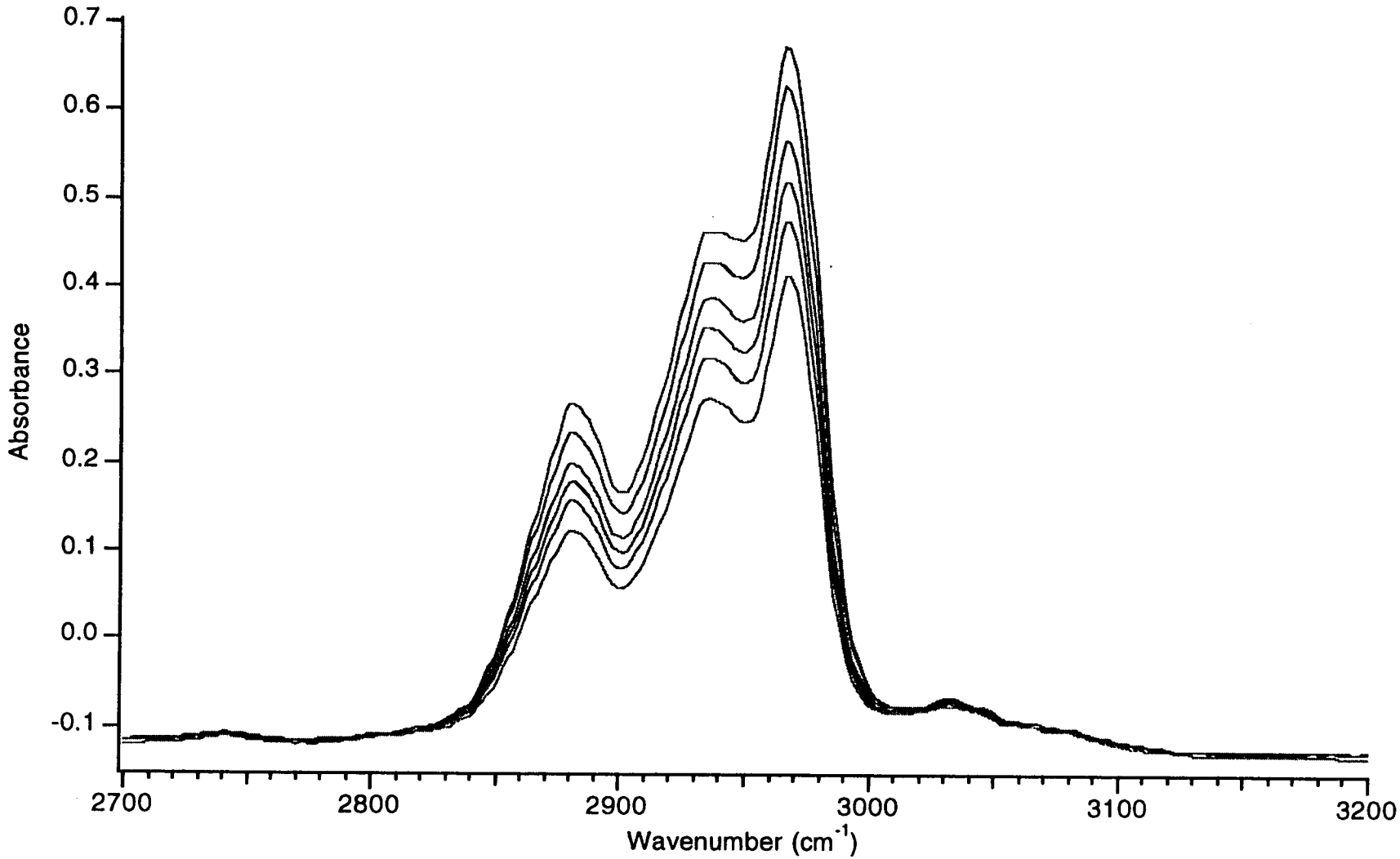

Figure 6.2. Consecutive scans of the gaspad vapor effluent taken between June 27, 11:50 PM and June 28, 1:57 AM at 6 minute intervals are overlaid and displayed without modification of the raw data. The integrated band intensity of the alkyl C-H stretch region indicates that the alkane concentration changes by more than 50% during the measurement interval. In contrast, the integrated band intensity of the water region from 2000 to 1590 cm^{-1} shows a deviation from the mean value of less than 1%. Some of the scans obtained during the collection interval have been removed for clarity.

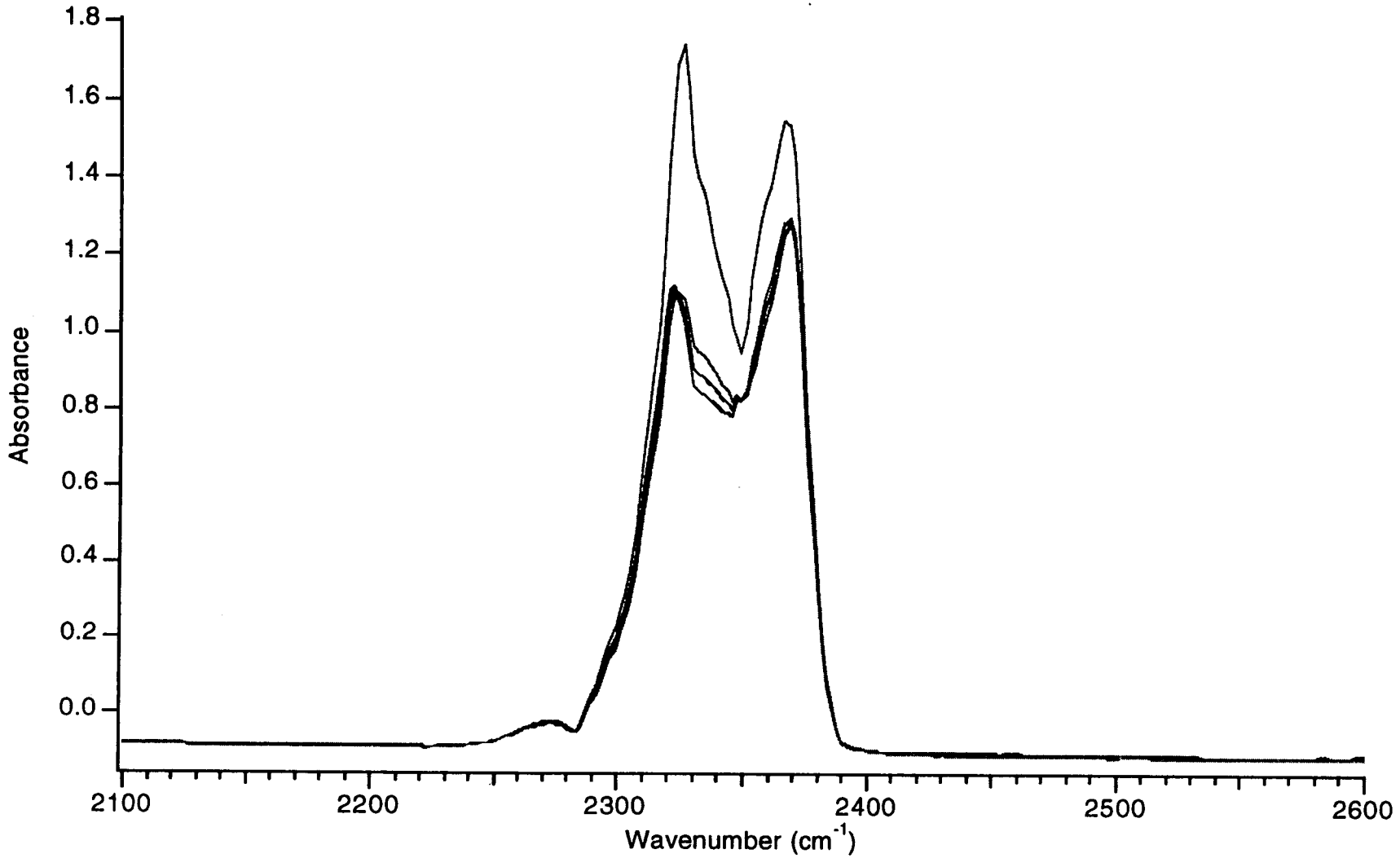

Figure 6.3. The CO_2 stretch absorption is relatively constant over the measurement interval.

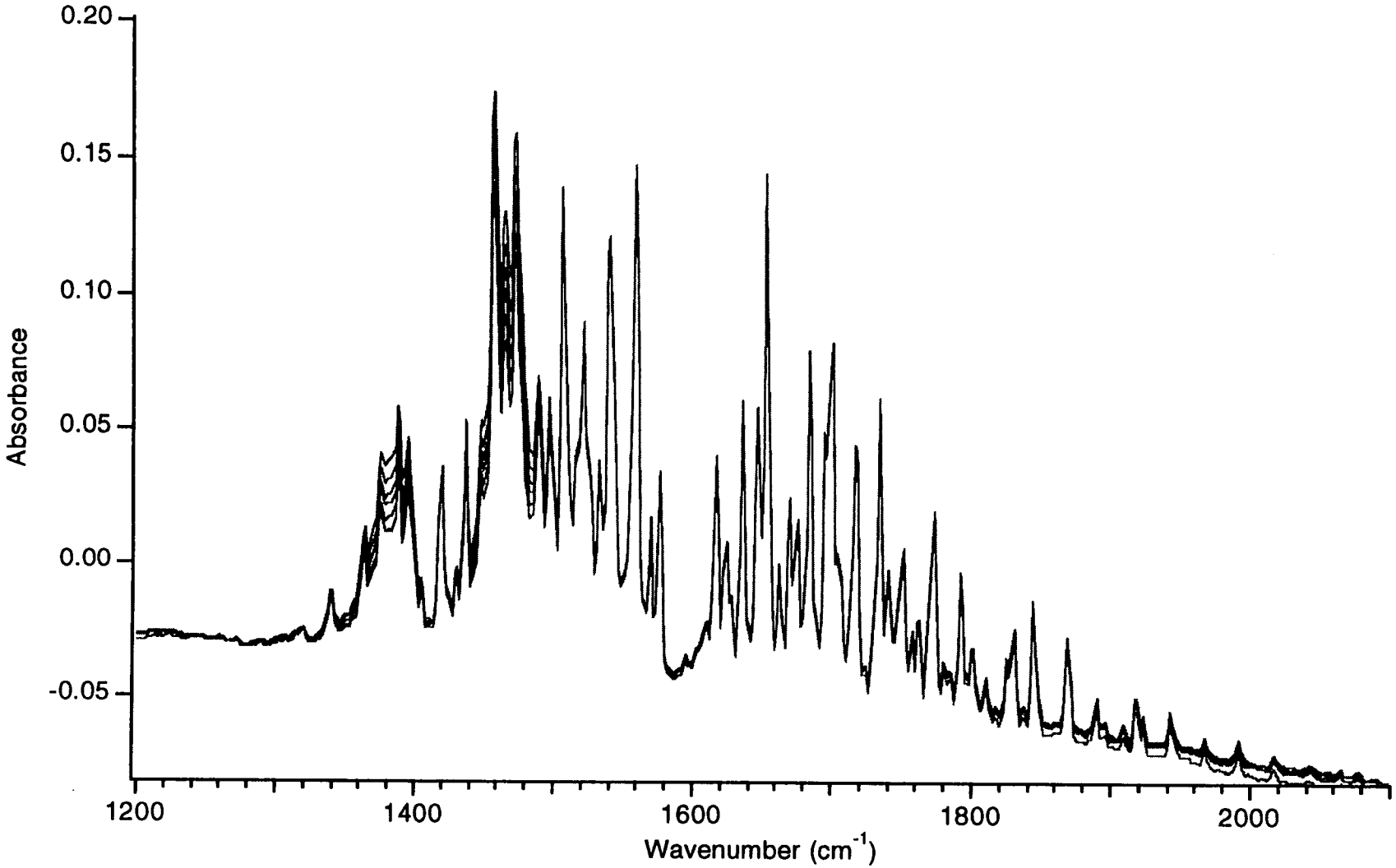

Figure 6.4. Consecutive scans of the gaspad vapor effluent taken at 6 minute intervals are overlaid. There is remarkable consistency in the water envelop as one might expect with a saturated water vapor concentration. However, the alkane bending region (1350-1450 cm^{-1}) that overlaps the water manifold shows conspicuous intensity variation. The integrated band intensity of the water region from 2000 to 1590 cm-1 shows a deviation from the mean value of less than 1%. Some of the scans obtained during the collection interval have been removed for clarity.

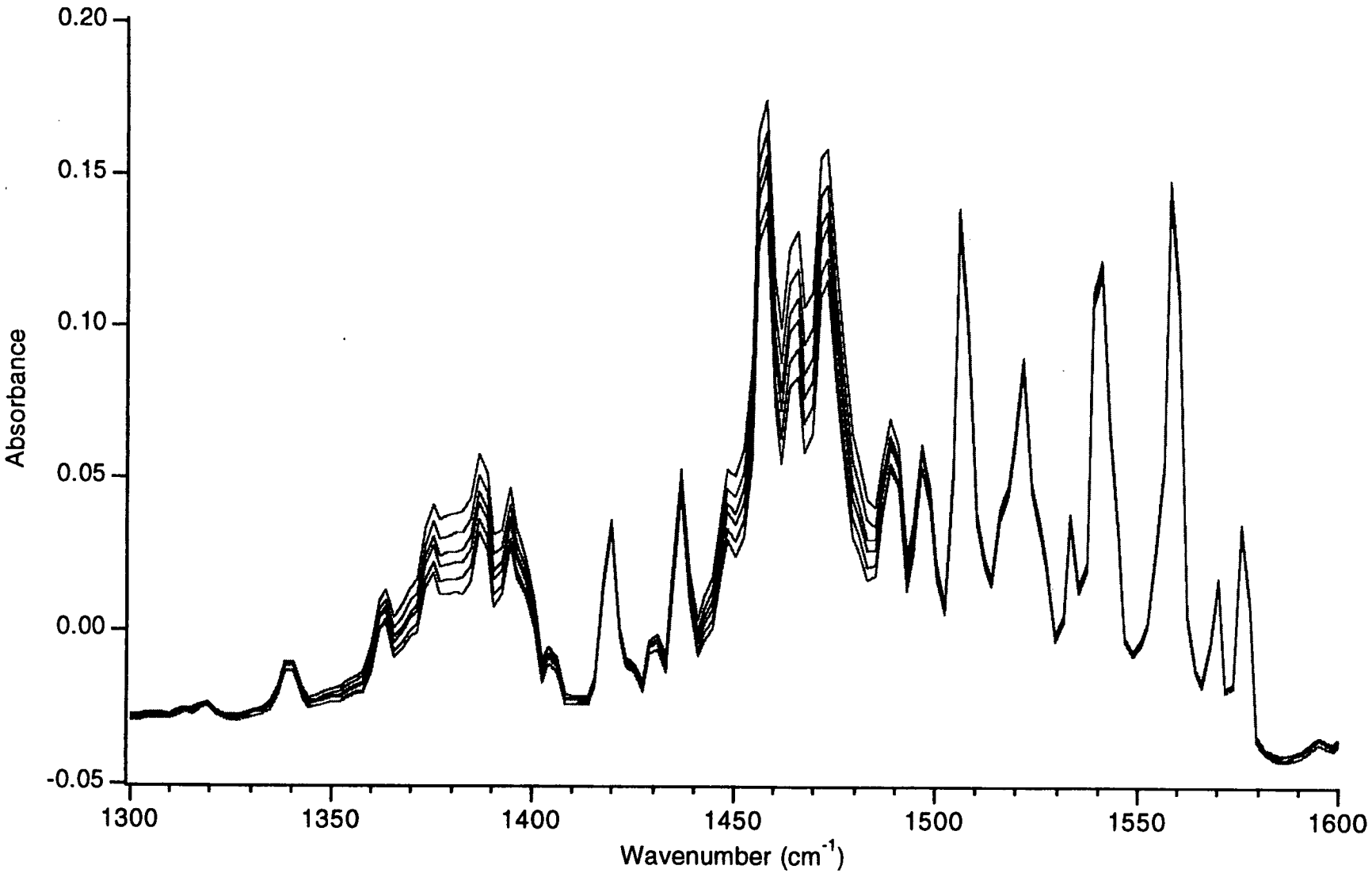

Figure 6.5. Consecutive scans of the gaspad vapor effluent taken between June 27, 11:50 PM and June 28, 1:57 AM at 6 minute intervals are overlaid and displayed without modification of the raw data. An expanded view of the C-H and O-H bending regions shows the remarkable consistency of the water envelop and the changing intensity of the alkane absorbances (1350-1450 cm^{-1}). Some of the scans obtained during the collection interval have been removed for clarity.

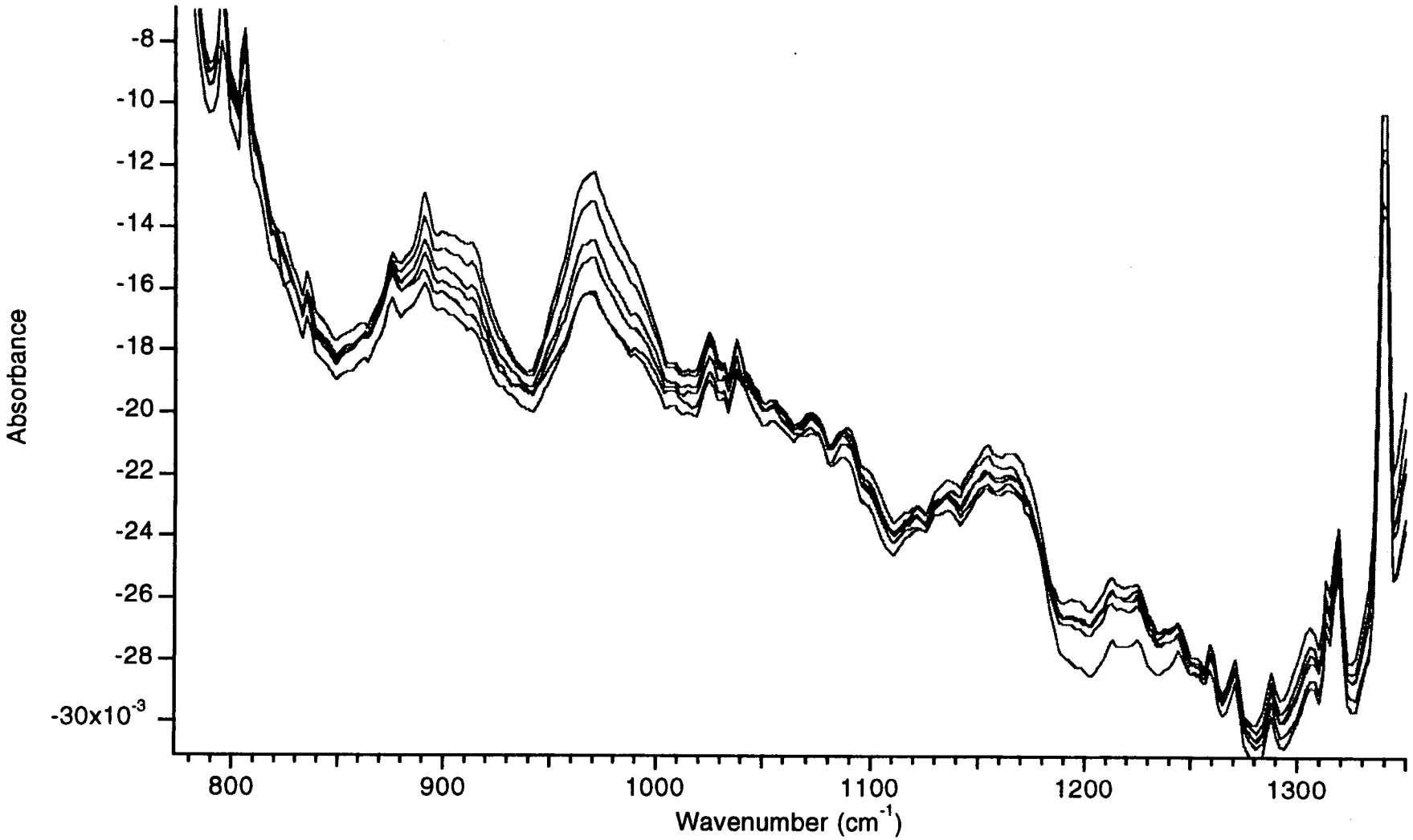

Figure 6.6. Consecutive scans of the gaspad vapor effluent taken between June 27, 11:50 PM and June 28, 1:57 AM at 6 minute intervals are overlaid and displayed without modification of the raw data. This expanded view of the fingerprint region shows that the intensity variation is not spectral noise but represents absorbances that most likely result from dilute aromatic constituents in the effluent vapor and from low intensity vibrations of the more concentrated aliphatic effluent components.

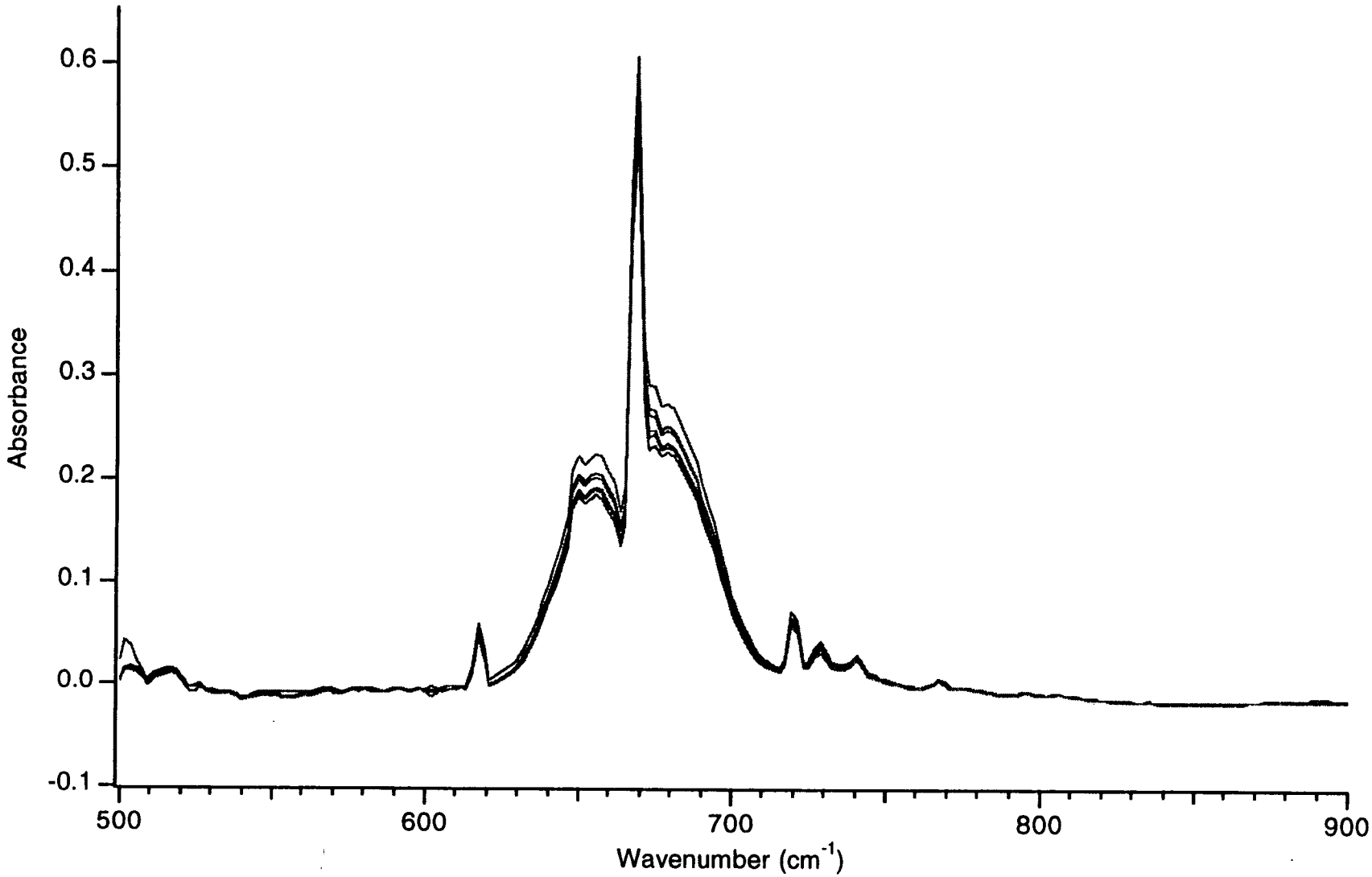

Figure 6.7. Consecutive scans of the gaspad vapor effluent taken between June 27, 11:50 PM and June 28, 1:57 AM at 6 minute intervals are overlaid and displayed without modification of the raw data. The region of the fundamental CO_2 bending vibration is shown with some of the scans removed for clarity.

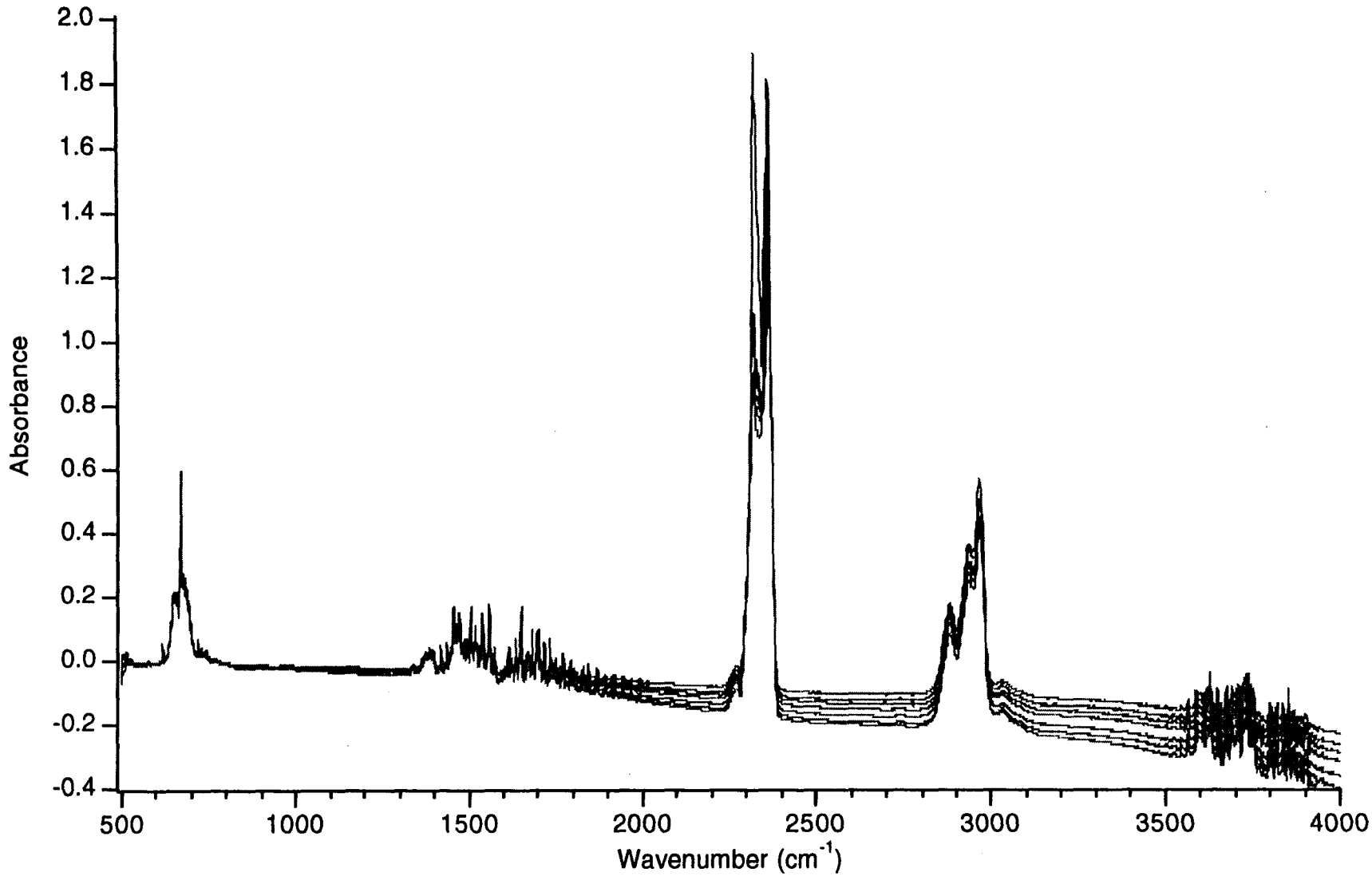

Figure 7. Over relatively short time intervals (2 hours) the baseline remains quite constant, as was shown in Figure 6.1; however, the overlaid scans in this figure were collected over 17 hours and show a substantial shift in the baseline. This problem, which may result from a drifting source and could be overcome simply by obtaining a background spectrum at more frequent intervals.

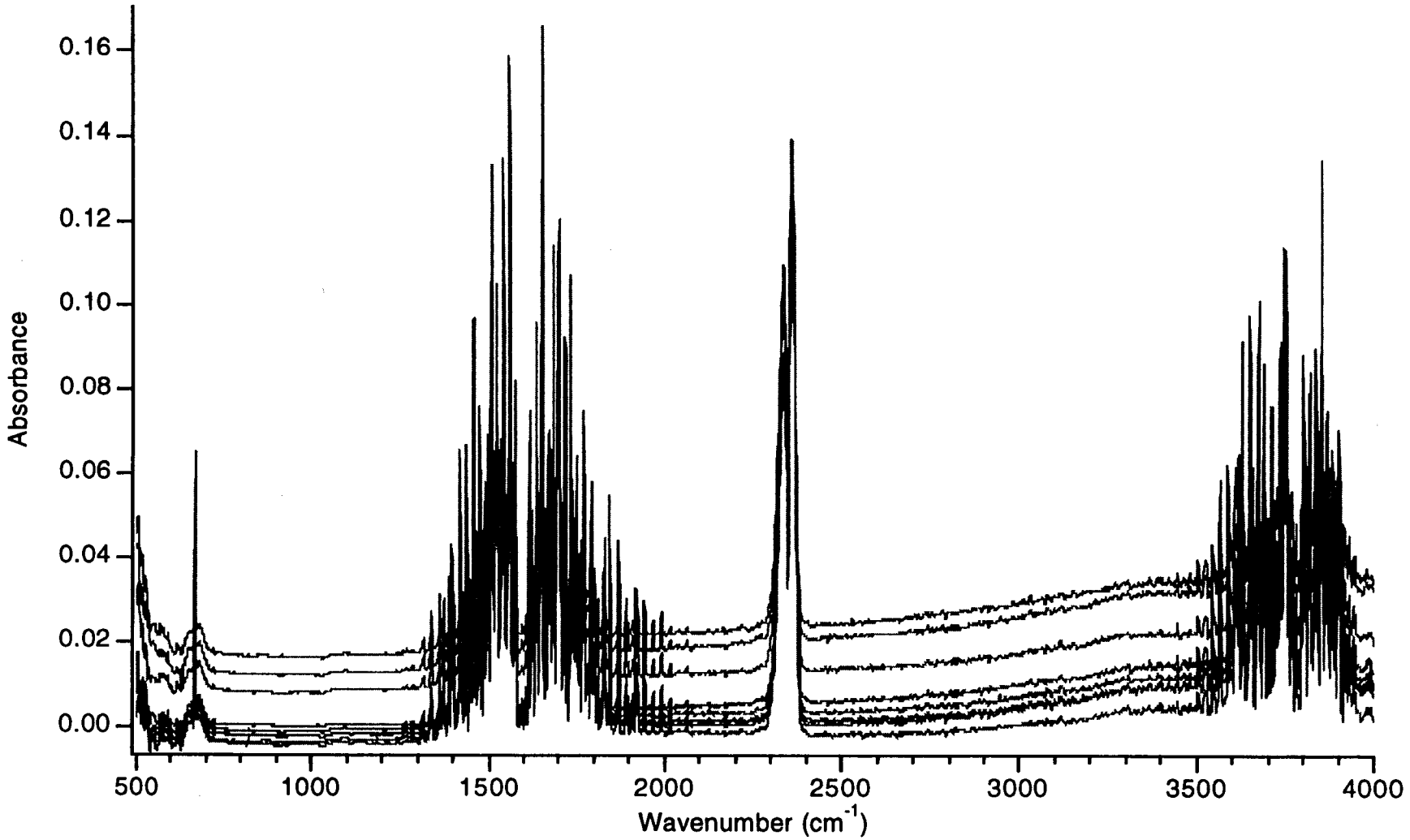

Figure 8. Overlay of room air spectra taken to evaluate instrument stability. These spectra, collected with the same instrument parameters as were used to collect the vapor effluent data, were obtained in the laboratory. Although the baseline drifted by almost 20% of the spectra's maximal absorbance value, the integrated band intensities for the water bending manifold (2100-1200 cm^{-1}) varied by less than 1.5% and the CO_2 intensity (2500-2200 cm^{-1}) varied by less than 3%. However, as the baseline value increased, so to did the integrated band intensities (see Figure 9).

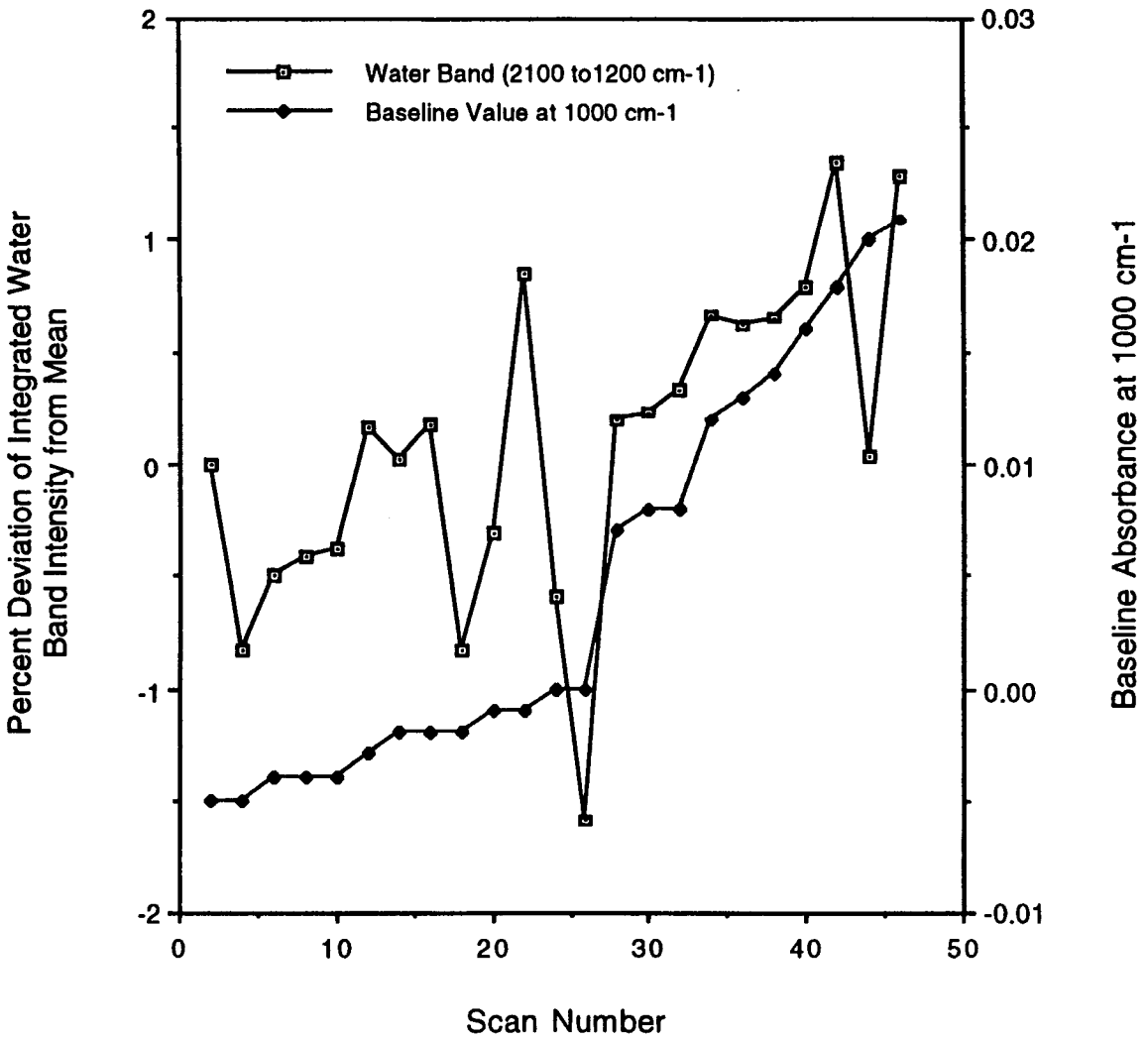

Figure 9. The integrated band intensities of the water region (2100 to 1200 cm^{-1}) from 46 spectra of laboratory room air collected at 6 minute intervals are shown in the plot along with the change in their baseline absorbance values. The data suggest that these two trends are related and that it may be necessary to address the problem of the drifting baseline to insure that the integrated peak data is representative of vapor concentration.

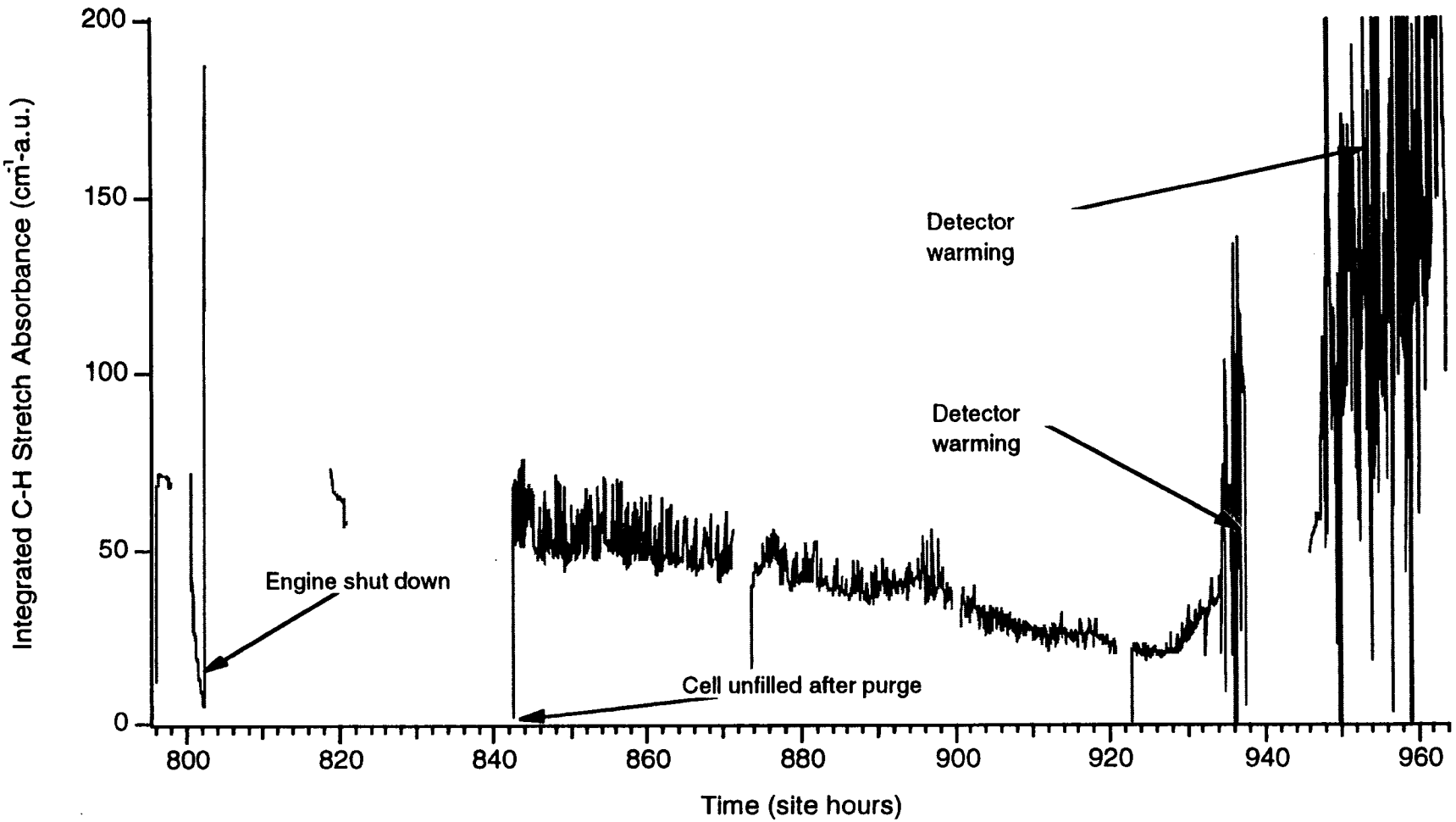

Figure 10. The integrated band intensity of the C-H stretching absorbance (2700-3000 cm^{-1}) for each scan is plotted against the collection time. The initial data was collected sporadically because modifications were made in the instrumentation and data collection routines. The vertical lines at the start of each collection interval result from incomplete purging of nitrogen after collecting the background spectra. One or two scan times were required to completely flush the gas cell with effluent vapor. The up-swing in the data at 920 h corresponds to the start of steam injection at 897 h into well 819. The portions of the graph that show intense variation (940 h and beyond) are thought to be periods when the MCT detector warmed because the liquid nitrogen in the deware had been expended.

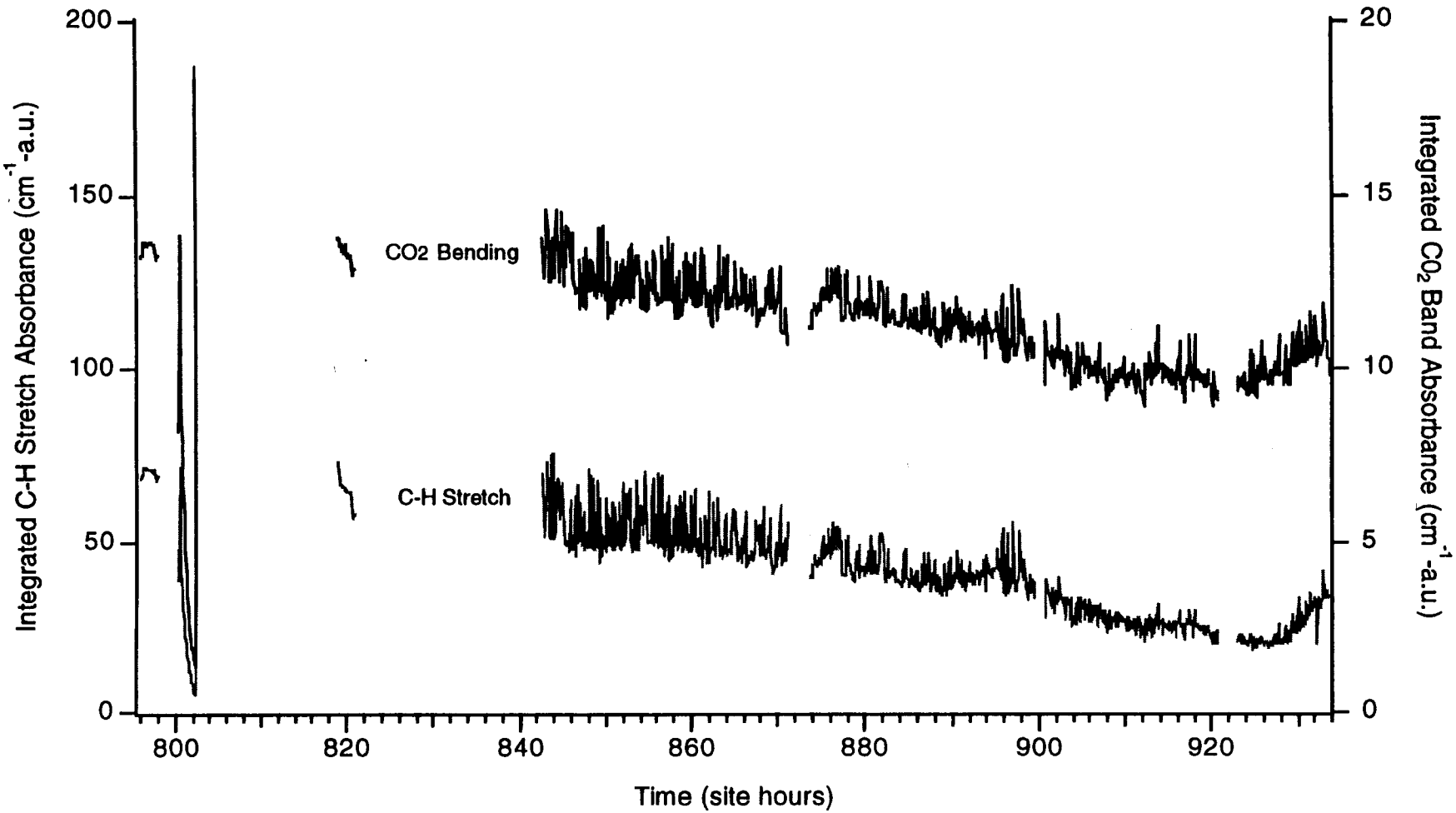

Figure 11. The integrated band intensity of the C-H stretching absorbance (2700-3000 cm^{-1}) for each scan is plotted with its intensity on the left ordinate and the corresponding scale for the CO_2 bending absorbance (600-800 cm^{-1}) is on the right ordinate. The data show the concentrations of both CO_2 and the alkane components are decreasing as the vacuum extraction proceeds. The CO_2 concentration declines only about 20% over the monitoring period while the alkane concentration is reduced by nearly 65%. The fluctuations in the integrated band values may represent real changes in the gas concentrations that result from "bumping" or other phenomena that occur during the extraction process. The up-swing in the CO_2 and alkane concentrations at 920 h corresponds to steam injection into well 819 at 897 h.

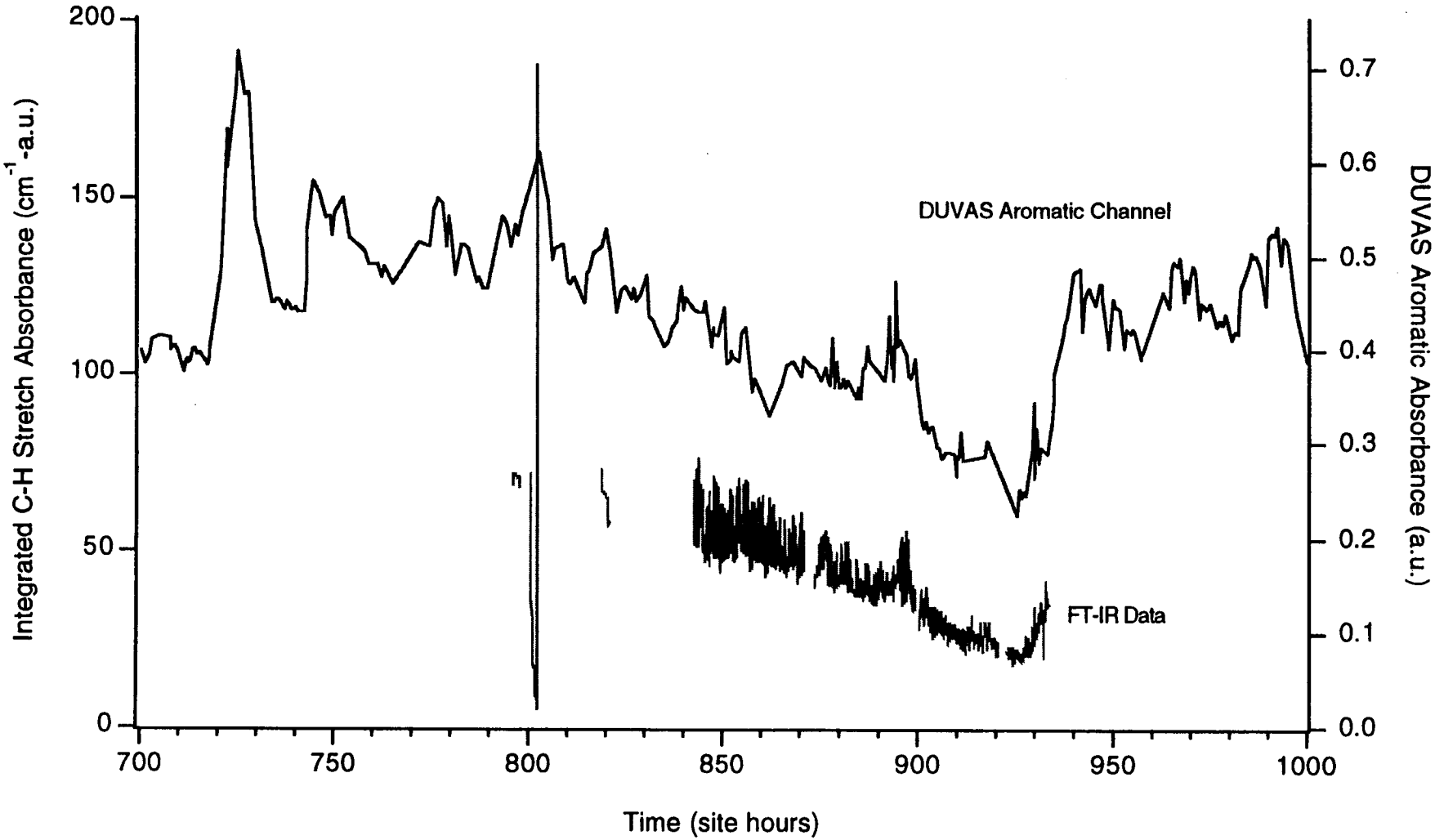

Figure 12. The integrated band intensity of the C-H stretching absorbance (2700-3000 cm^{-1}) for each scan is plotted with its intensity on the left ordinate and the corresponding scale for the aromatic signal from the DUVAS system is on the right ordinate. Although the DUVAS system was operating for a longer period during the demonstration, the data show that both instruments followed the same trend as the concentrations of analytes declined as the vacuum extraction progressed. Both instruments detect the increase in organic components in the effluent vapor as steam injection commences at 897 h.

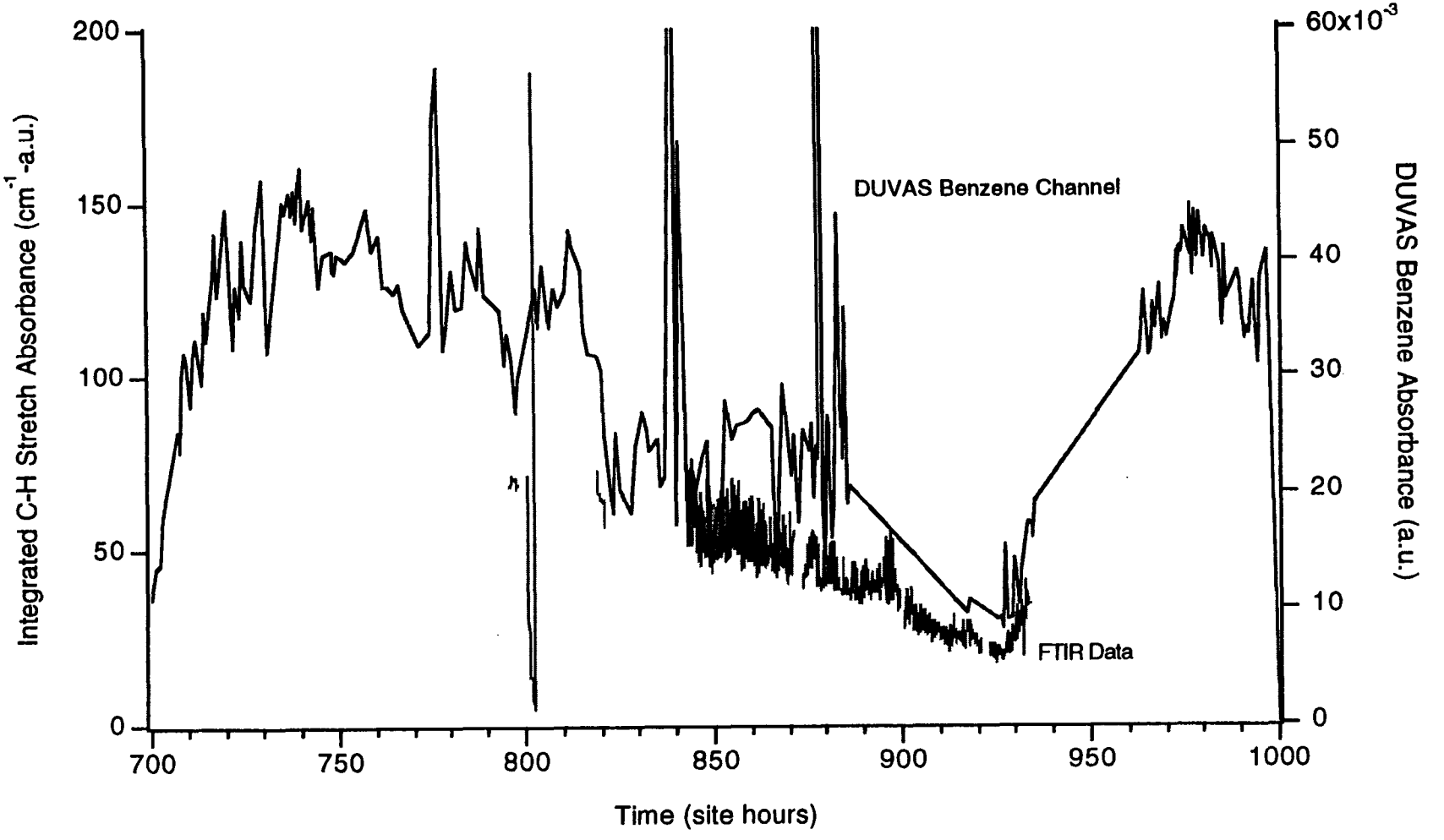

Figure 13. The integrated band intensity of the C-H stretching absorbance (2700-3000 cm^{-1}) for each scan is plotted with its intensity on the left ordinate and the corresponding scale for the benzene signal from the DUVAS system is on the right ordinate. The straight lines in the DUVAS data between 860 and 960 h were times that the benzene channel was not in operation. Nevertheless, both instruments exhibit good correlation between the data types and follow the same trend as the concentrations of analytes decline during the vacuum extraction process. Both instruments detect the increase in organic components in the effluent vapor as steam injection commences at 897 h.

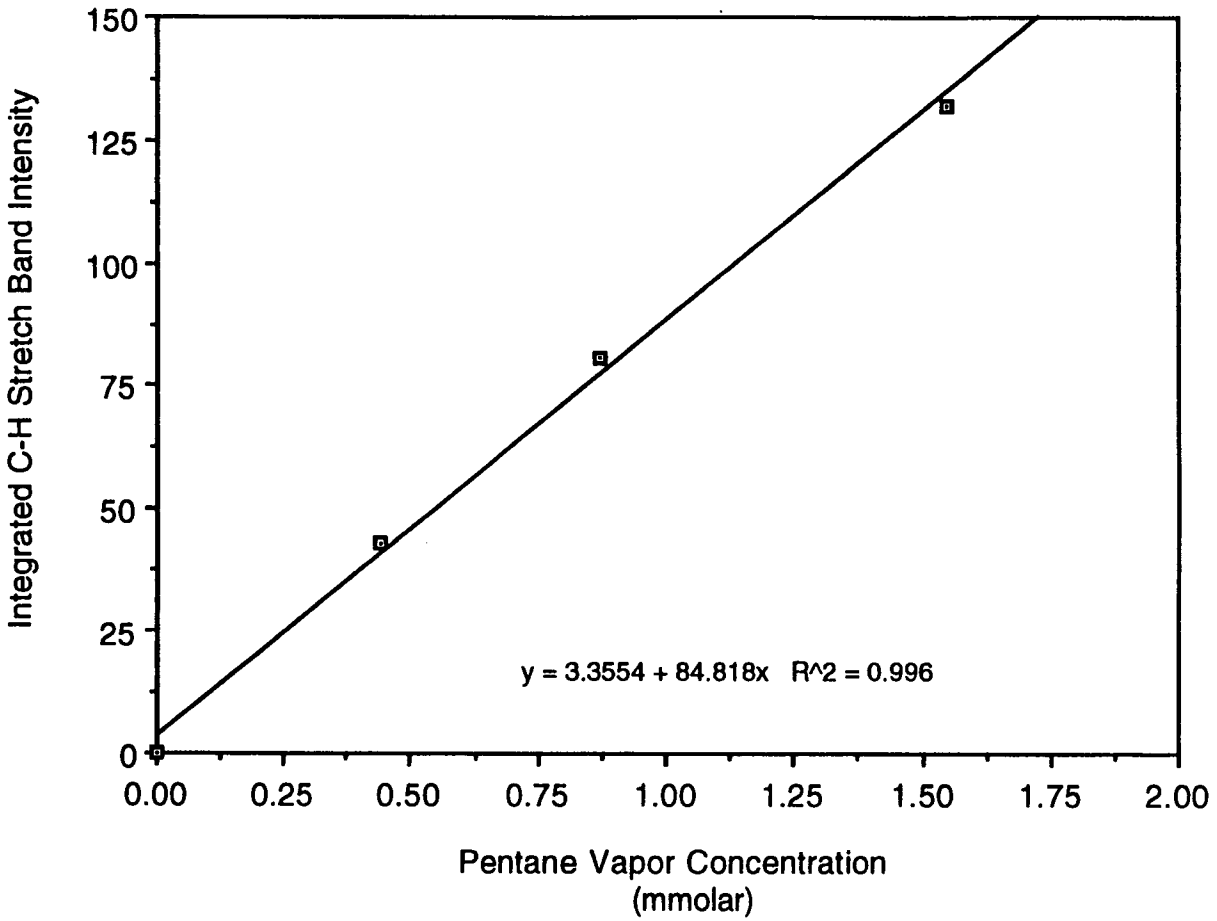

Figure 14. The integrated C-H stretching band intensity of pentane is used as a standard for calibrating the FT-IR response to the alkane vapor effluent. The concentration of alkane is reported as millimoles of pentane per liter of gas. From the integrated band intensities of Figure 10, the estimated alkane concentration, based on the molar absorptivity of the combined CH_3 and CH_2 stretching modes, is about 0.6 mmolar, which represents about 15,000 ppm of alkane in the vapor stream.